Supplemental Information

Table of Contents

Figure S1. Sequence similarity network of TSs (IPR034686) from bacteria at an e-value threshold of 10-70.[1] Functionally characterized TSs are colored (green, C10; orange, C11; magenta, C15; blue, C20) and their major products are shown. AlbS is shown as blue with yellow border. Related to Fig. 2.

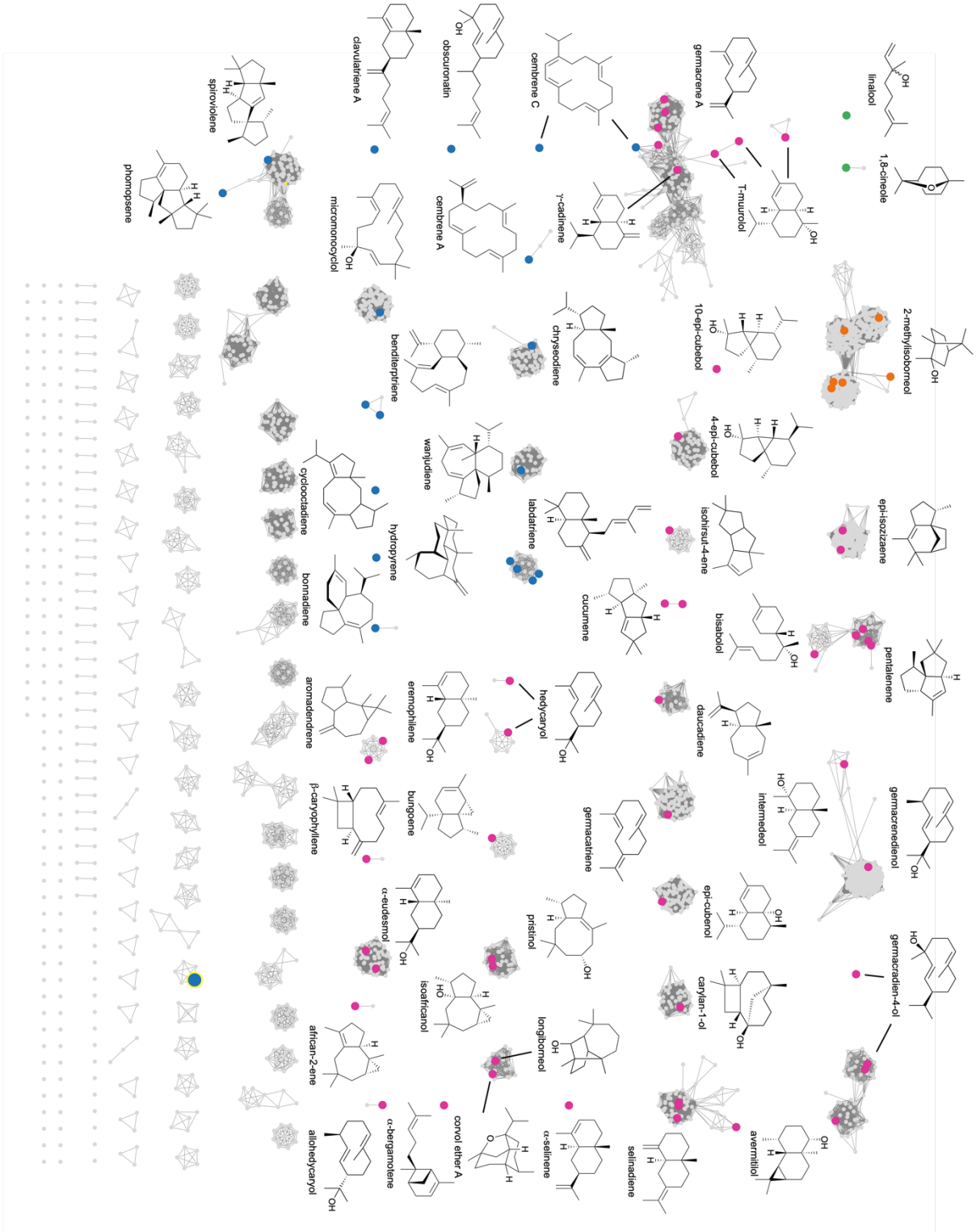

Figure S2. Sequence alignment. Residues are colored based on conservation (red box with white residue shows identity, red residue similarity, and blue frame similarity across groups). The alignment was created with ClustalW[2] and rendered with ESPript.[3] The conserved DDxxD, NSE, and WxxxxxRY motifs are labeled with purple, brown, and light blue boxes. Residues targeted for mutation are highlighted by black arrows. Accession numbers of proteins are given in the methods section.

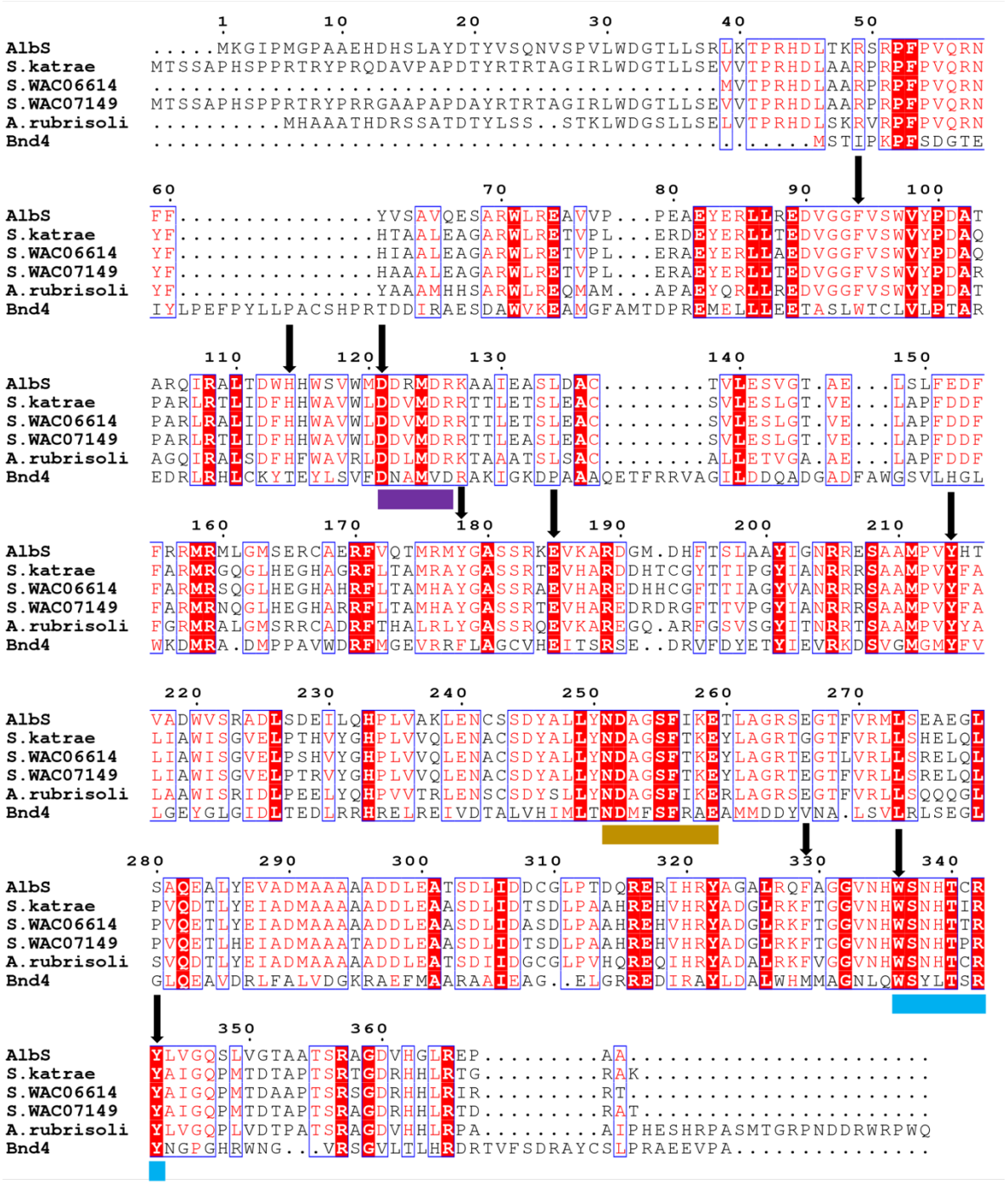

Figure S3. SDS-PAGE of purified AlbS and mutants. AlbS, with its His tag, is 46.5 kDa. Samples shown below are elutions from Ni-NTA affinity chromatography. Y214A, W336A, W336H, F94A, H114T, F329A, Y214W, and Y214I were insoluble. F94W, H114A, Y214L, and Y214H were sparingly soluble but not active.

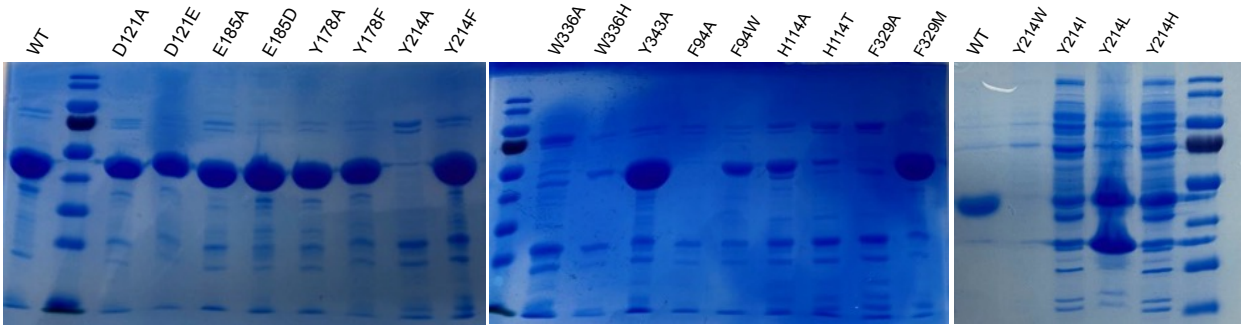

Figure S4. EIMS of β-elemene (**3**). The fragmentation and retention index (RI = 1398) matched the literature (RI = 1390).[4]

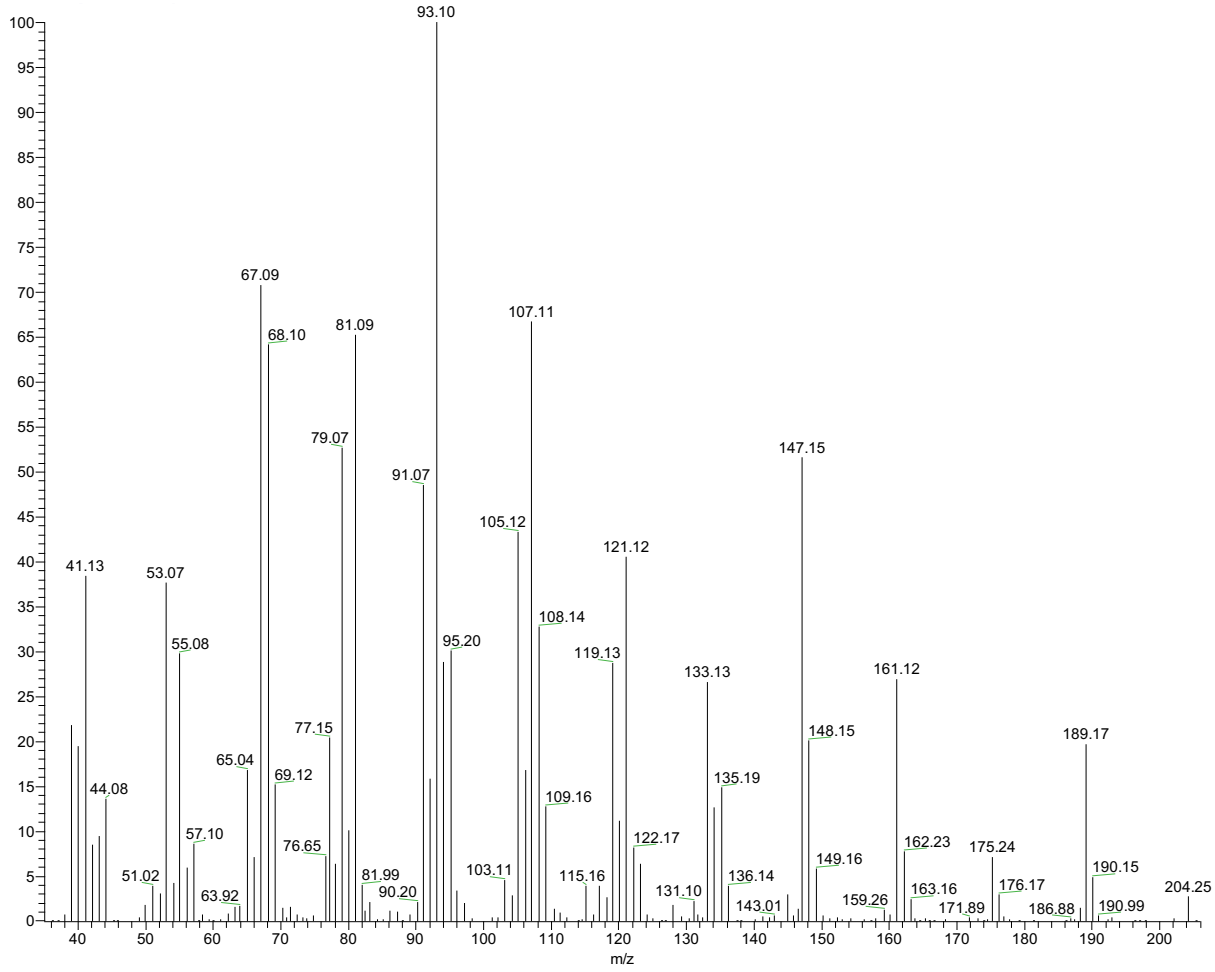

Figure S5. EIMS of shyobunol (**4**). The fragmentation and retention index (RI = 1521) matched the literature (RI = 1521).[5]

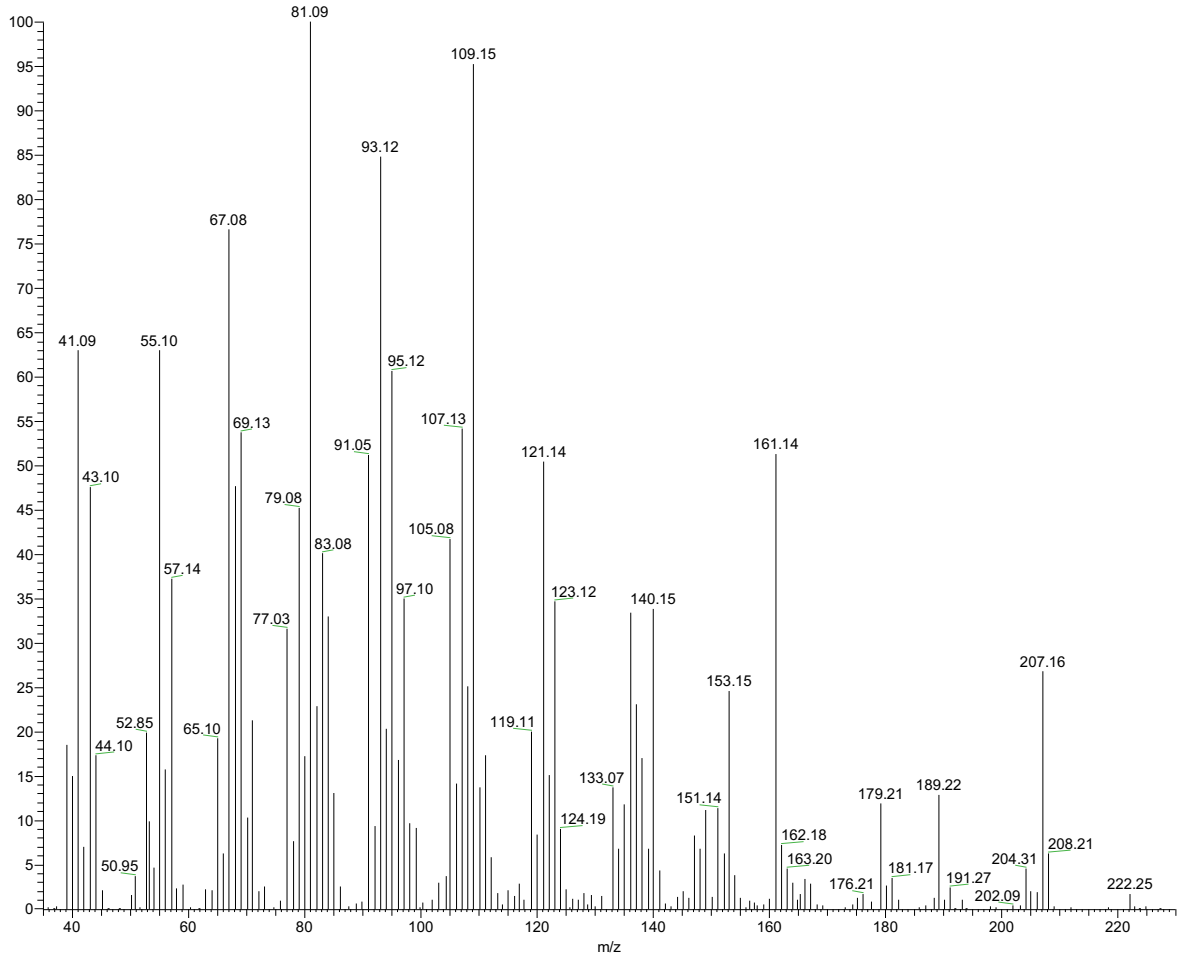

Figure S6. EIMS of elemol (**5**). The fragmentation and retention index (RI = 1558) matched the literature (RI = 1549).[4]

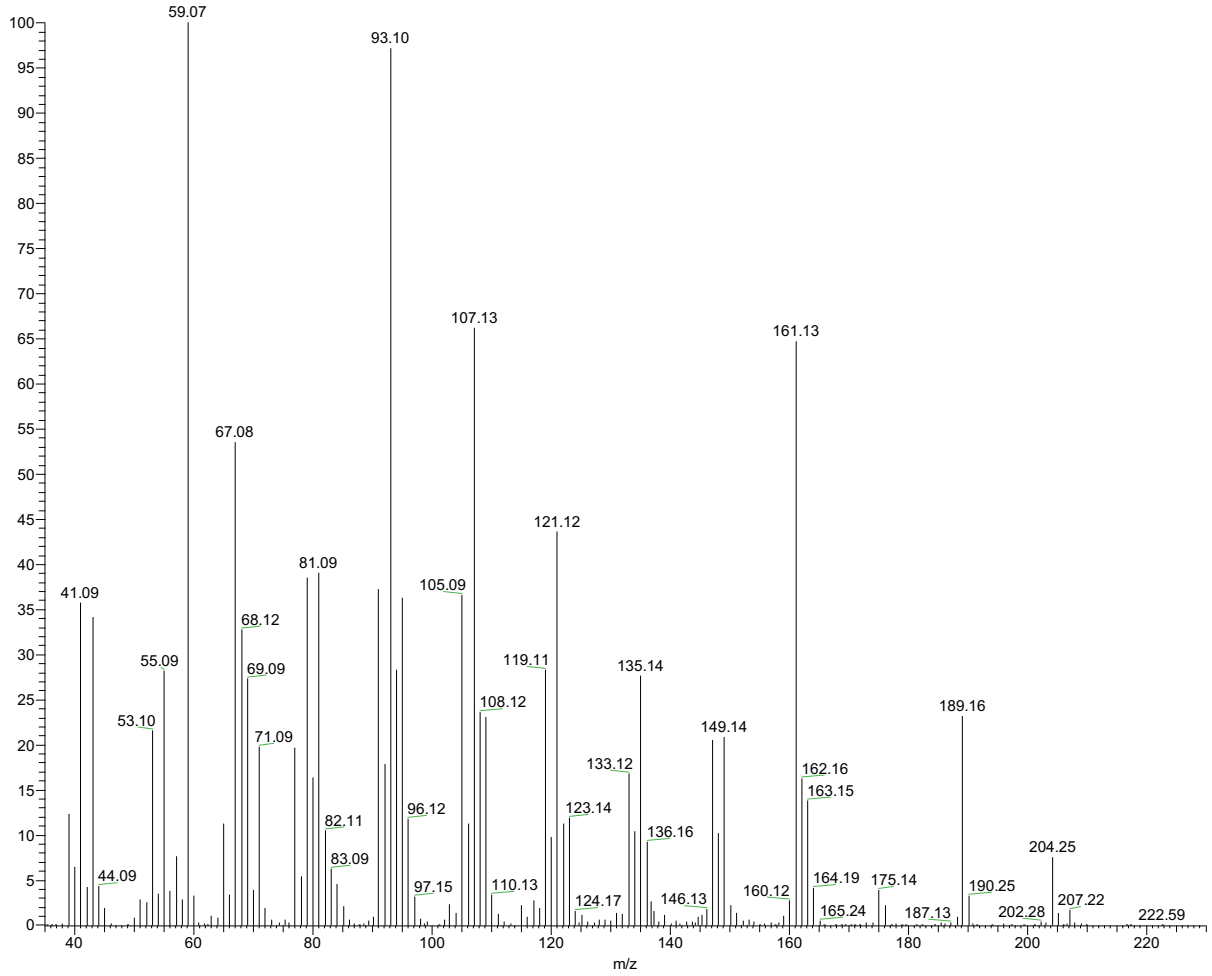

Figure S7. EIMS of *trans*-nerolidol (**6**). The fragmentation and retention index (RI = 1567) matched the literature (RI = 1563).[4]

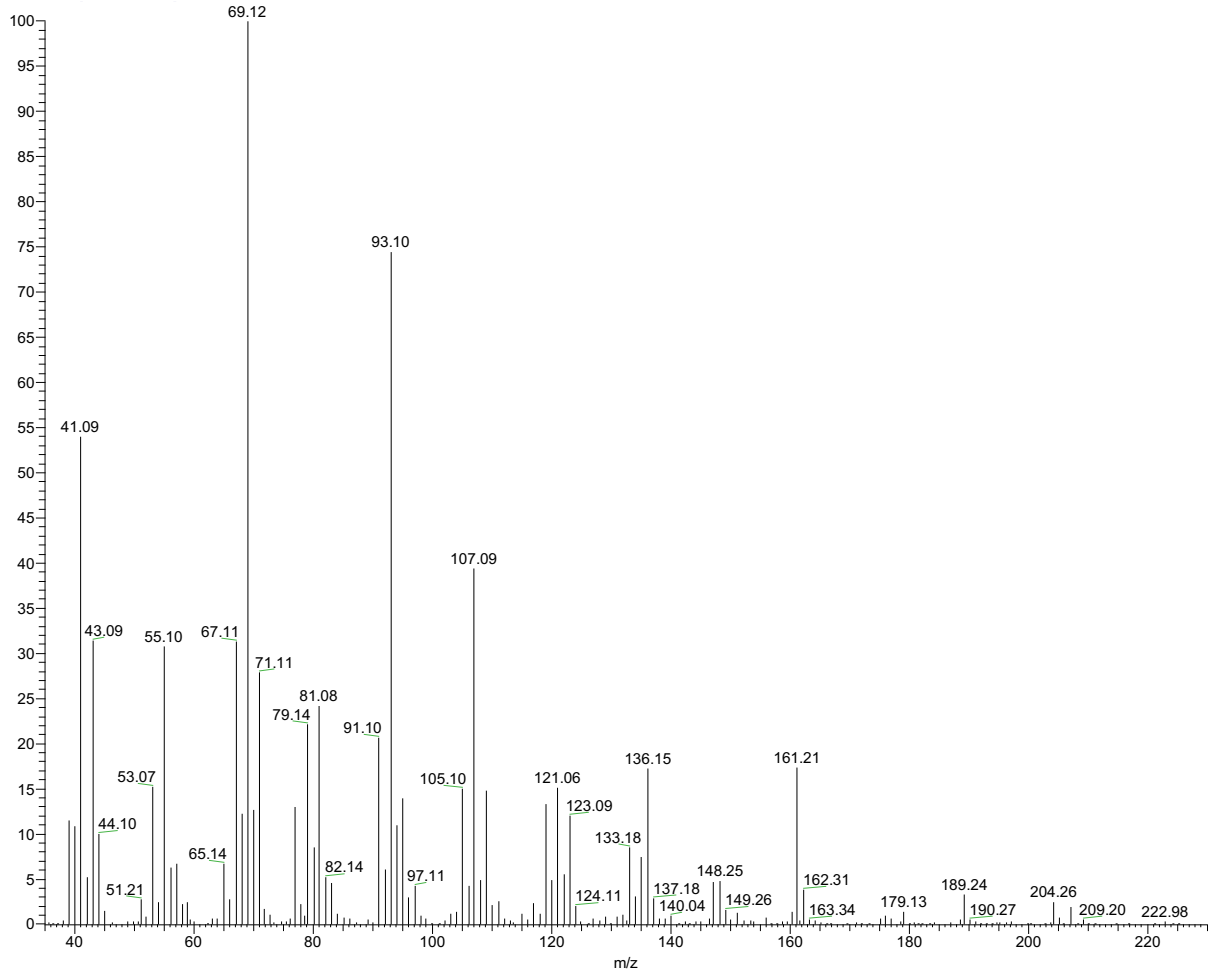

Figure S8. EIMS of *epi*-α-cadinol (**7**). The fragmentation and retention index (RI = 1632) matched the literature(RI = 1640).[4]

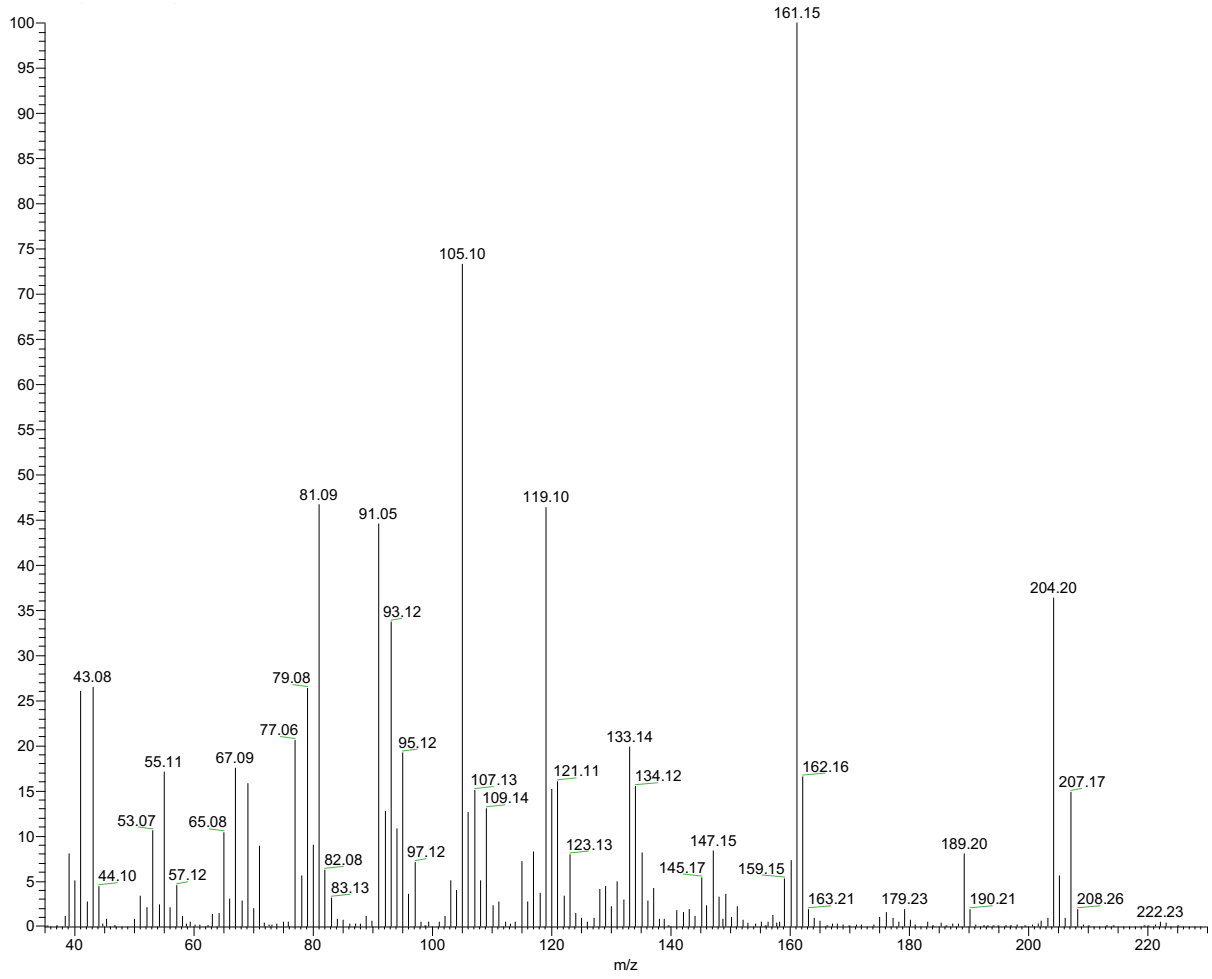

Figure S9. EIMS of albireticulene (**1**). (top) **1**; (middle) 11-^{2}H-**1**; (bottom) 1,11-$^{2}H_{2}$-**1**.

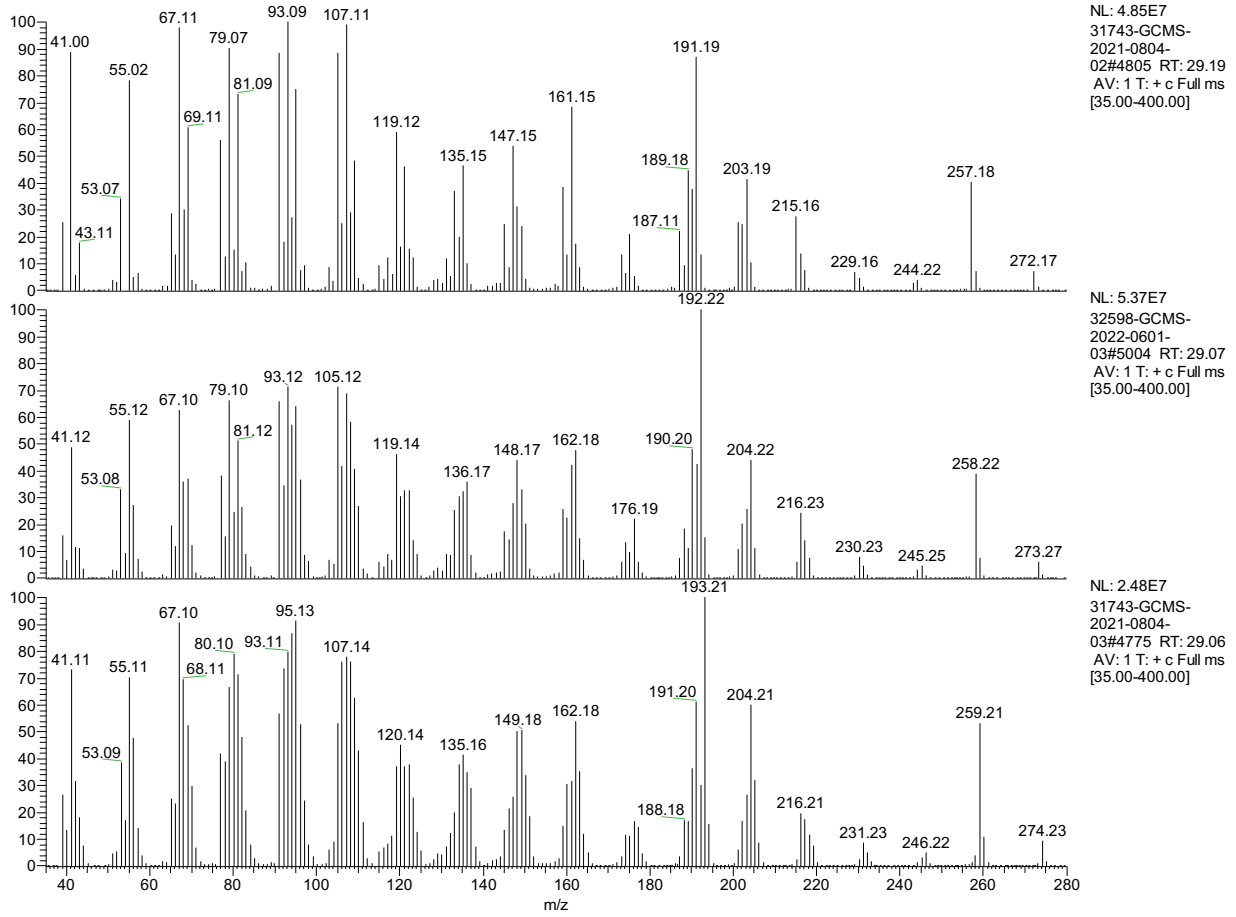

Figure S10. ^{1}H NMR spectrum of albireticulene (**1**) in toluene-d_8 (600 MHz).

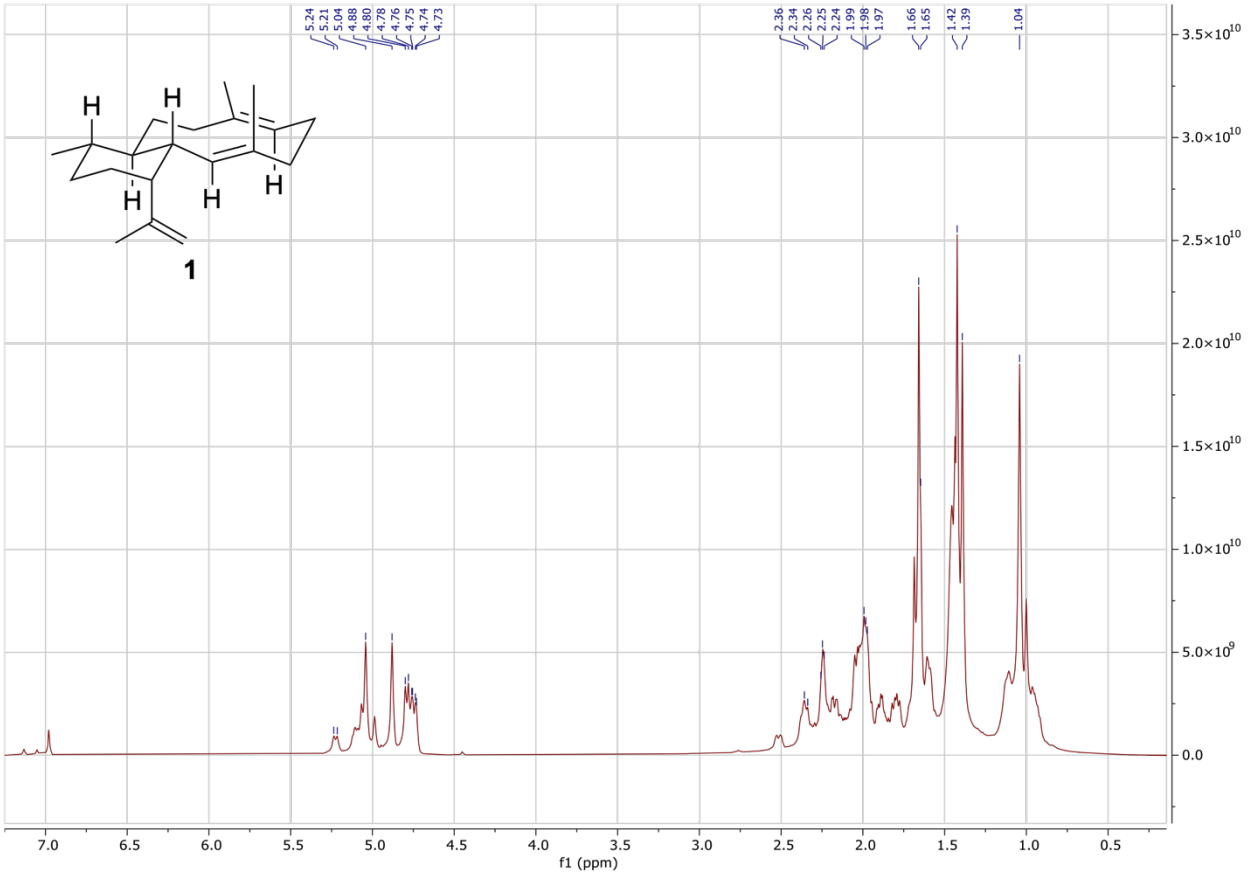

Figure S11. ^{13}C NMR spectrum of albireticulene (**1**) in toluene-d_8 (151 MHz).

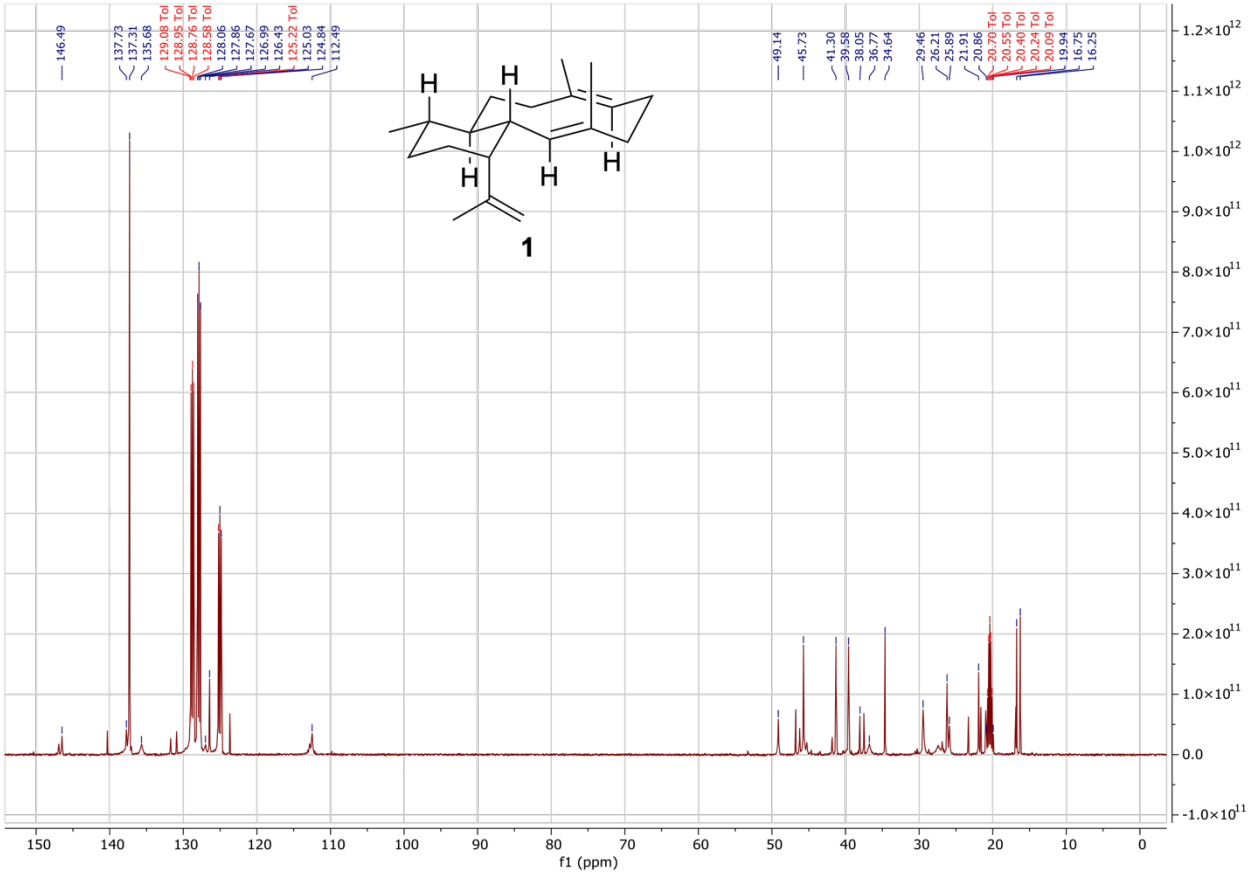

Figure S12. HSQC spectrum of albireticulene (**1**) in toluene-d_8. Blue cross peaks represent –CH or –CH_3; orange represent –CH_2.

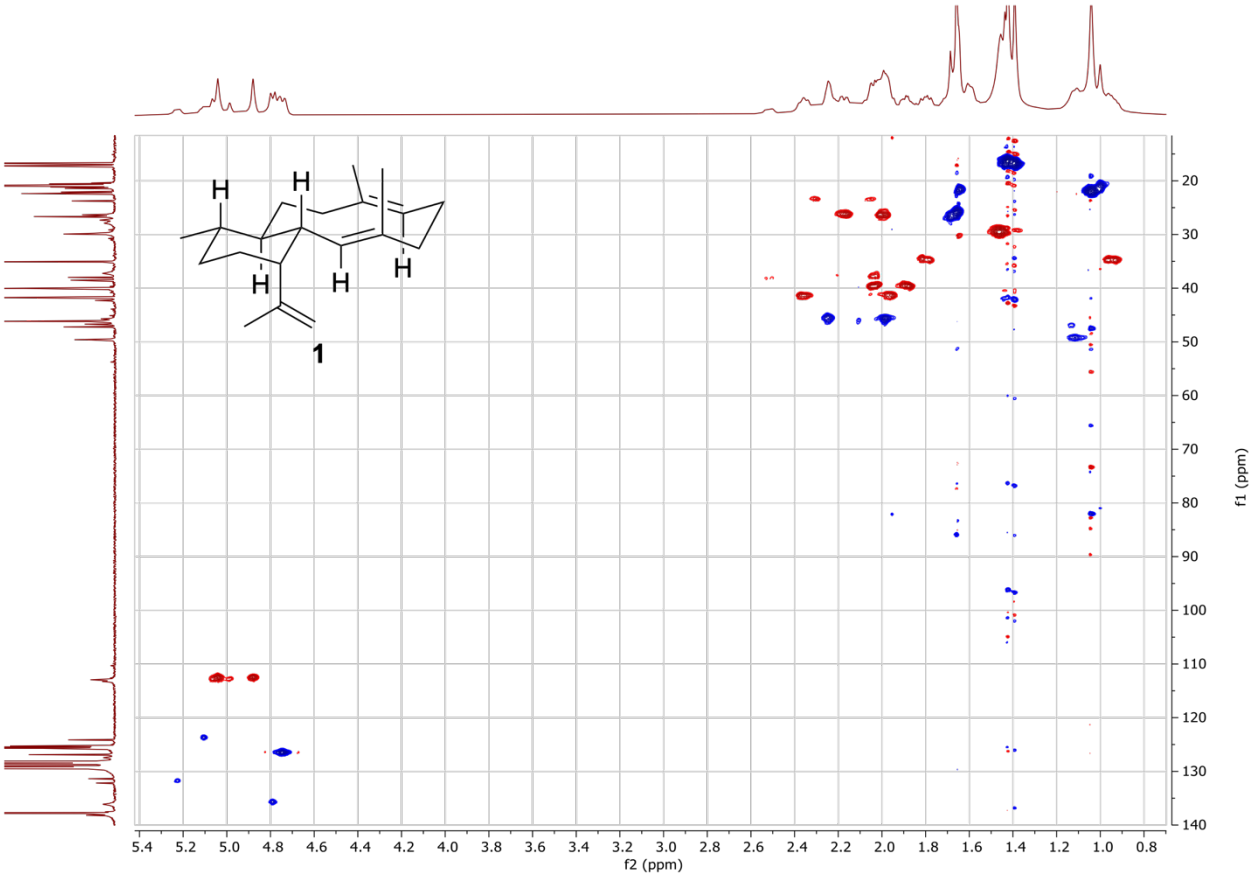

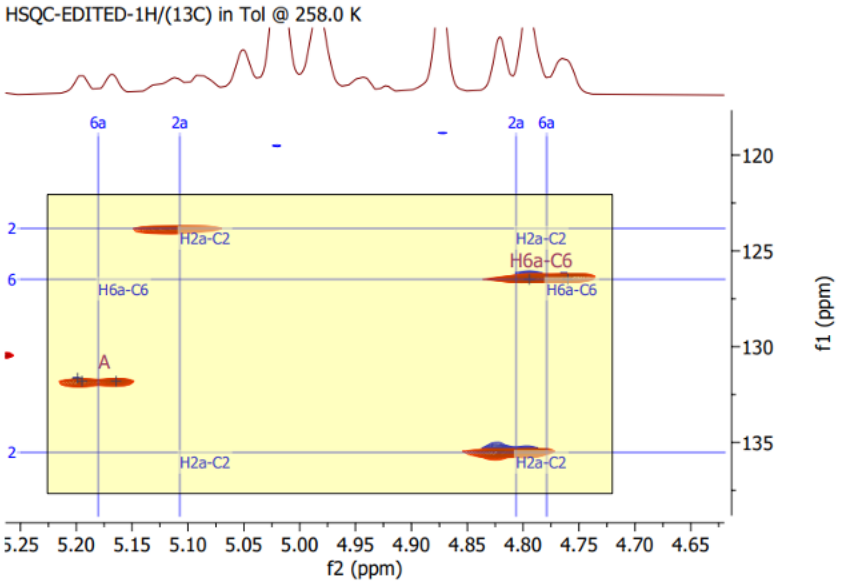

Figure S13. HMBC spectrum of albireticulene (**1**) in toluene-d_8 (600 MHz).

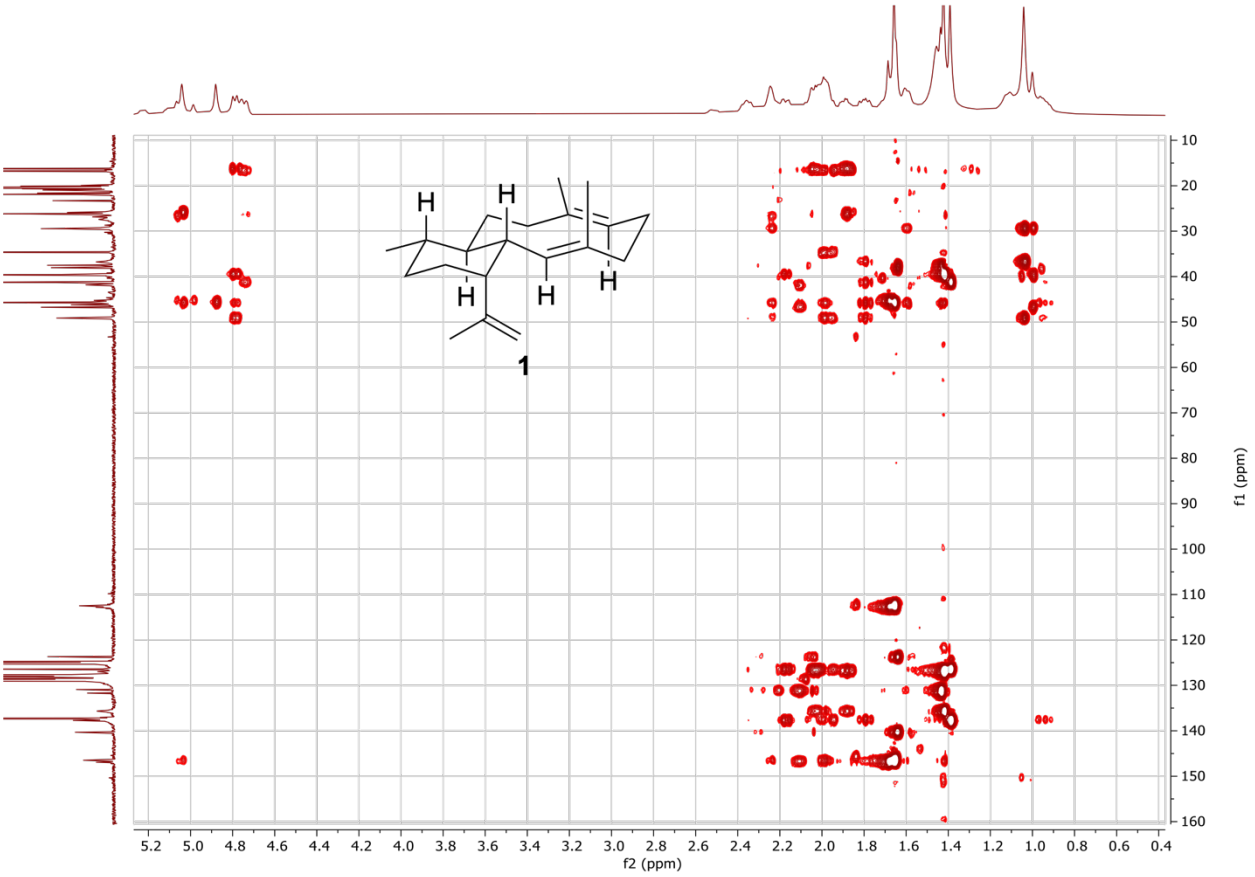

Figure S14. COSY spectrum of albireticulene (**1**) in toluene-d_8 (600 MHz).

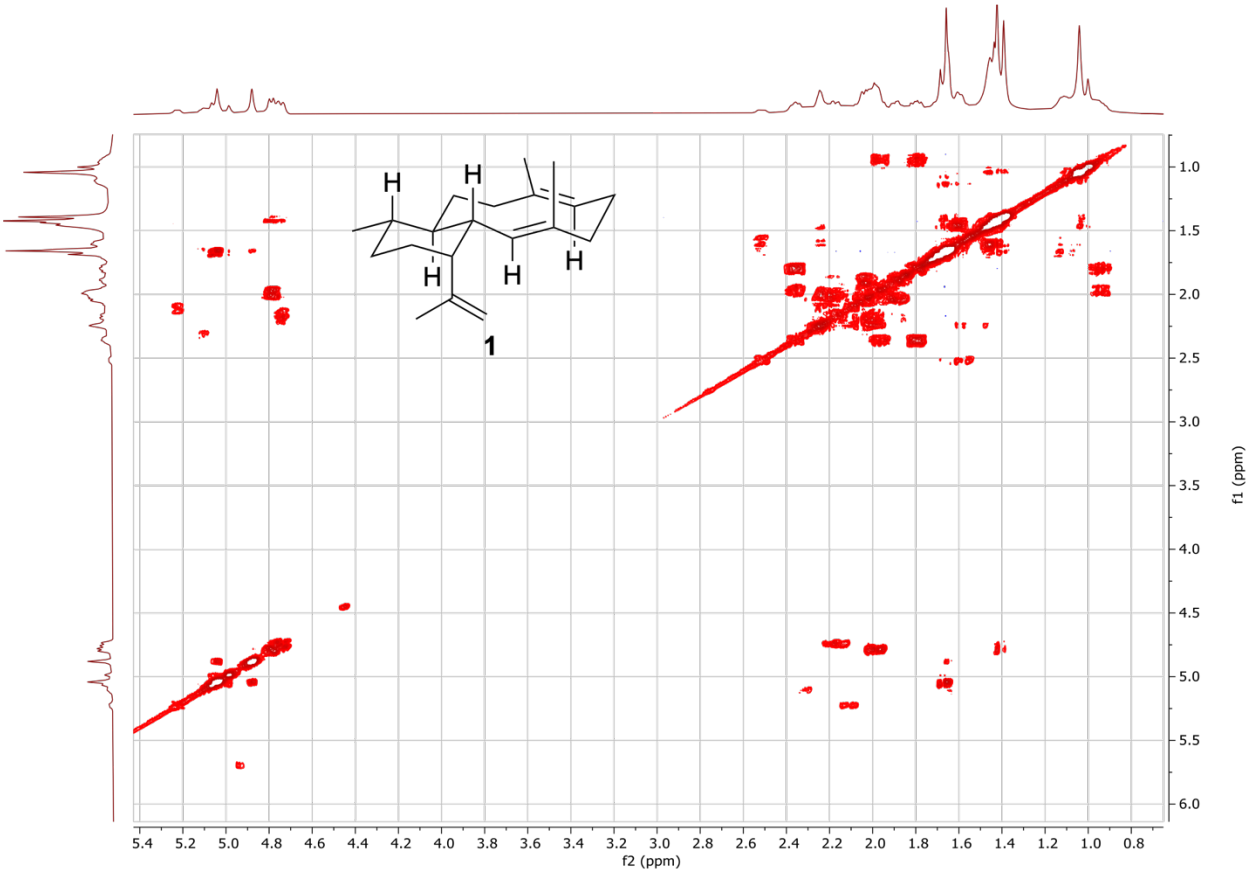

Figure S15. TOCSY spectrum of albireticulene (**1**) in toluene-d_8.

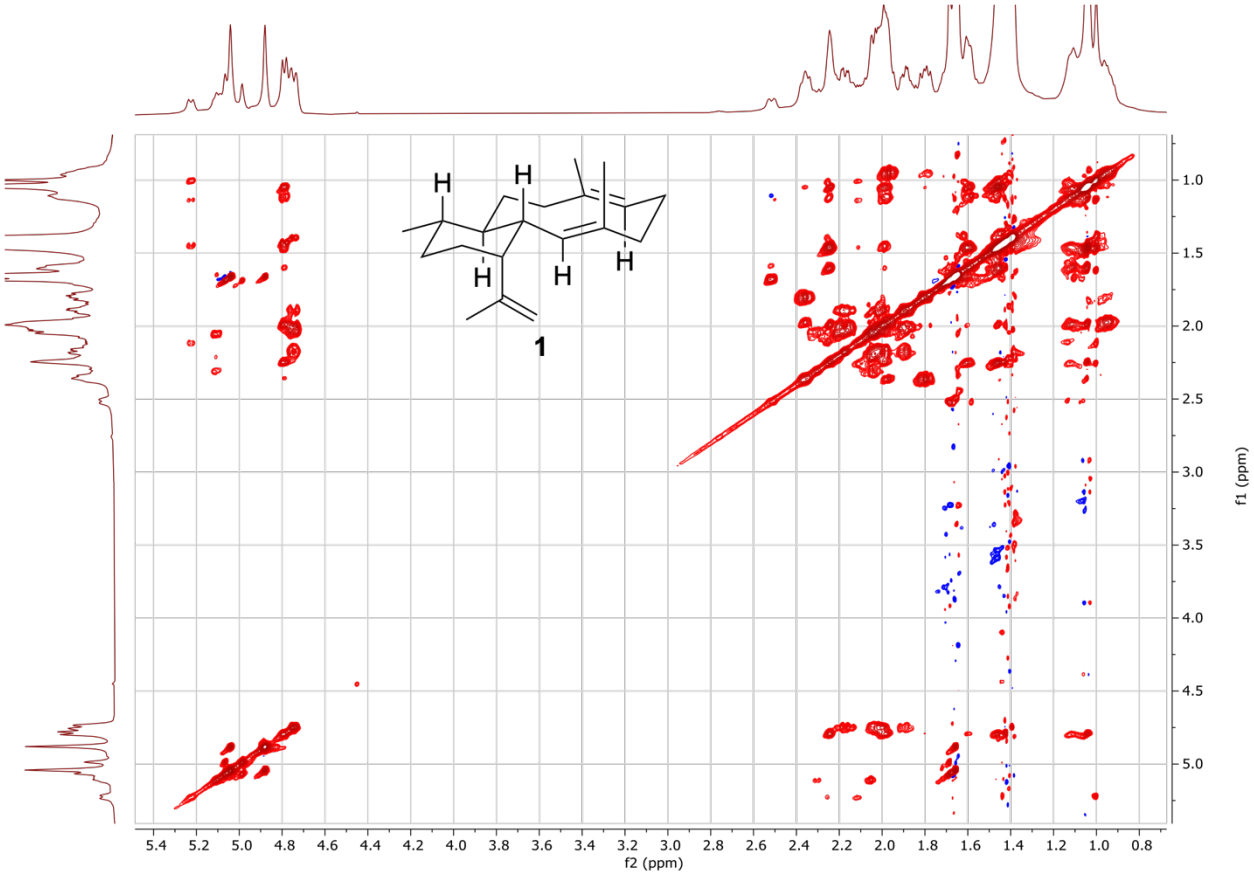

Figure S16. IPAP-HMBC NMR spectra of albireticulene (**1**) in toluene-d_8. 1D traces of $^{3}J_{(H\text{-}2,C\text{-}20)}$ (top) and $^{3}J_{(H\text{-}6,C\text{-}19)}$ (bottom) coupling constants supporting the C-2/C-3 and C-6/C-7 alkenes are *E* configurations.

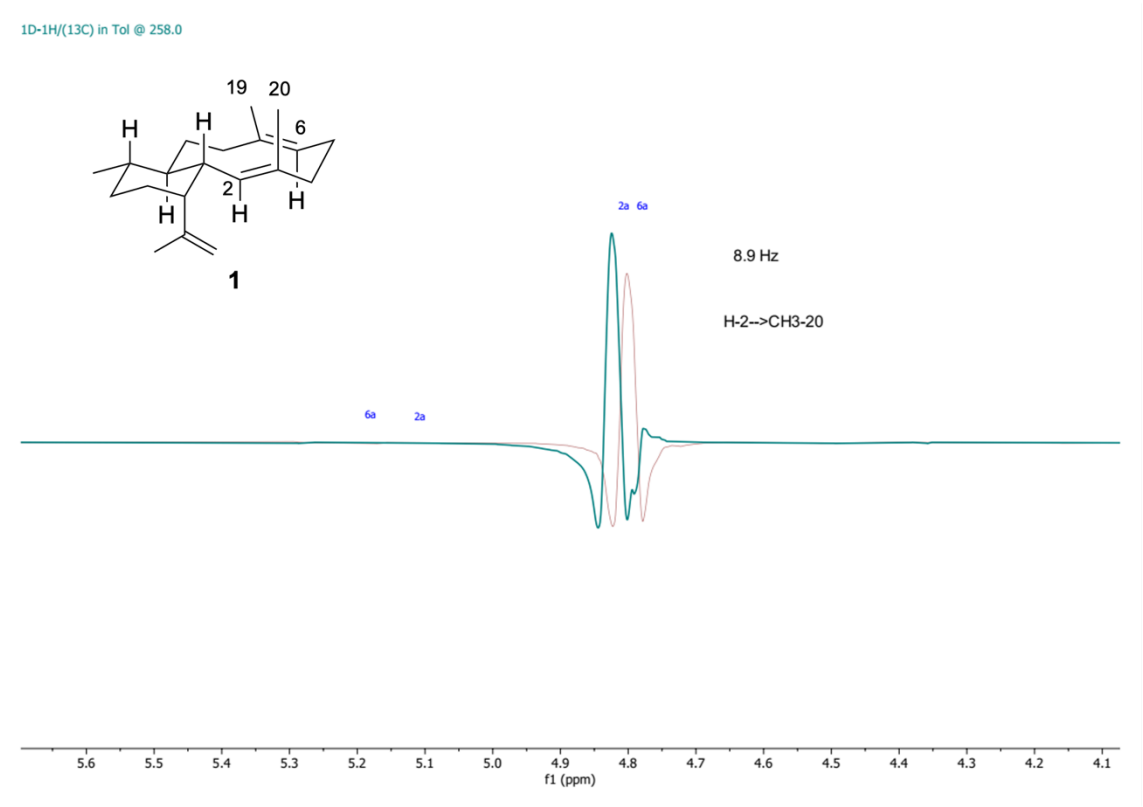

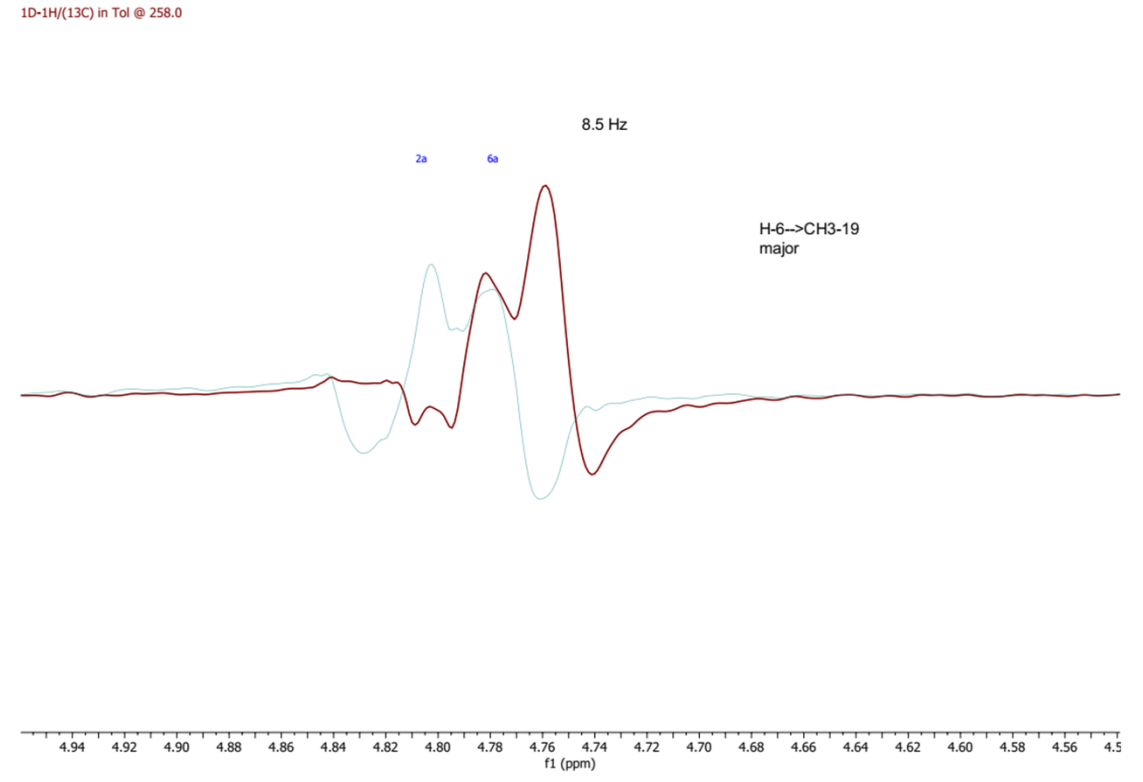

Figure S17. IPAP-HMBC NMR spectra of the minor conformer of albireticulene (**1**) in toluene-d_8. 1D trace of $^{3}J_{(H\text{-}6,C\text{-}19)}$ coupling constant support the C-6/C-7 alkene is *E* configuration.

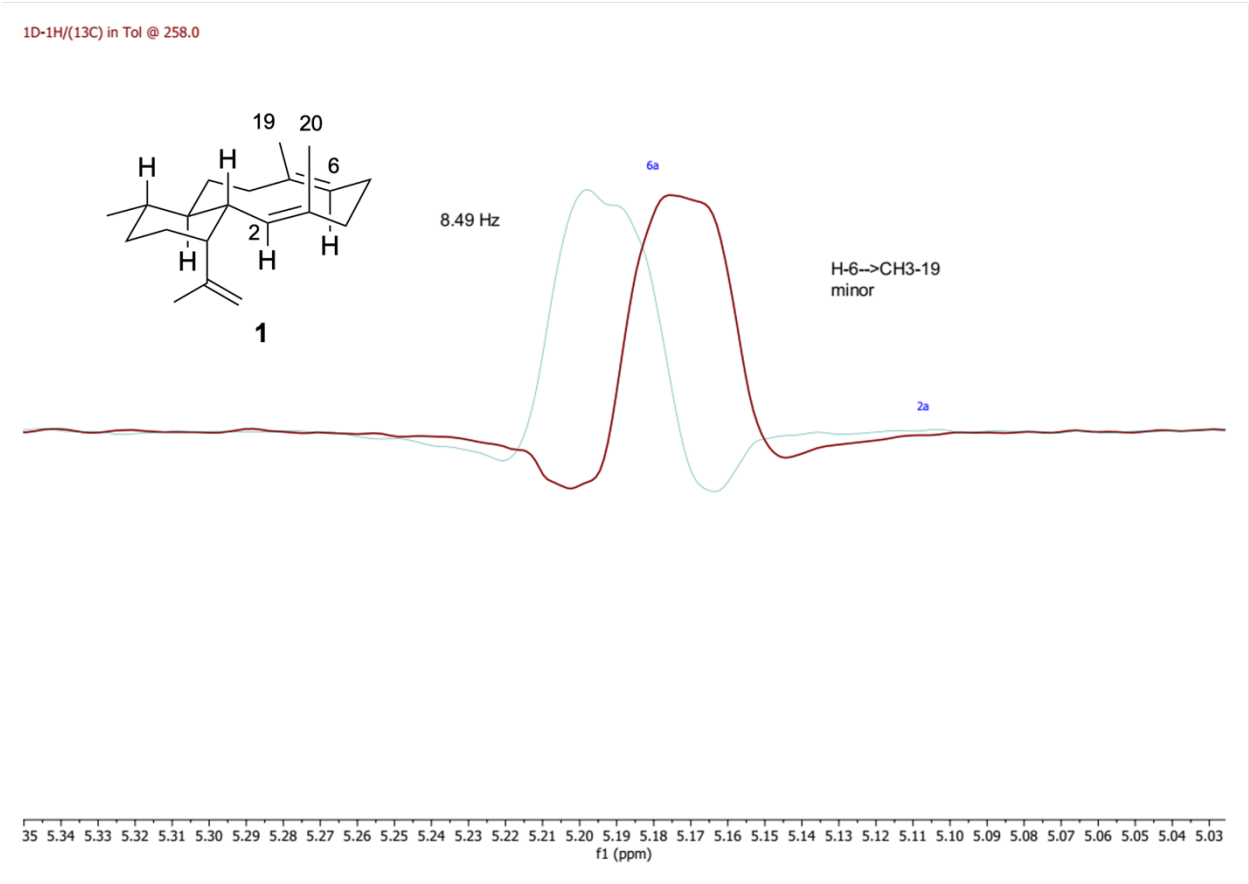

Figure S18. ^{1}H NMR spectrum of albireticulene (**1**) in benzene-d_6 (600 MHz).

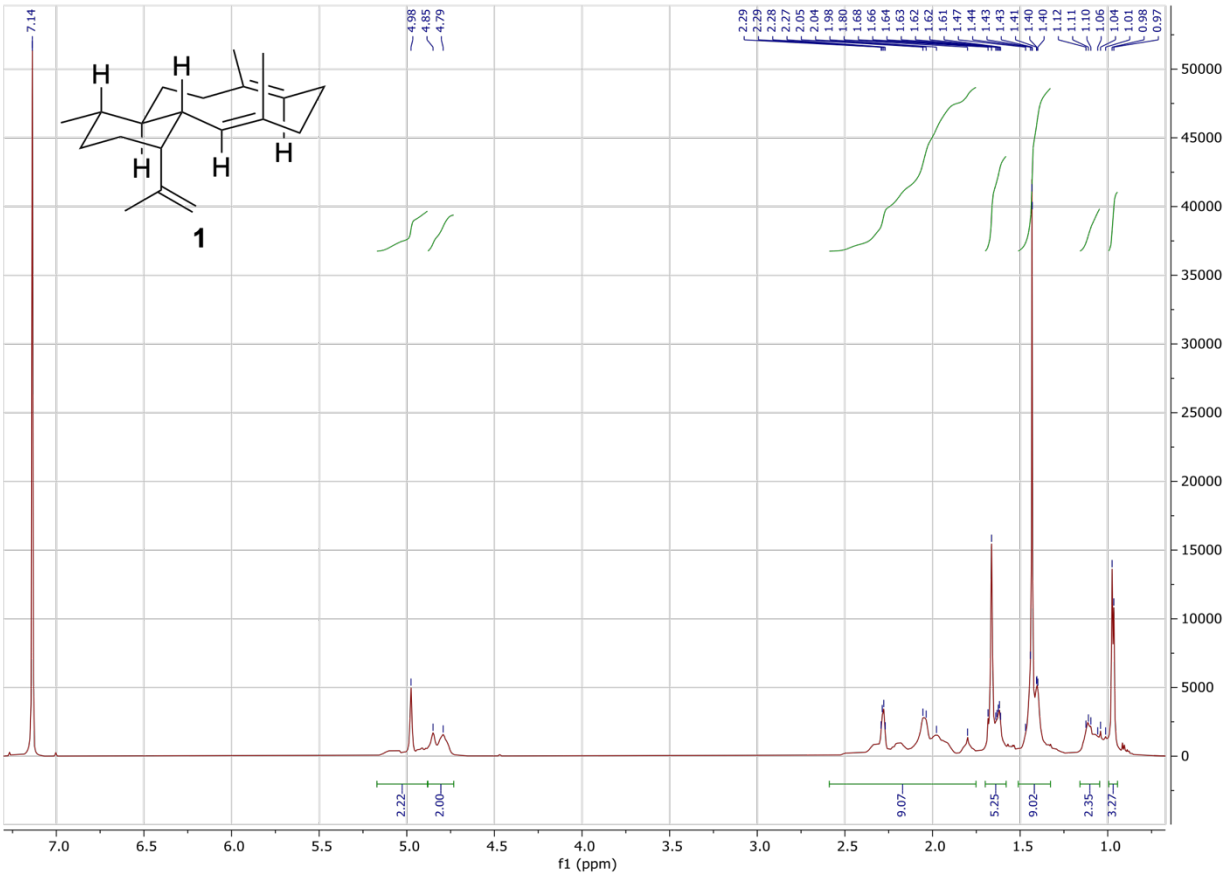

Figure S19. ^{13}C NMR spectrum of albireticulene (**1**) in benzene-d_6 (151 MHz).

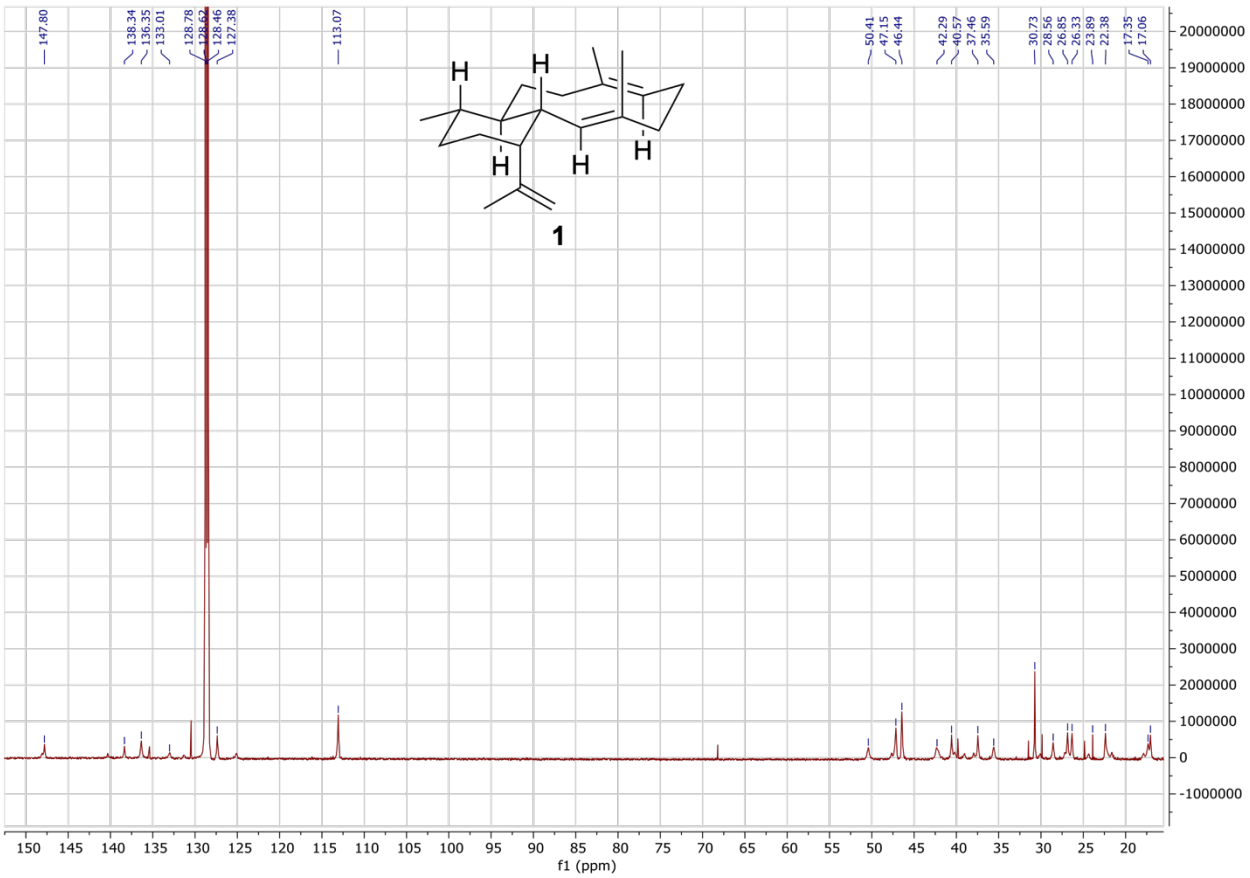

Figure S20. HSQC spectrum of albireticulene (**1**) in benzene-d_6. Blue cross peaks represent –CH or –CH_3; orange represent –CH_2.

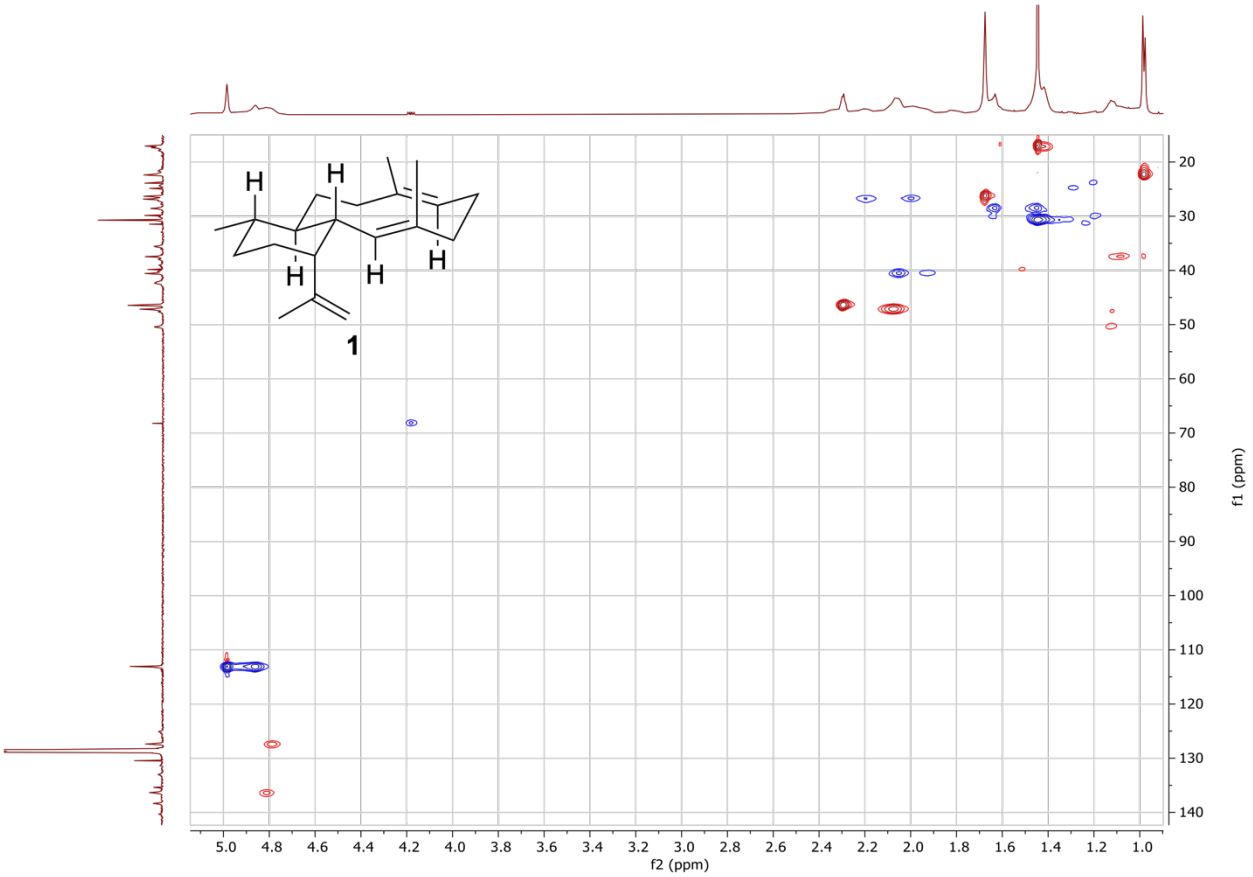

Figure S21. HMBC spectrum of albireticulene (**1**) in benzene-d_6 (600 MHz).

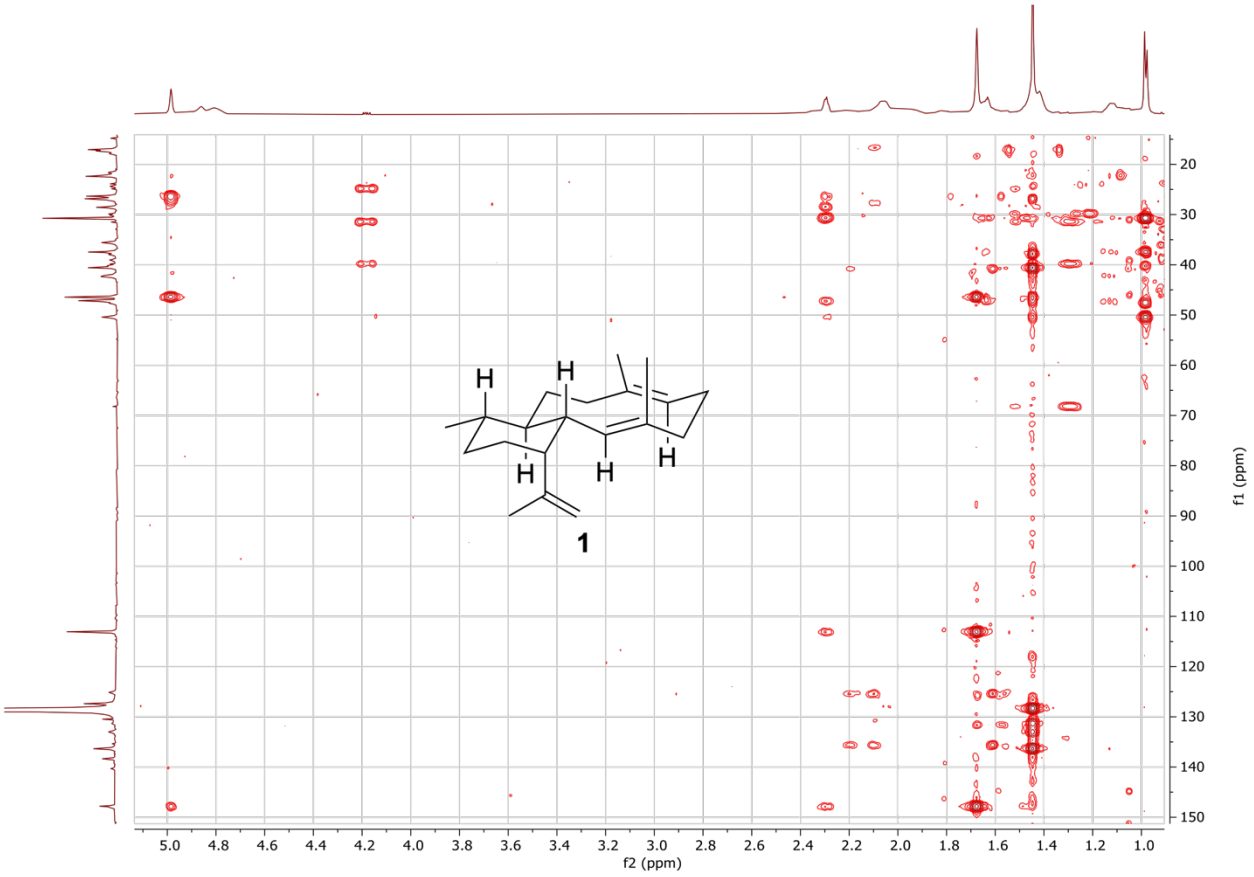

Figure S22. COSY spectrum of albireticulene (**1**) in benzene-d_6 (600 MHz).

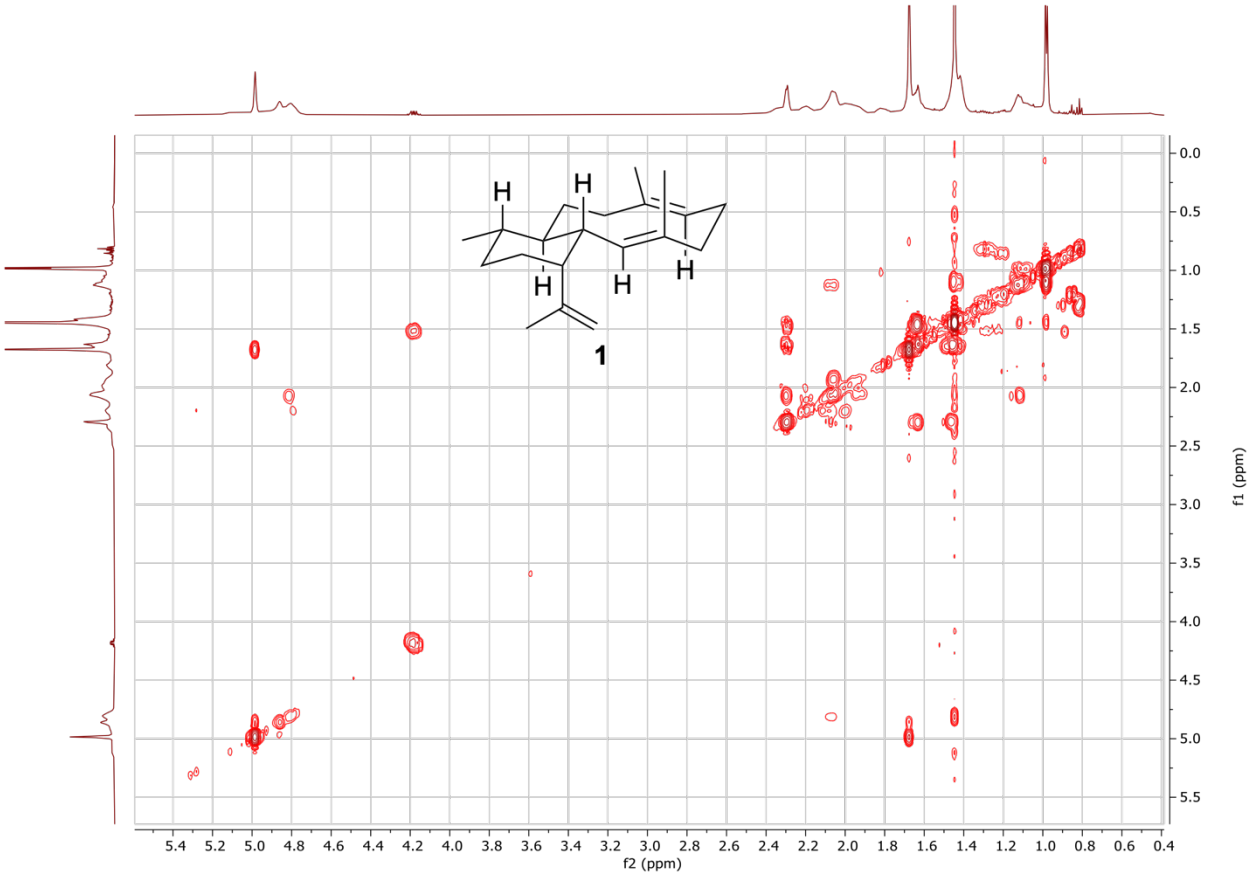

Figure S23. HPLC-UV analysis of the conversion of **1** into **8** and **9**. Related to Fig. 3D.

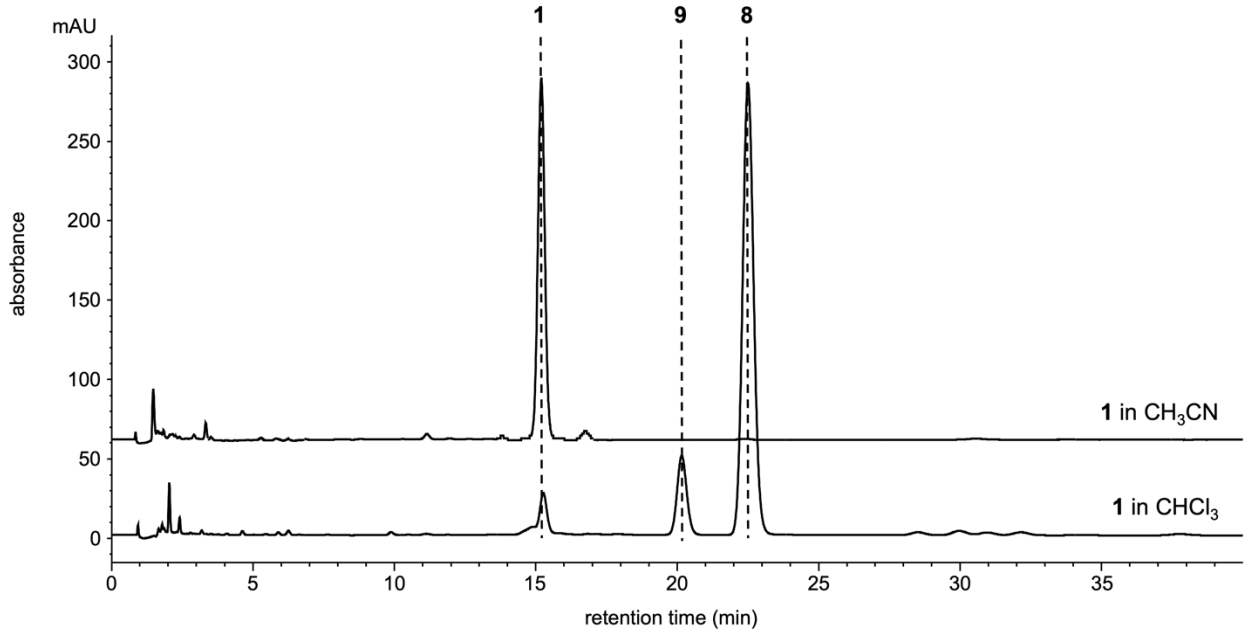

Figure S24. ^{1}H NMR spectrum of gersemiene A (**8**) in chloroform-*d* (600 MHz).

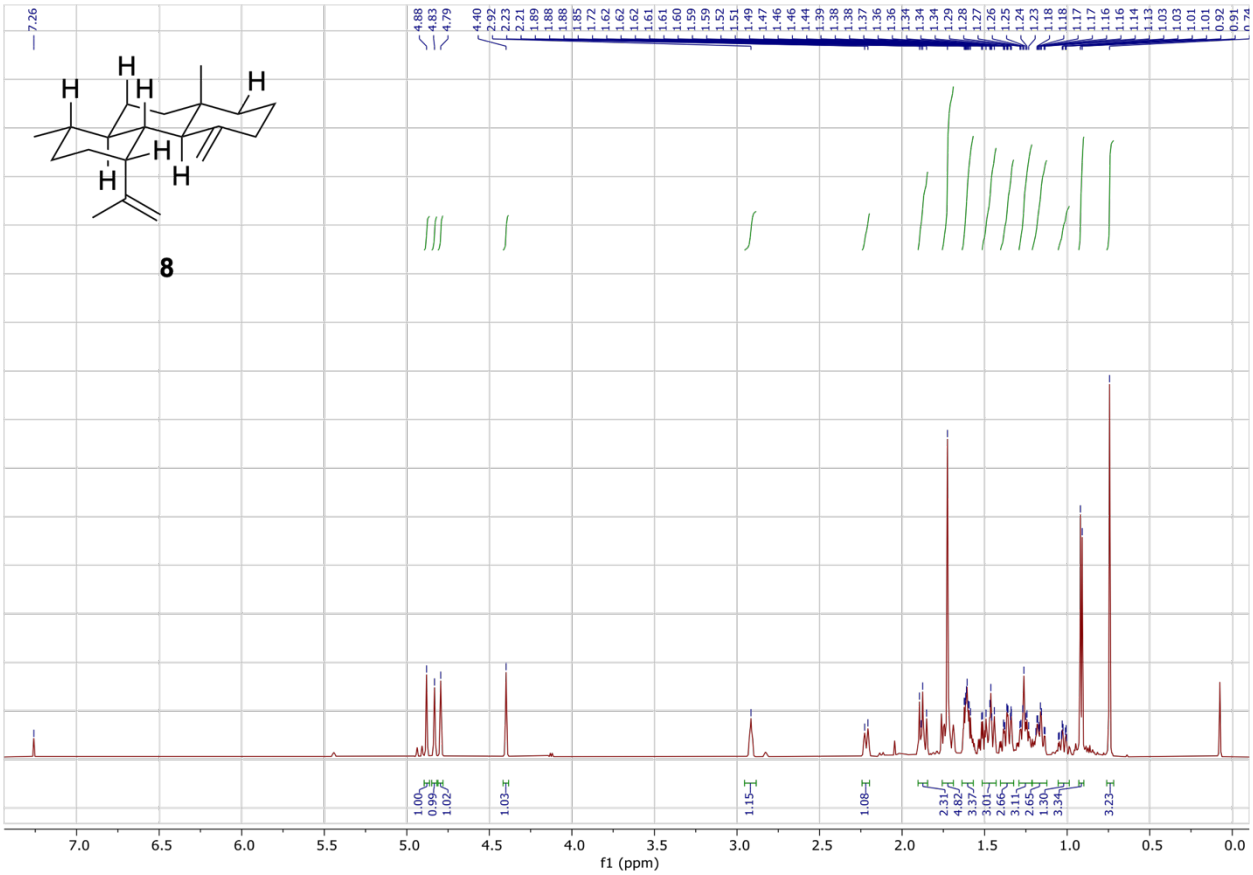

Figure S25. ^{13}C NMR spectrum of gersemiene A (**8**) in chloroform-*d* (151 MHz).

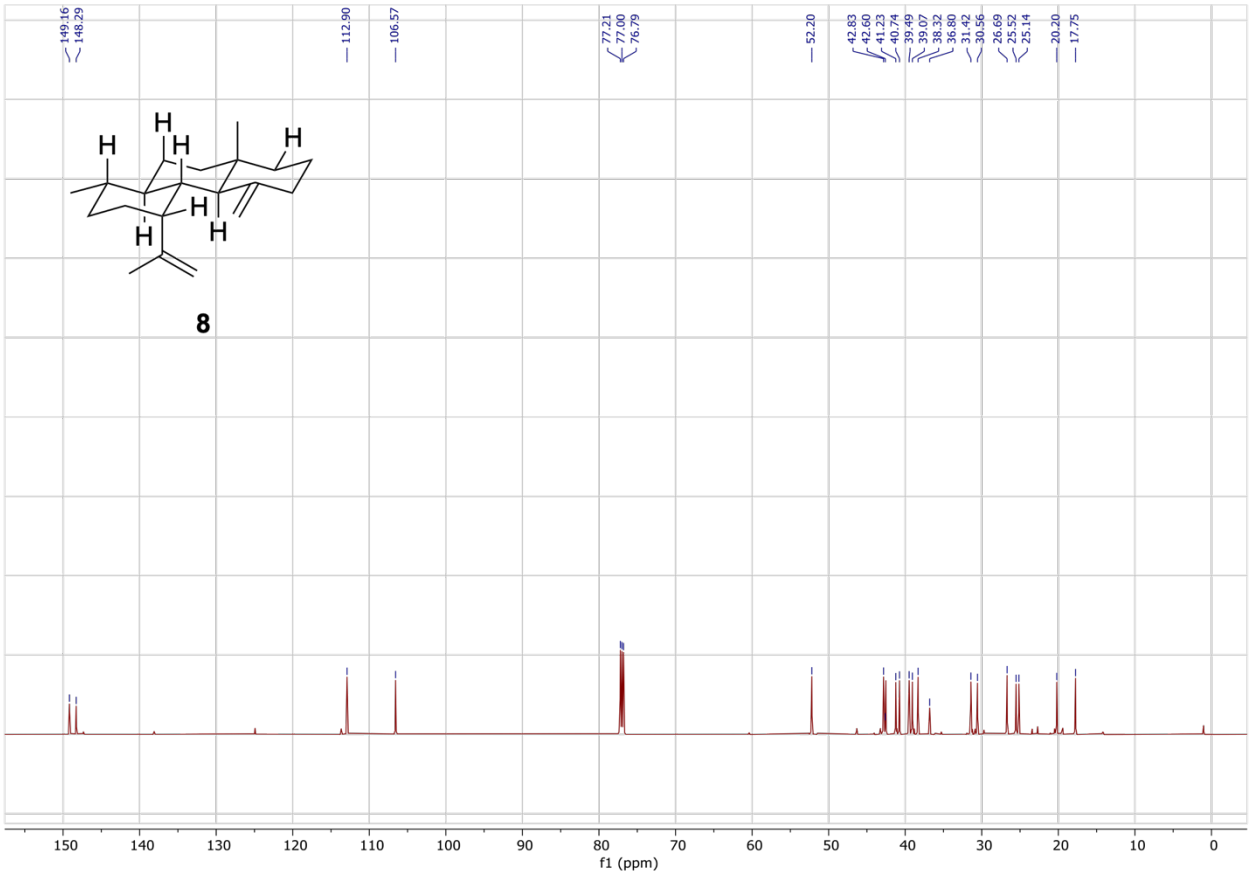

Figure S26. HSQC spectrum of gersemiene A (**8**) in chloroform-*d*. Blue cross peaks represent –CH or –CH_3; orange represent –CH_2.

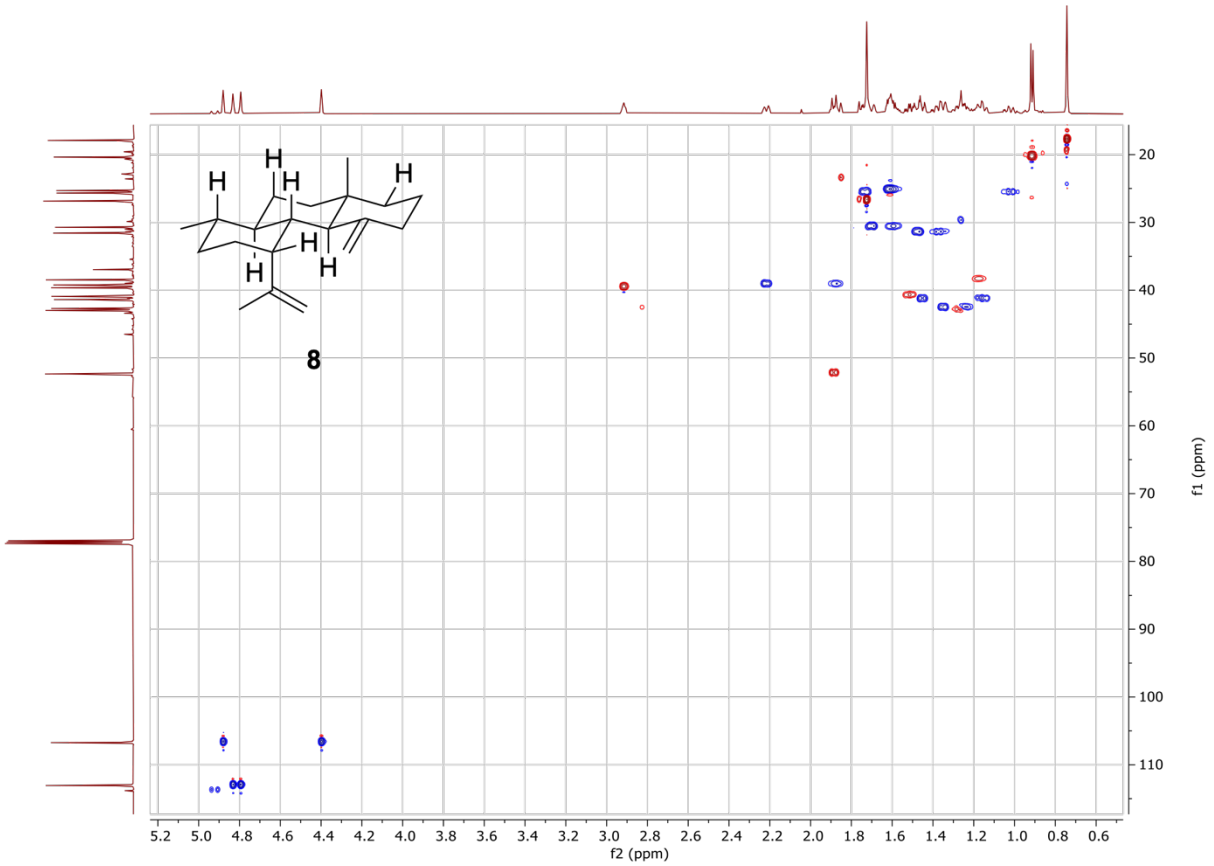

Figure S27. HMBC spectrum of gersemiene A (**8**) in chloroform-*d* (600 MHz).

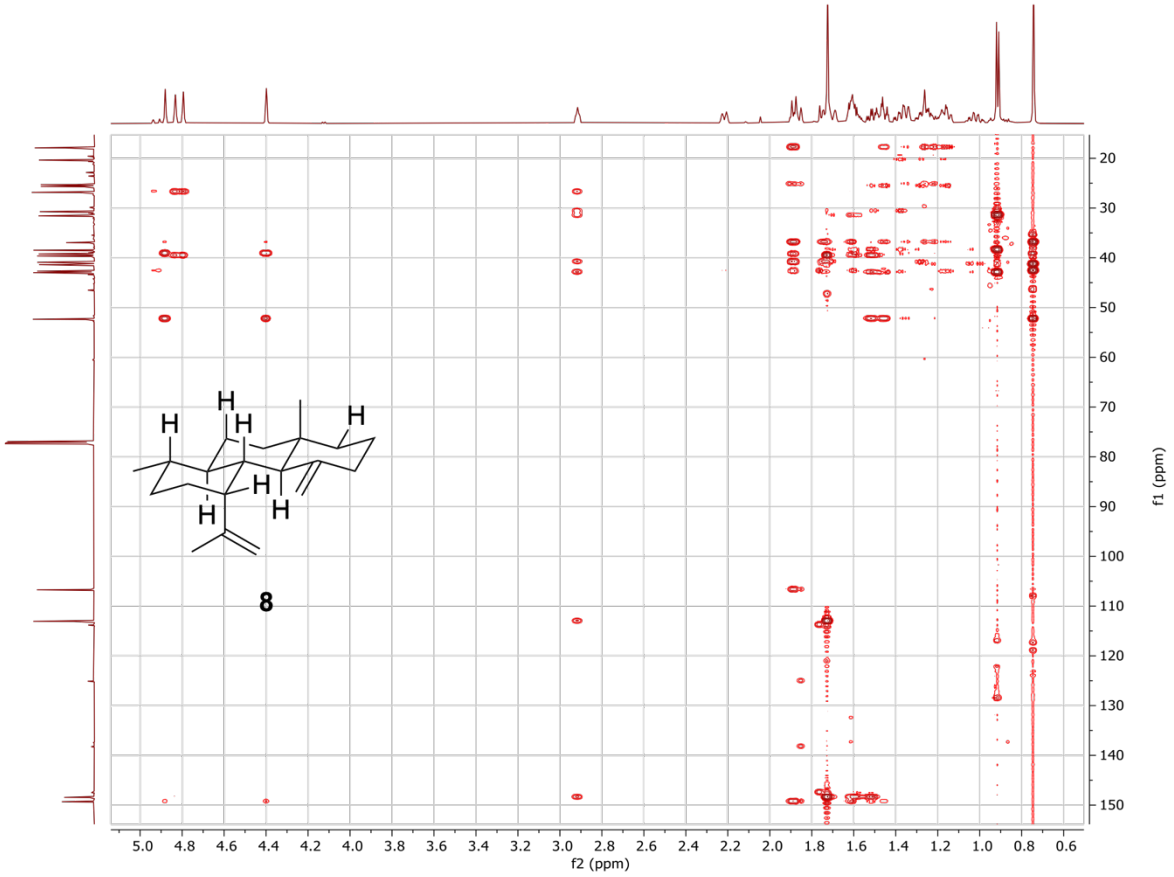

Figure S28. COSY spectrum of gersemiene A (**8**) in chloroform-*d* (600 MHz).

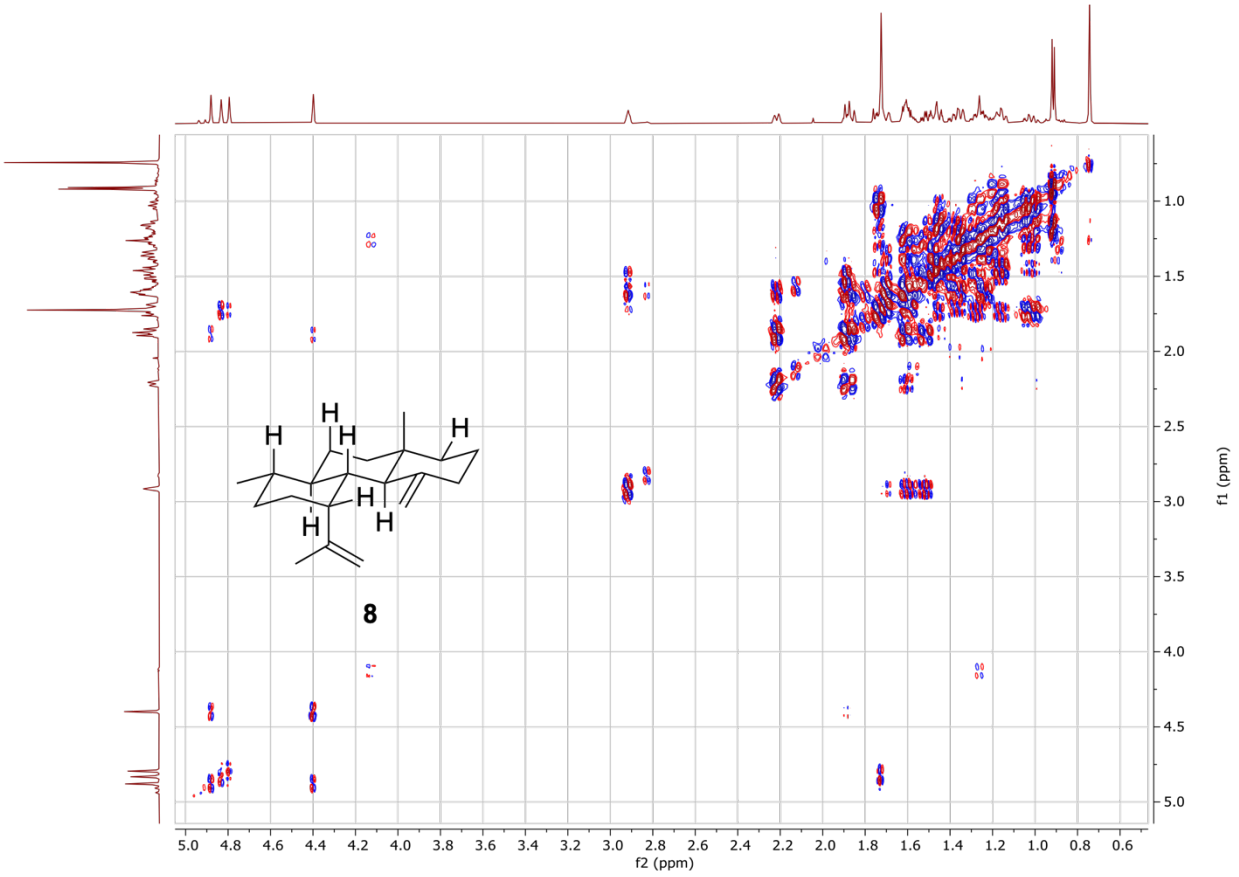

Figure S29. 1D TOCSY spectrum of gersemiene A (**8**) in chloroform-*d* (600 MHz) with selective excitation of H-14; mixing time = 120 ms.

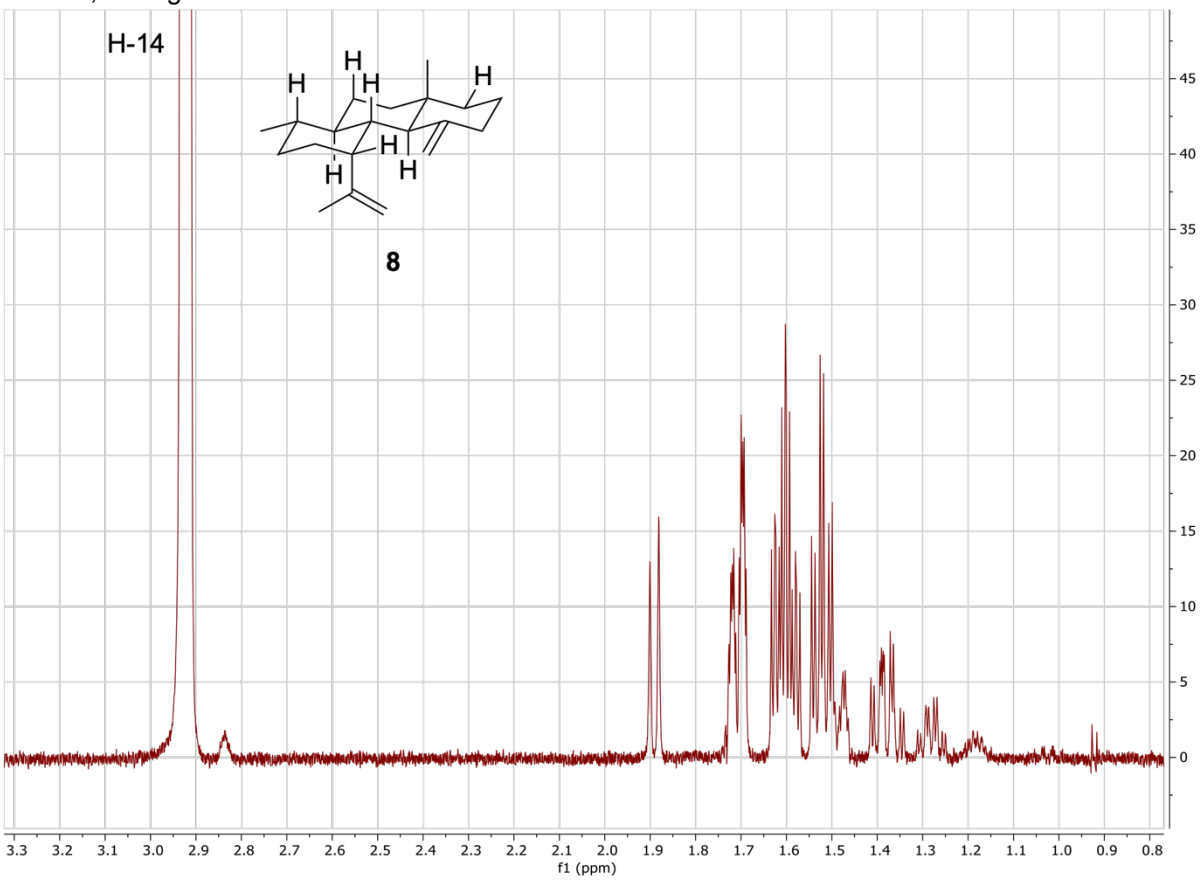

Figure S30. 1D NOESY spectrum of gersemiene A (**8**) in chloroform-*d* (600 MHz) with selective excitation of C-19; mixing time = 300 ms.

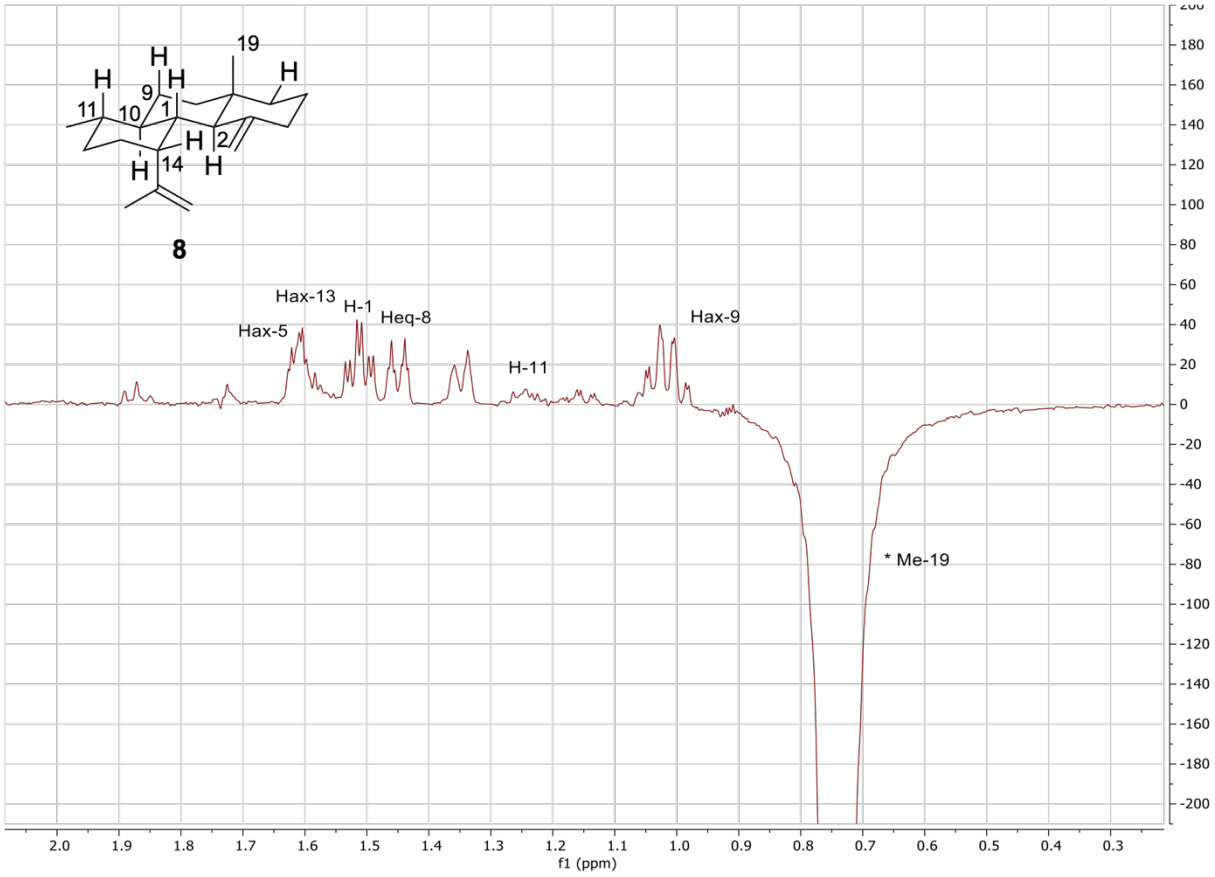

Figure S31. 1D traces of $^{3}J_{(H\text{-}2,C\text{-}19)}$ and $^{3}J_{(H\text{-}14,C\text{-}10)}$ coupling constants from IPAP-HMBC NMR spectrum of gersemiene A (**8**) in chloroform-*d*.

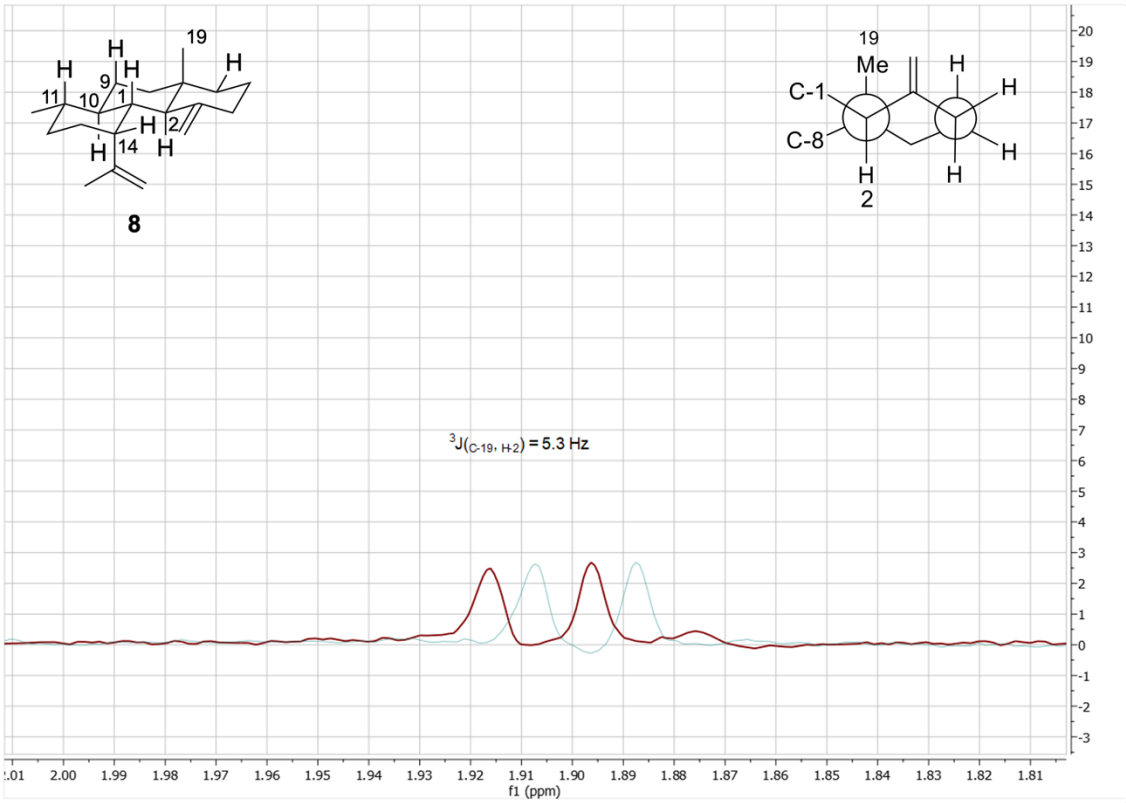

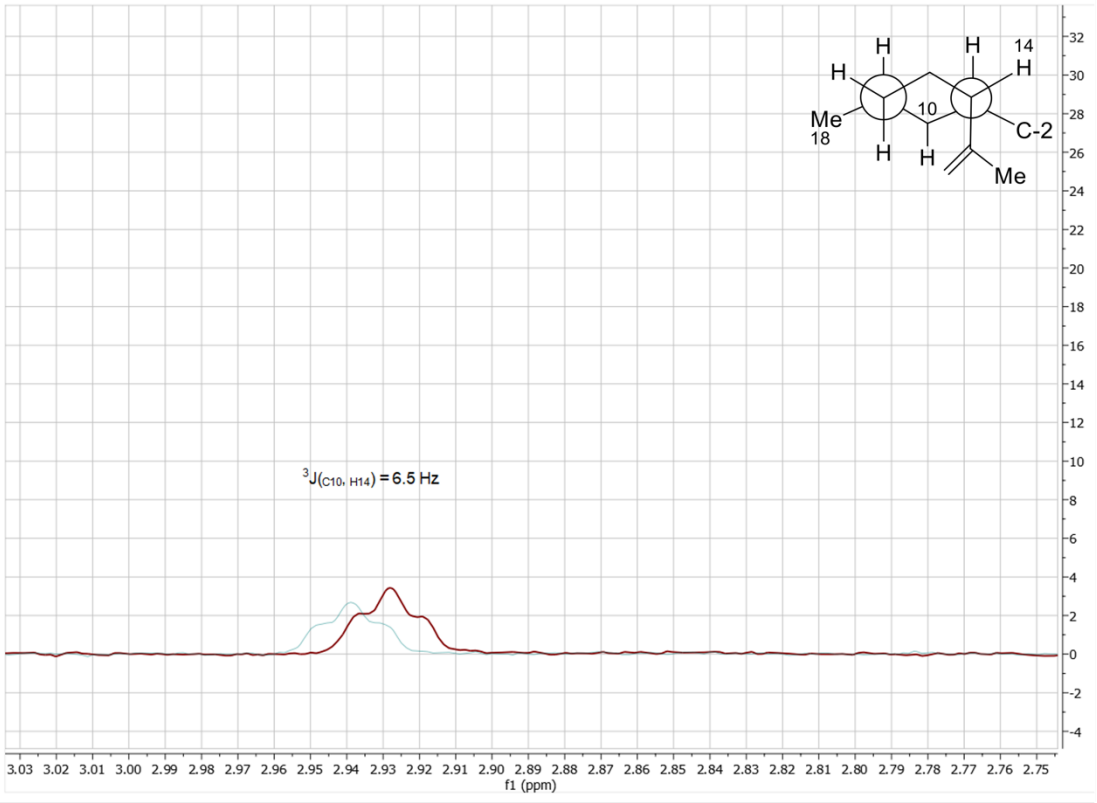

Figure S32. 1D traces of $^{3}J_{(H\text{-}2,C\text{-}10)}$, $^{3}J_{(H\text{-}12eq,C\text{-}10)}$, and $^{3}J_{(H\text{-}8eq,C\text{-}10)}$ coupling constants from IPAP-HMBC NMR spectrum of gersemiene A (**8**) in chloroform-*d*.

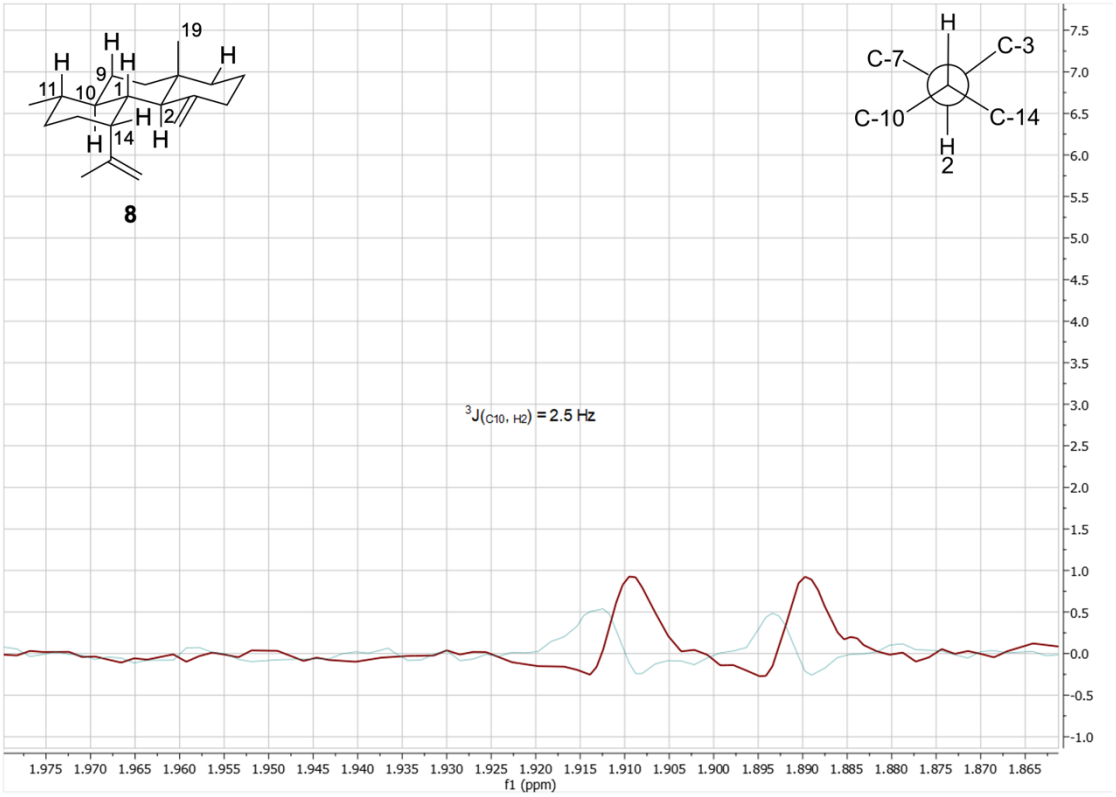

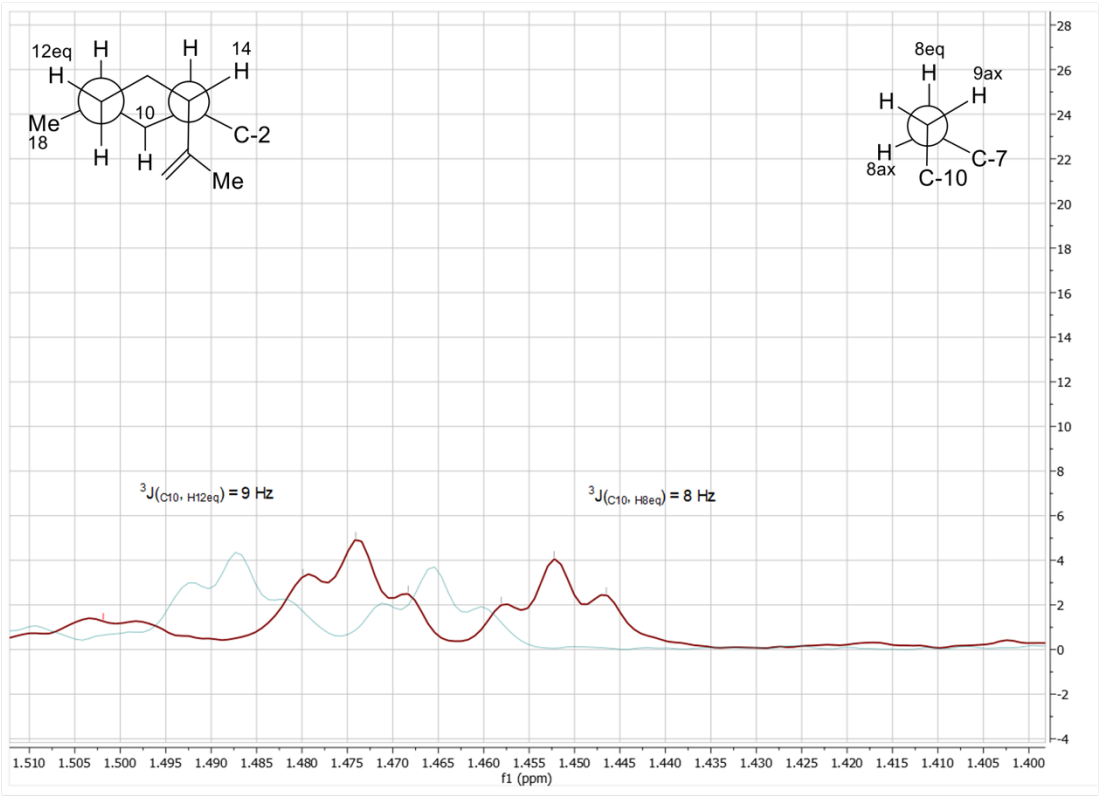

Figure S33. 1D traces of $^{3}J_{(H\text{-}14,C\text{-}12)}$ and $^{3}J_{(H\text{-}10,C\text{-}12)}$ coupling constants from IPAP-HMBC NMR spectrum of gersemiene A (**8**) in chloroform-*d*.

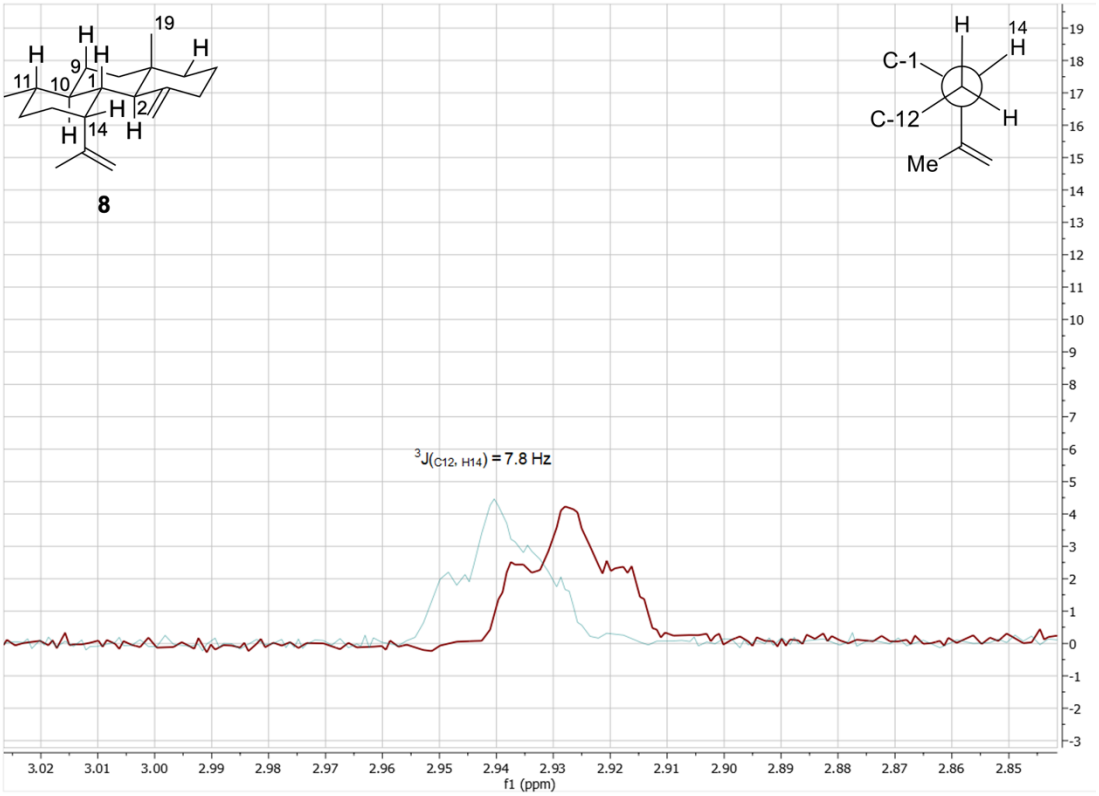

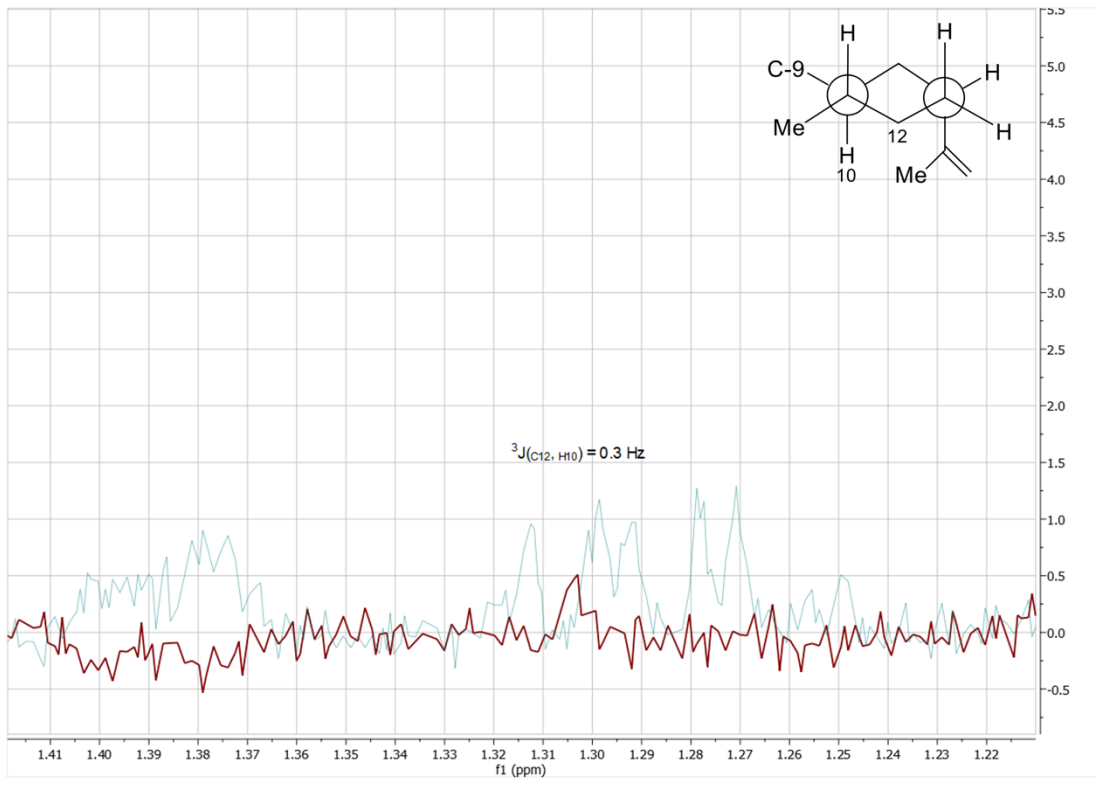

Figure S34. ^{1}H NMR spectrum of gersemiene B (**9**) in chloroform-*d* (600 MHz).

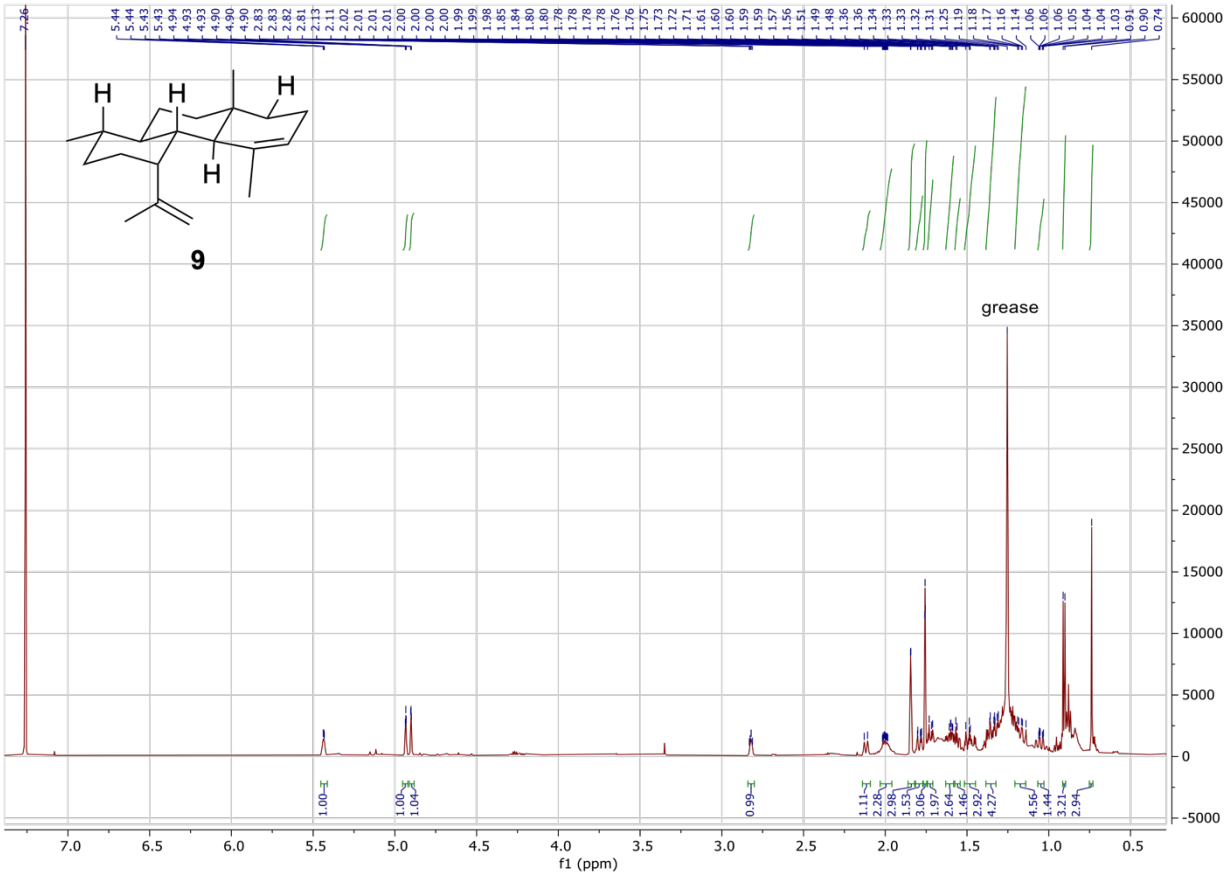

Figure S35. ^{13}C NMR spectrum of gersemiene B (**9**) in chloroform-*d* (151 MHz).

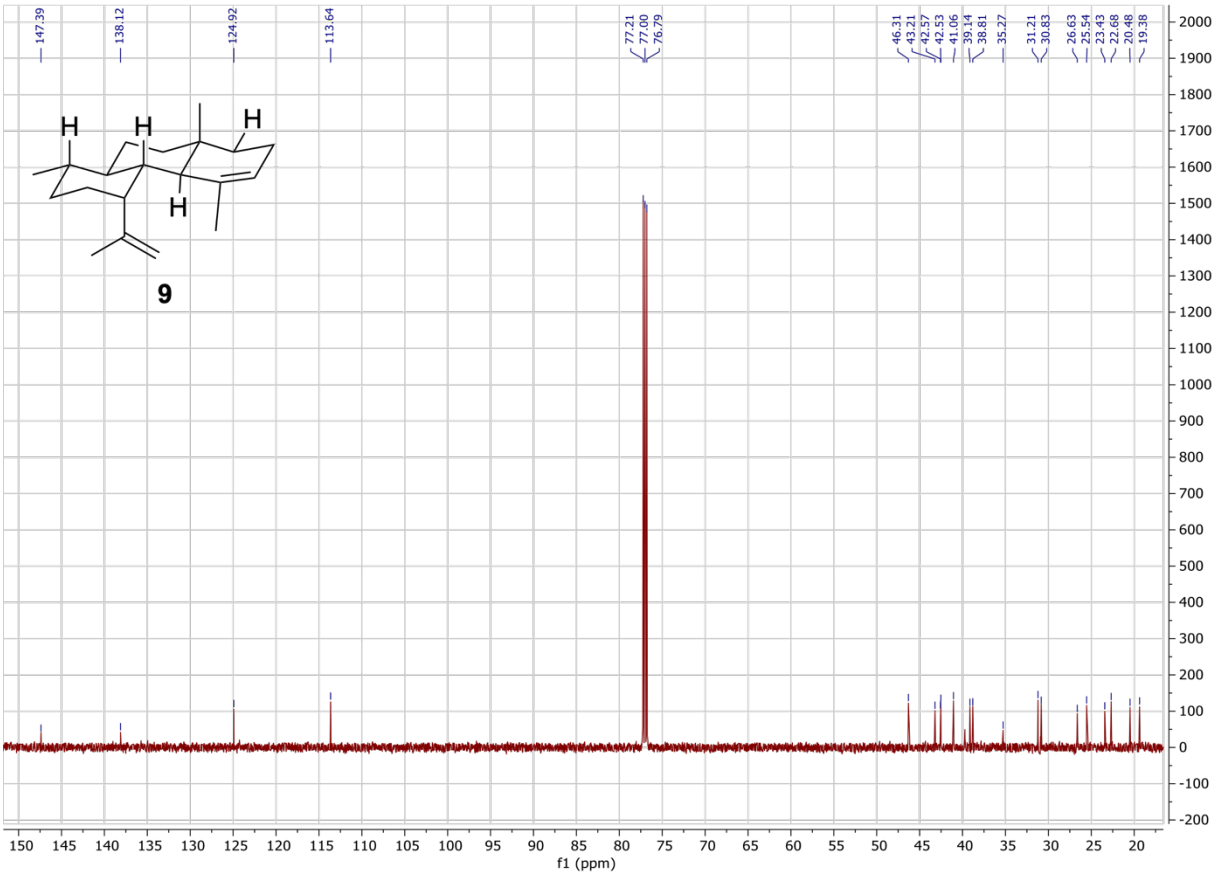

Figure S36. HSQC spectrum of gersemiene B (**9**) in chloroform-*d*. Blue cross peaks represent –CH or –CH_3; orange represent –CH_2.

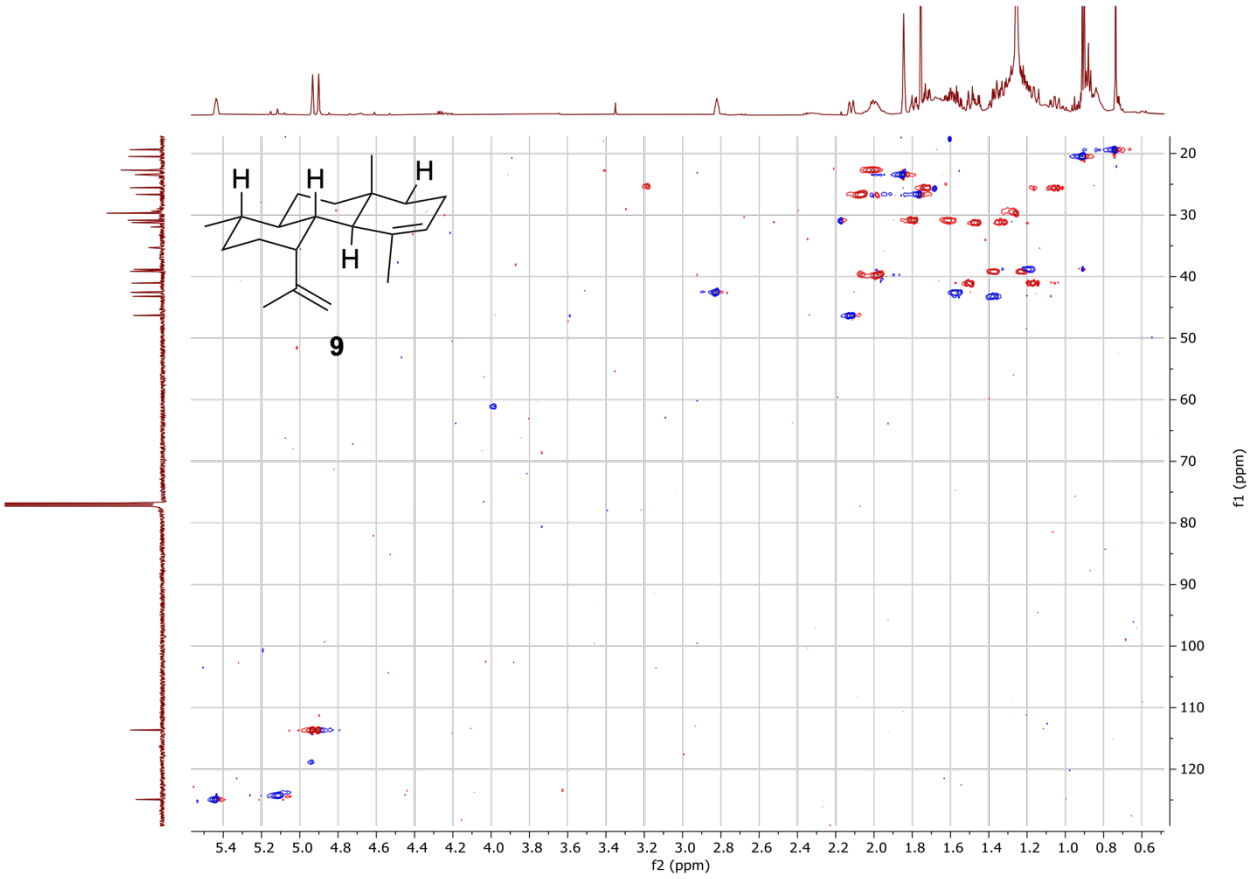

Figure S37. HMBC spectrum of gersemiene B (**9**) in chloroform-*d* (600 MHz).

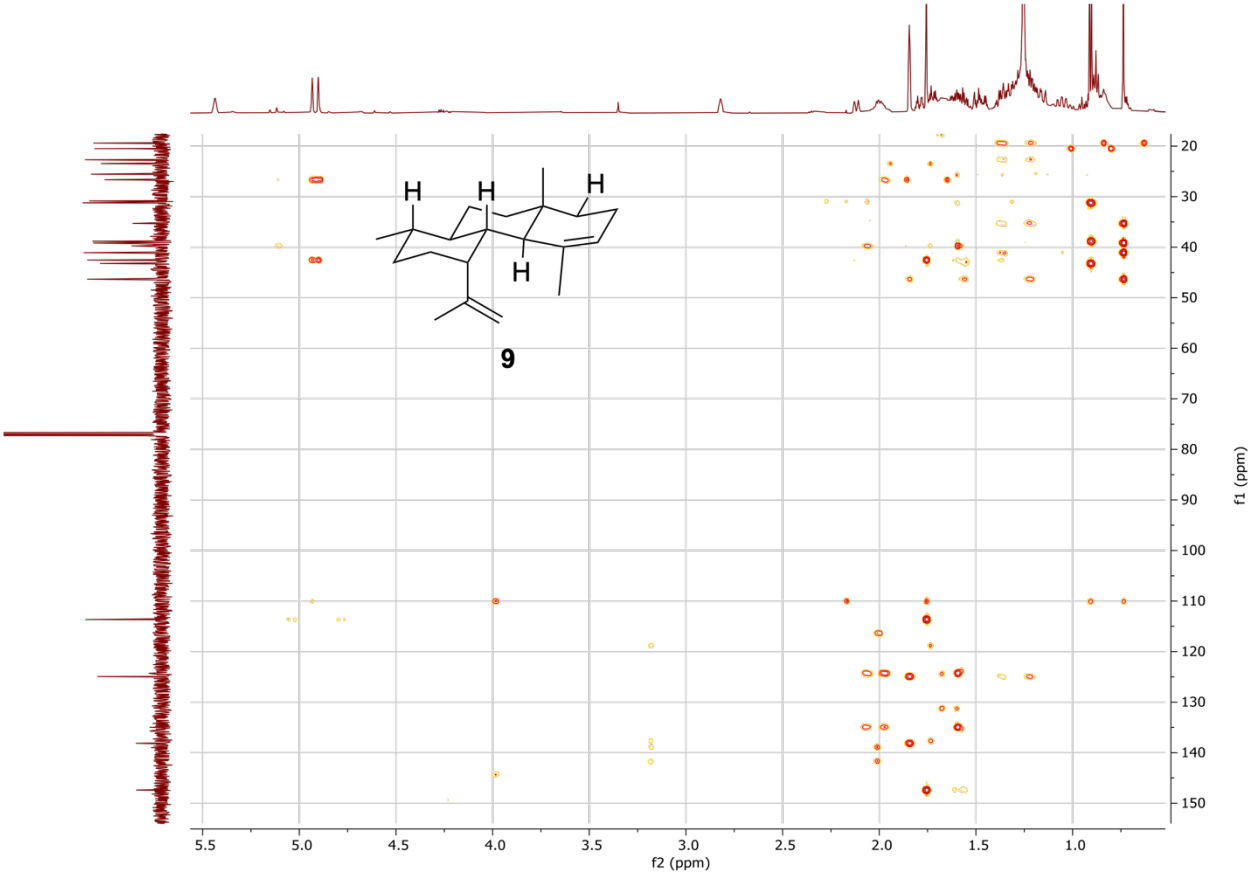

Figure S38. COSY spectrum of gersemiene B (**9**) in chloroform-*d* (600 MHz).

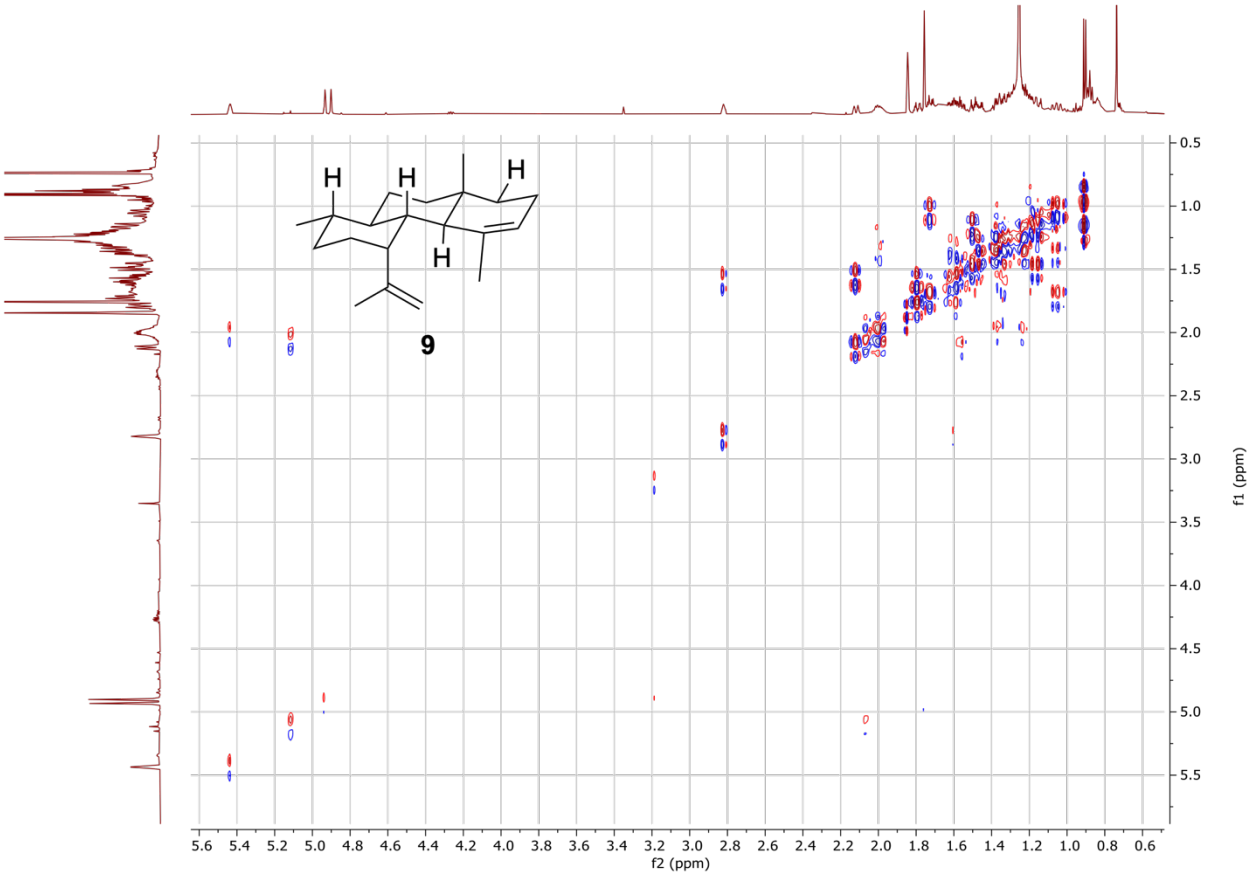

Figure S39. 1D TOCSY spectrum of gersemiene B (**9**) in chloroform-*d* (600 MHz) with selective excitation of H-1 (top; mixing time = 120 ms), H-14 (middle; mixing time = 120 ms), and H-2 (bottom; mixing time = 140 ms).

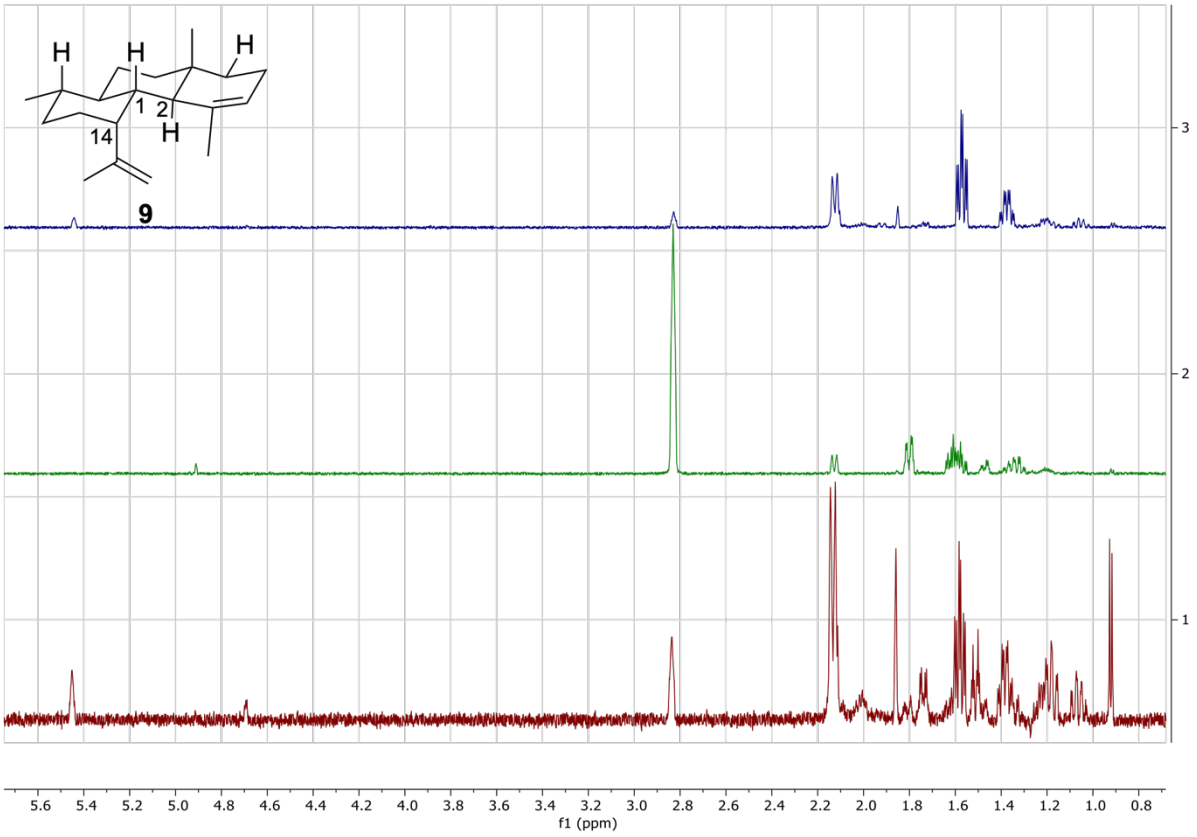

Figure S40. 1D NOESY spectrum of gersemiene B (**9**) in chloroform-*d* (600 MHz) with selective excitation of C-19; mixing time = 300 ms.

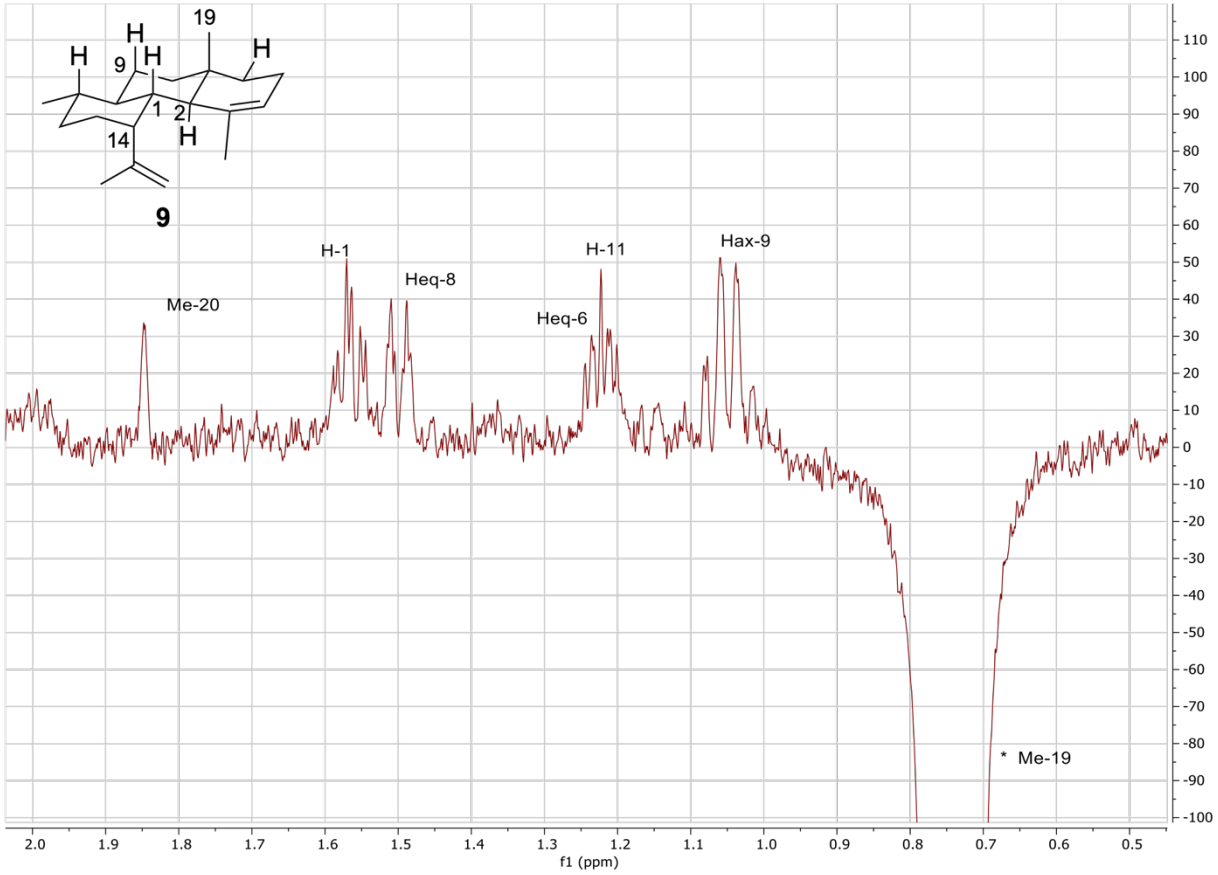

Figure S41. EIMS of gersemiene A (**8**).

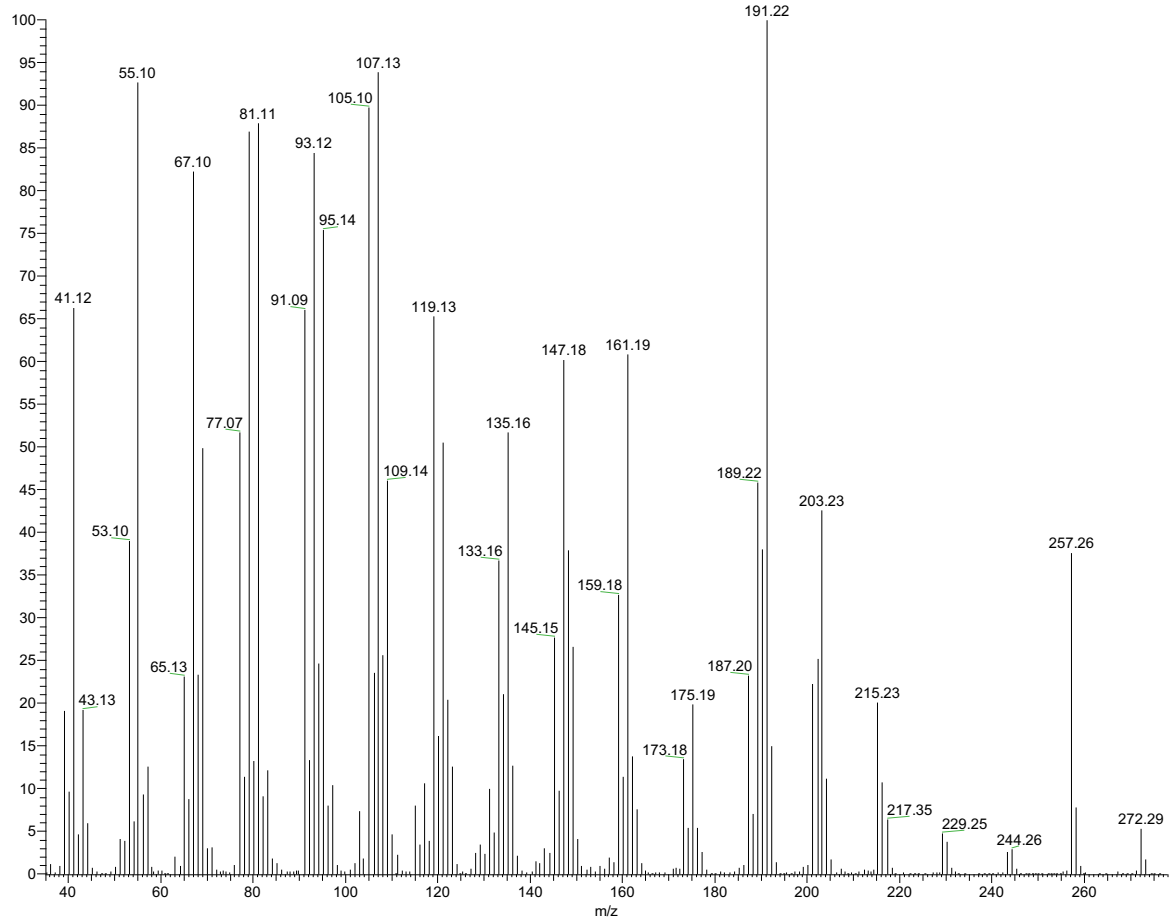

Figure S42. EIMS of gersemiene B (**9**).

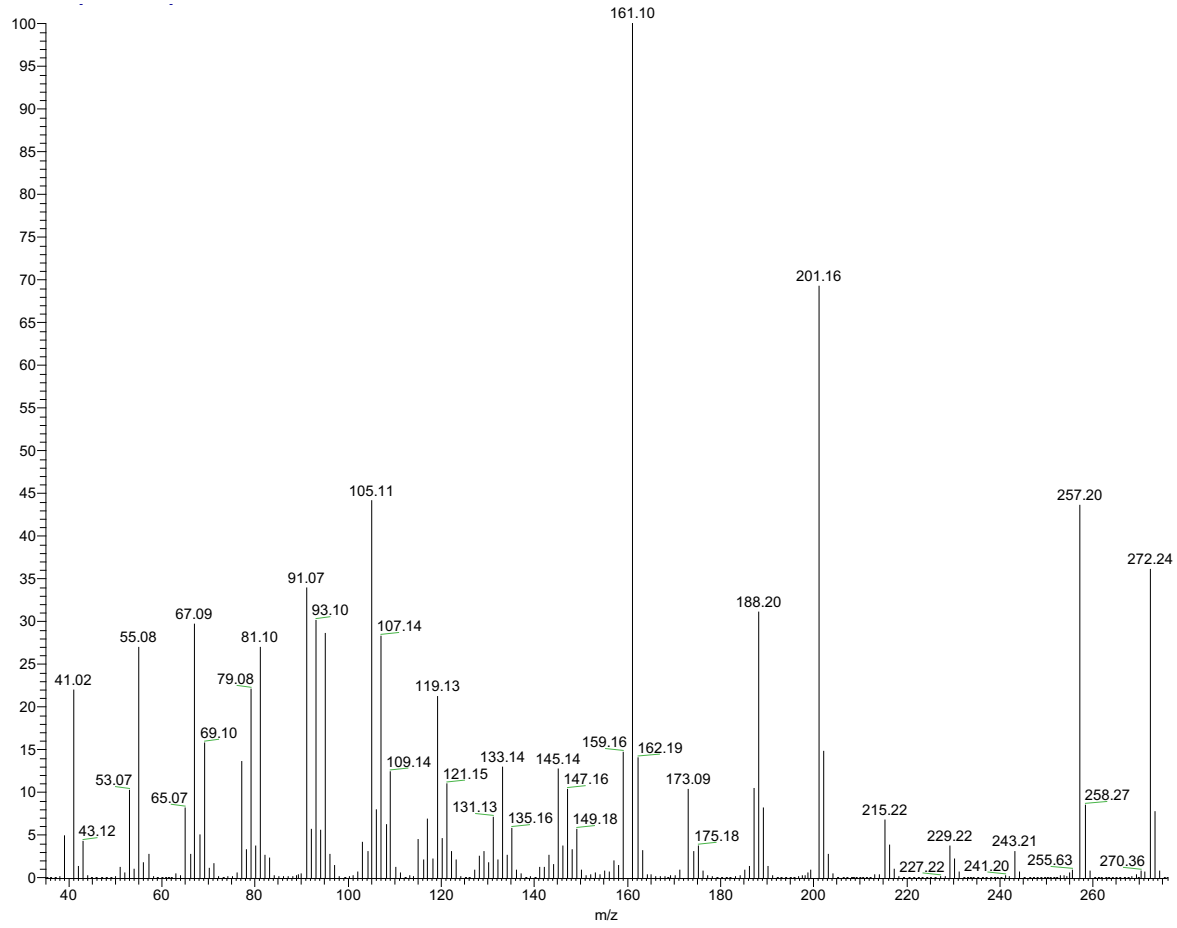

Figure S43. ^{1}H NMR spectrum of **10** in chloroform-*d* (600 MHz).

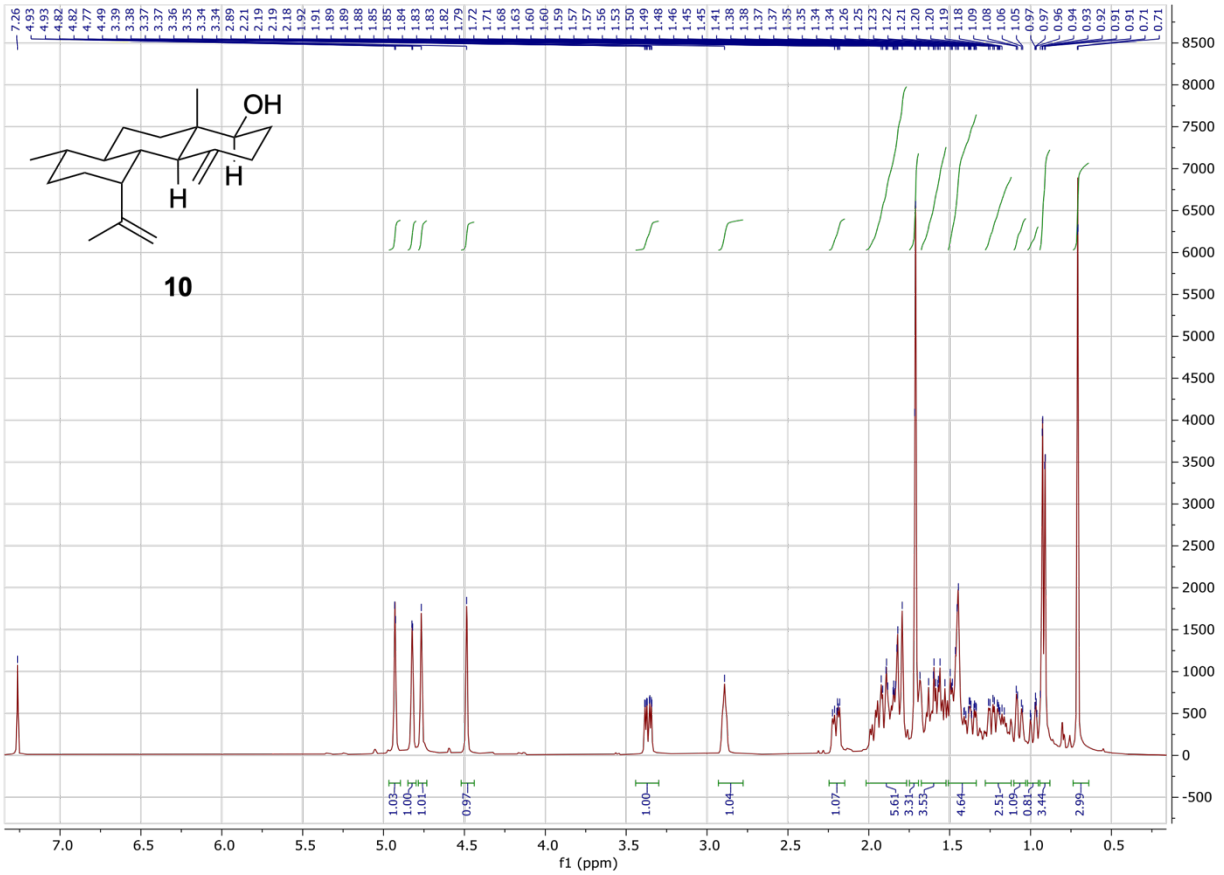

Figure S44. ^{13}C NMR spectrum of **10** in chloroform-*d* (151 MHz).

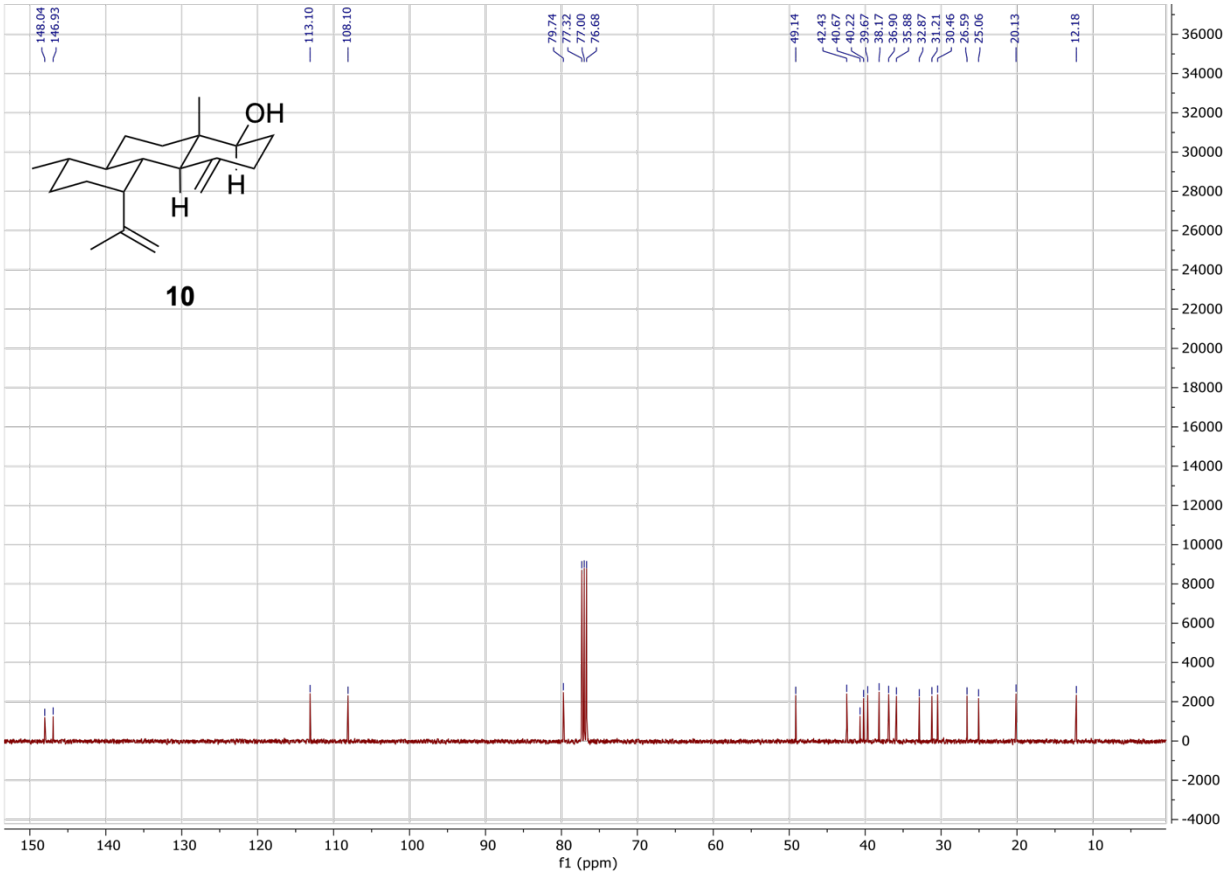

Figure S45. HSQC spectrum of **10** in chloroform-*d*. Blue cross peaks represent –CH or –CH_3; orange represent –CH_2.

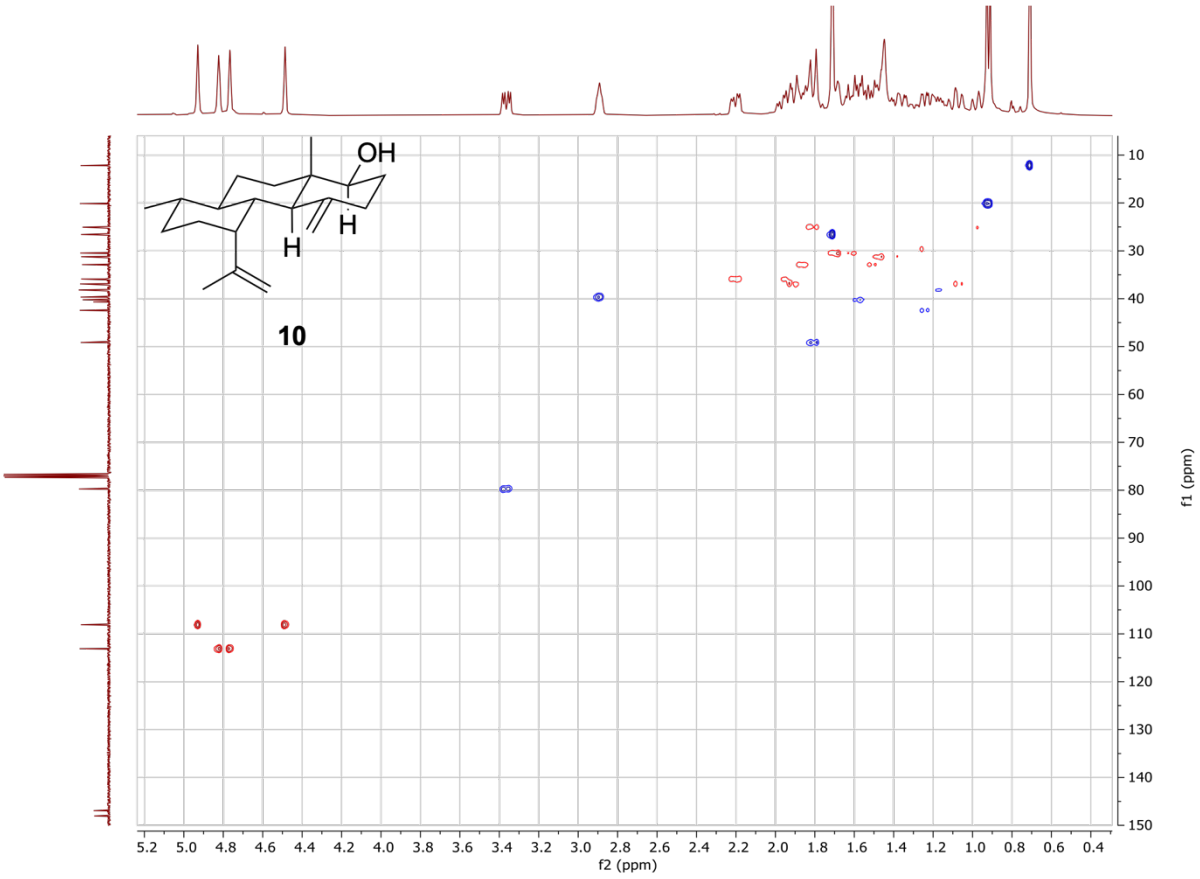

Figure S46. HMBC spectrum of **10** in chloroform-*d* (600 MHz).

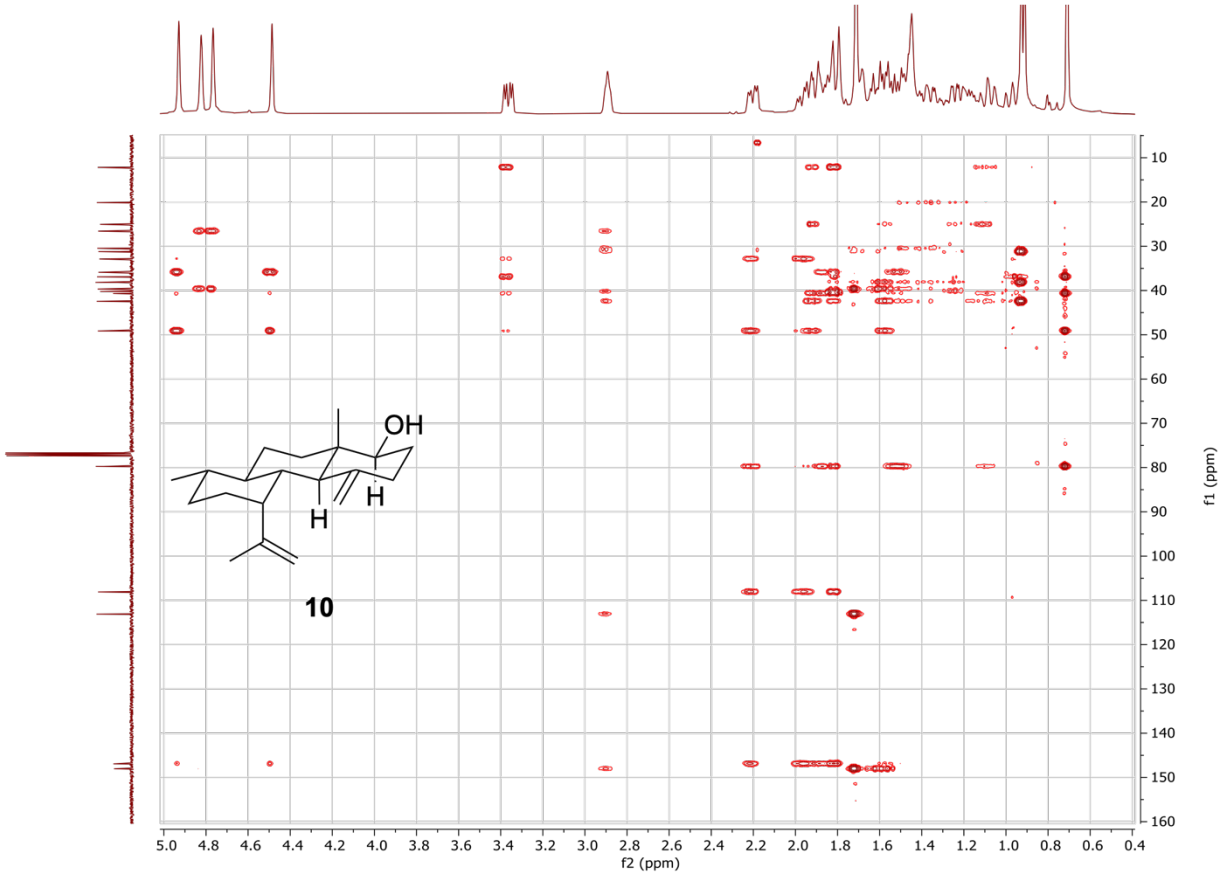

Figure S47. COSY spectrum of **10** in chloroform-*d* (600 MHz).

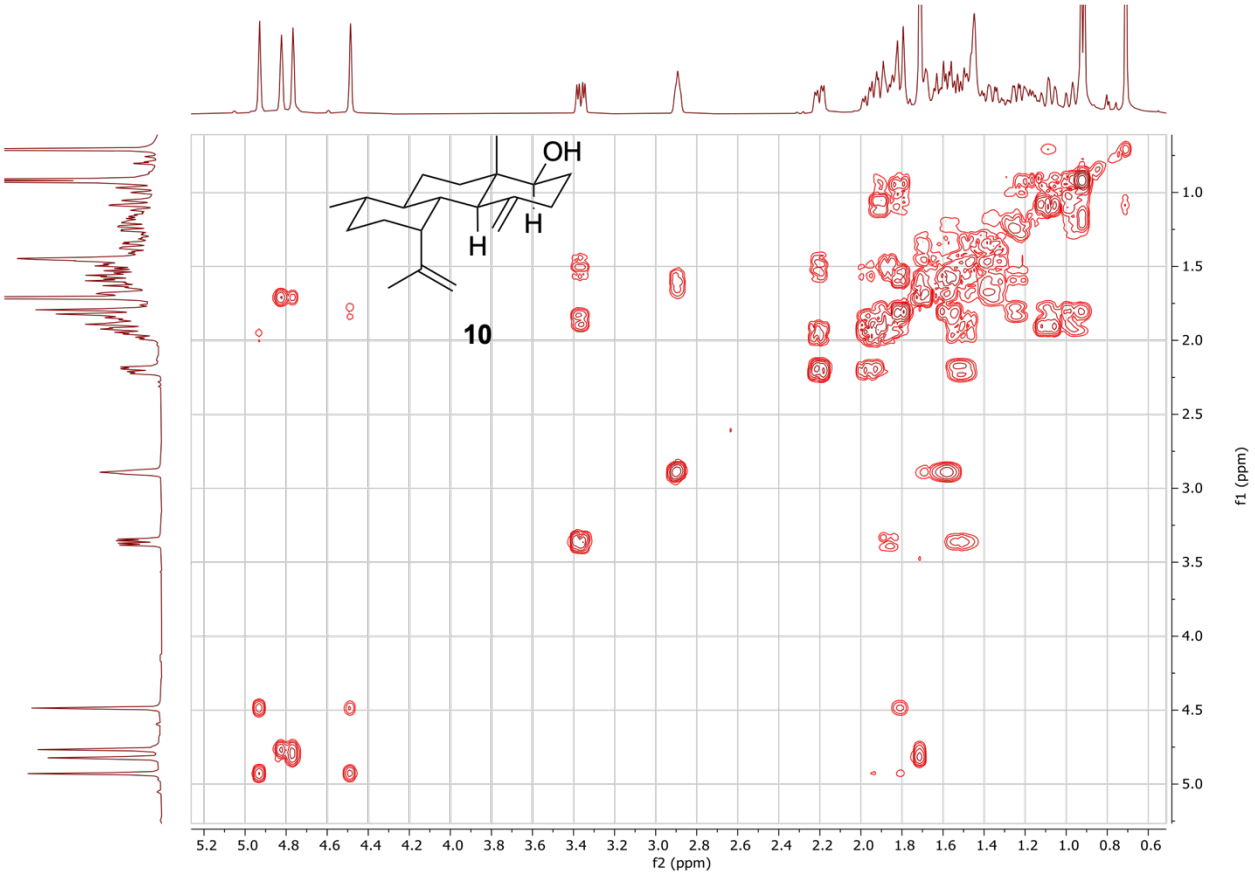

Figure S48. 1D selective gradient TOCSY spectrum of **10** in chloroform-*d* (600 MHz) with selective excitation of H-6.

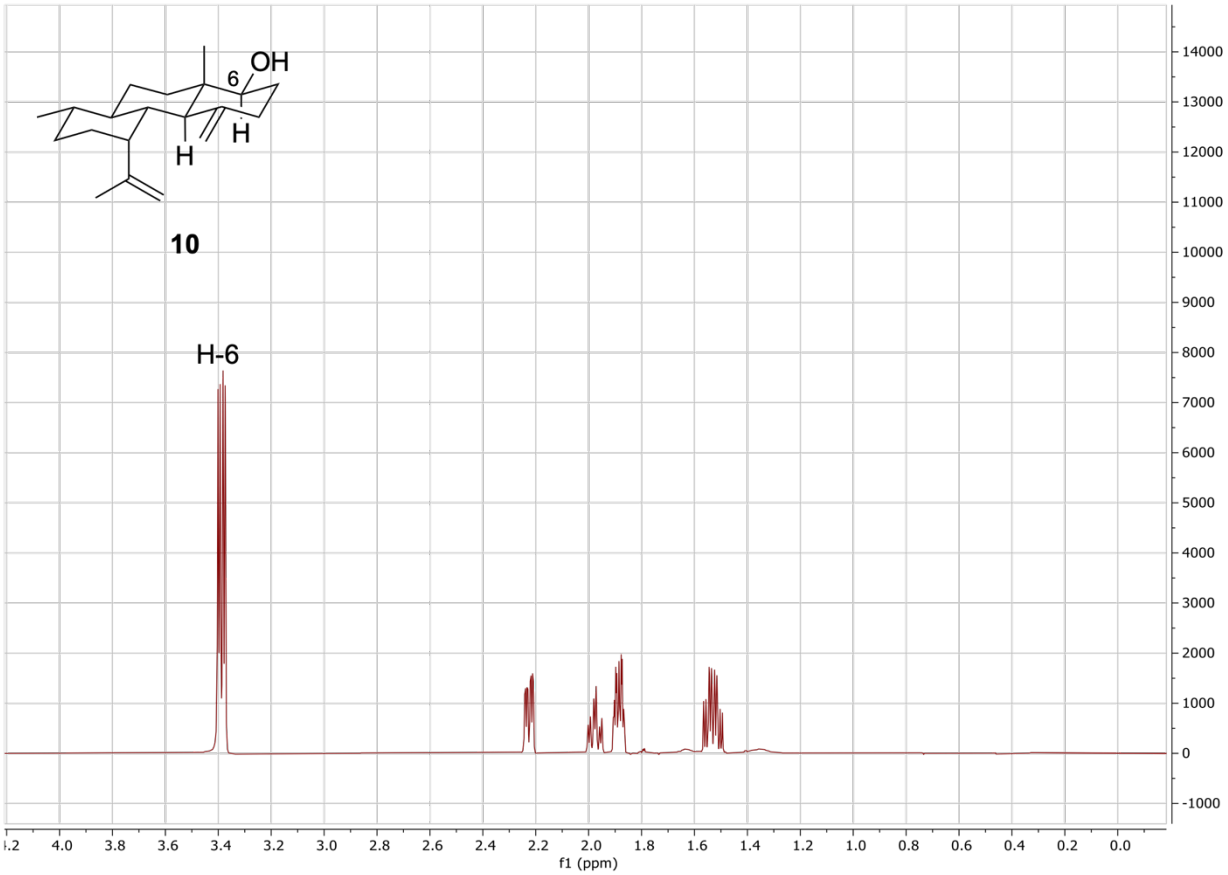

Figure S49. 1D NOESY spectrum of **10** in chloroform-*d* (600 MHz) with selective excitation of H-6; mixing time = 300 ms.

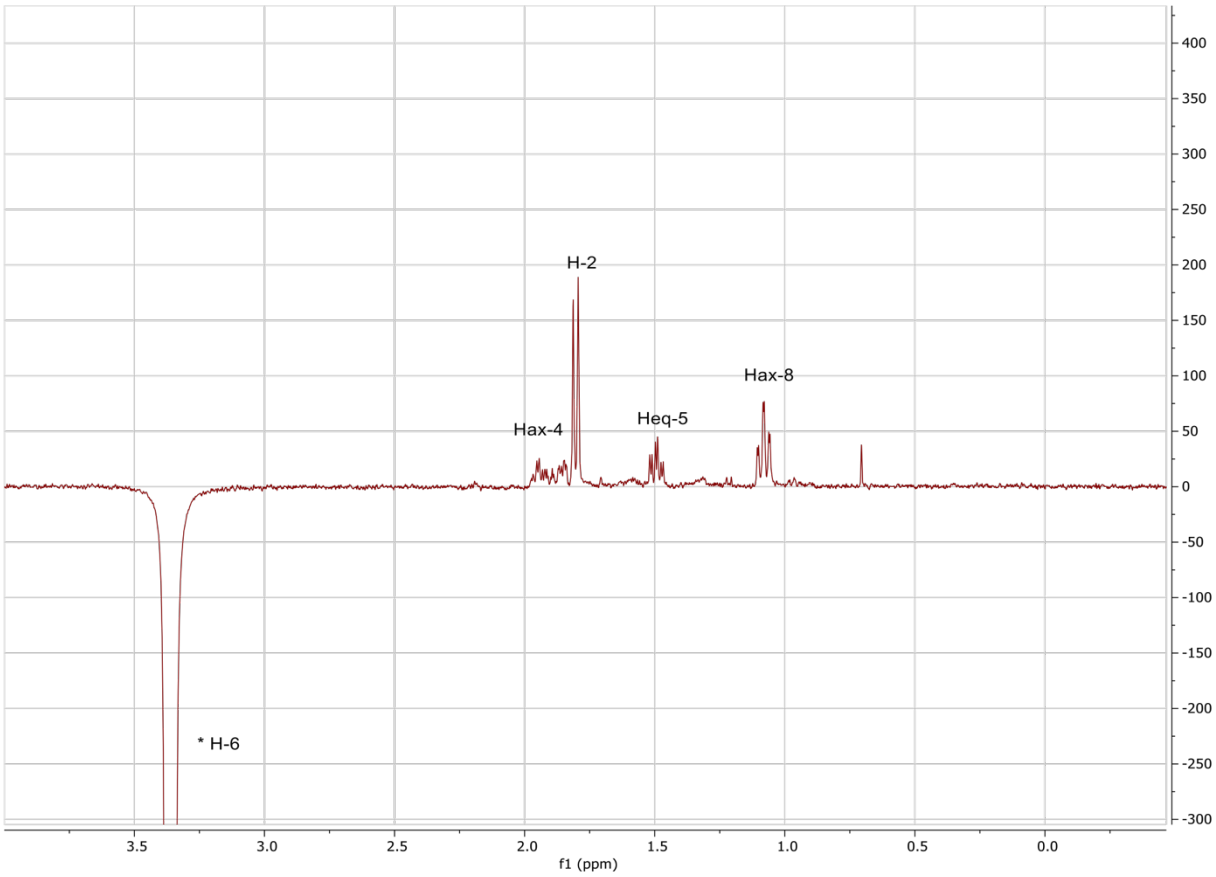

Figure S50. 1D NOESY spectrum of **10** in chloroform-*d* (600 MHz) with selective excitation of Me-19; mixing time = 300 ms.

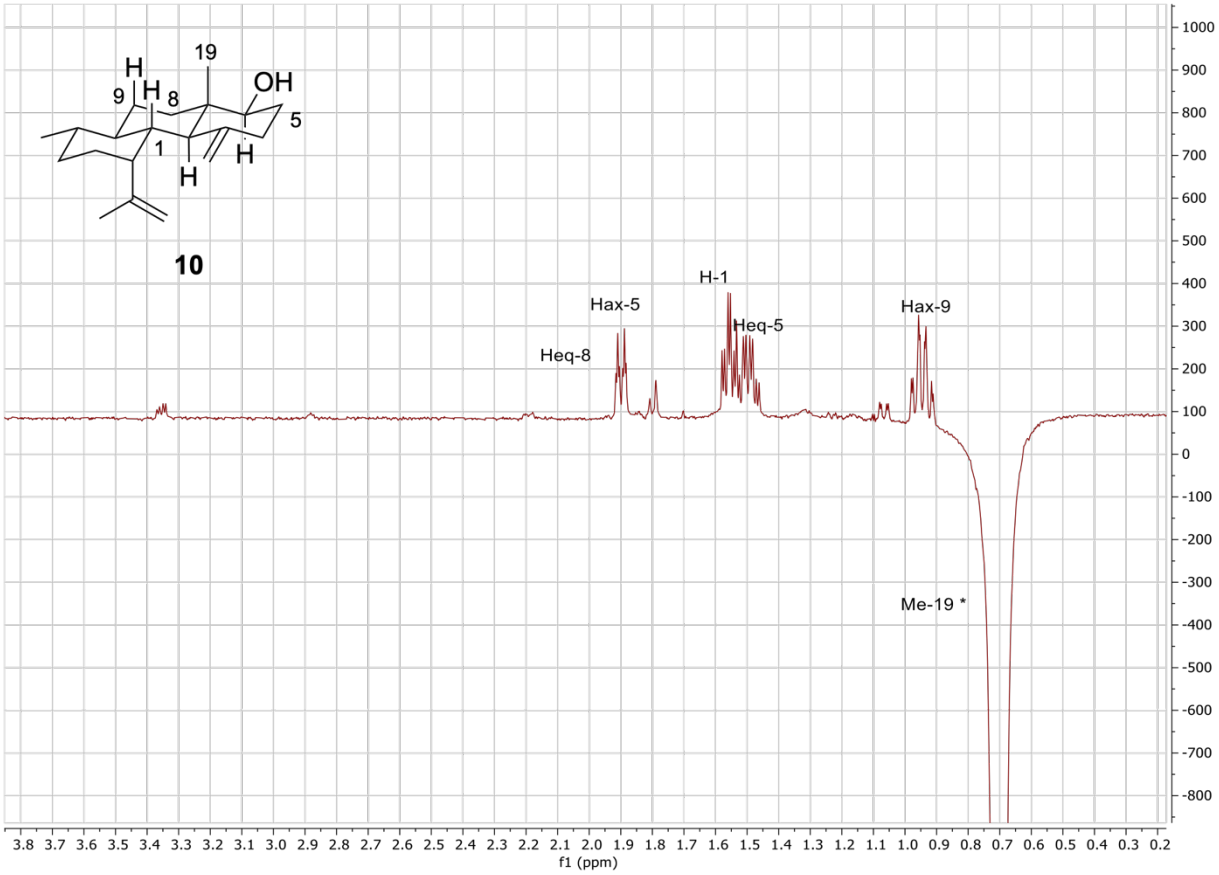

Figure S51. ^{1}H NMR spectrum of the (*S*)-MTPA ester of **10** (**11**) in chloroform-*d* (600 MHz).

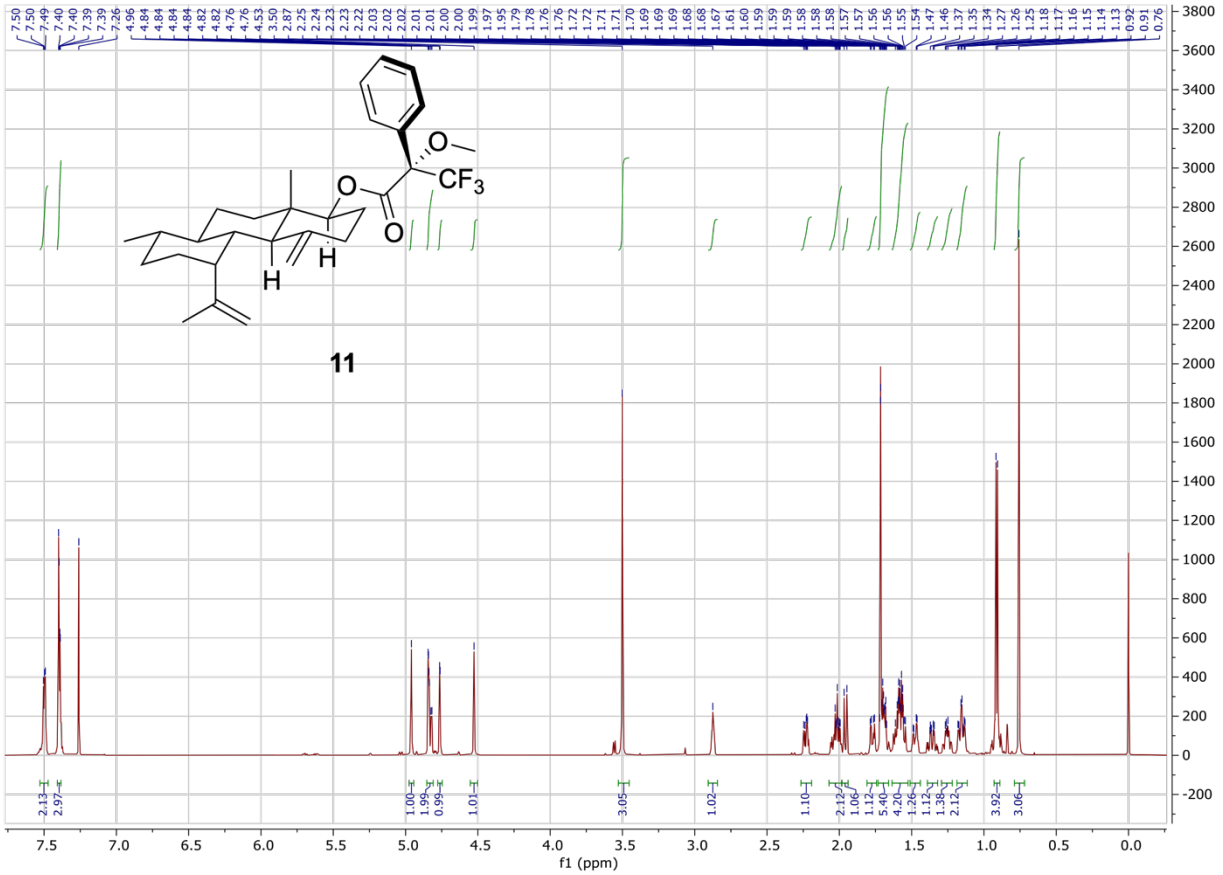

Figure S52. ^{13}C NMR spectrum of the (*S*)-MTPA ester of **10** (**11**) in chloroform-*d* (151 MHz).

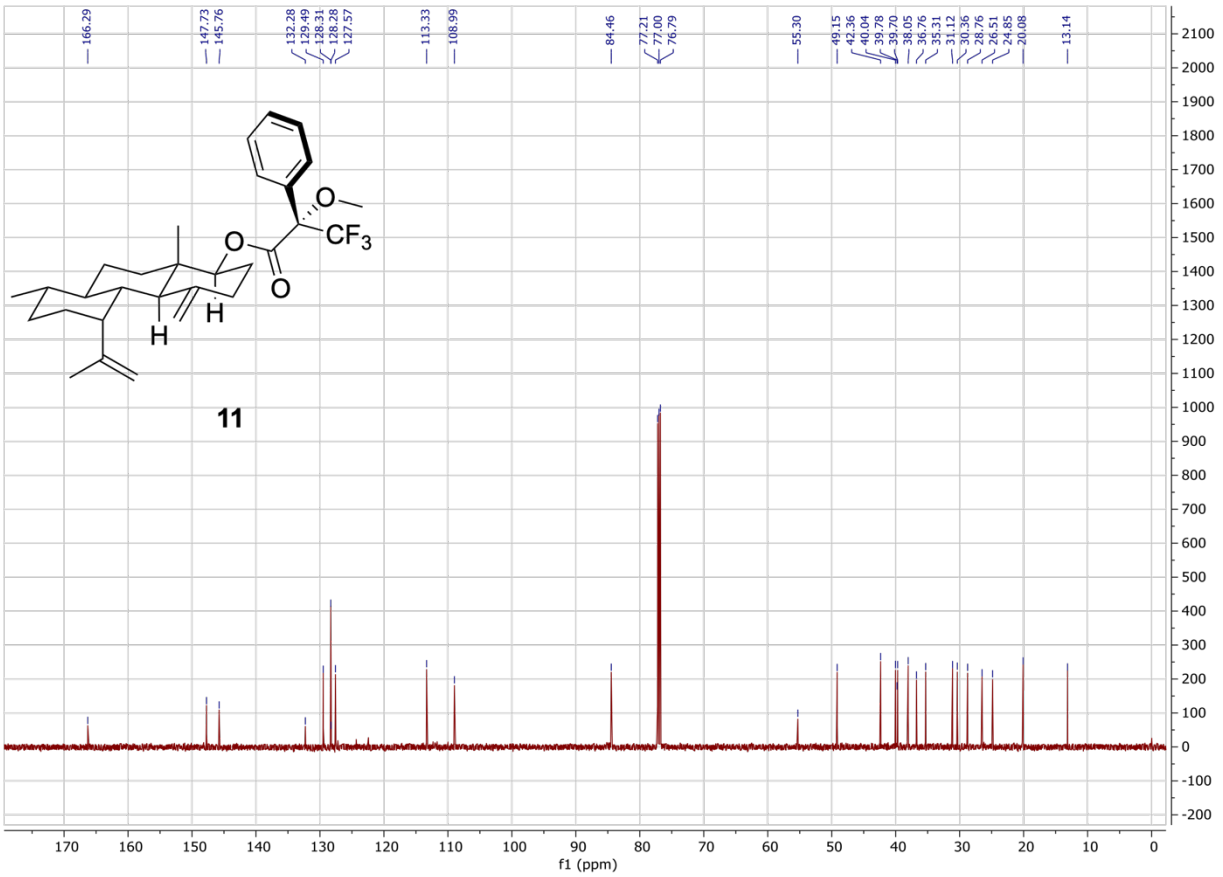

Figure S53. HSQC spectrum the (*S*)-MTPA ester of **10** (**11**) in chloroform-*d*. Blue cross peaks represent –CH or –CH_3; orange represent –CH_2.

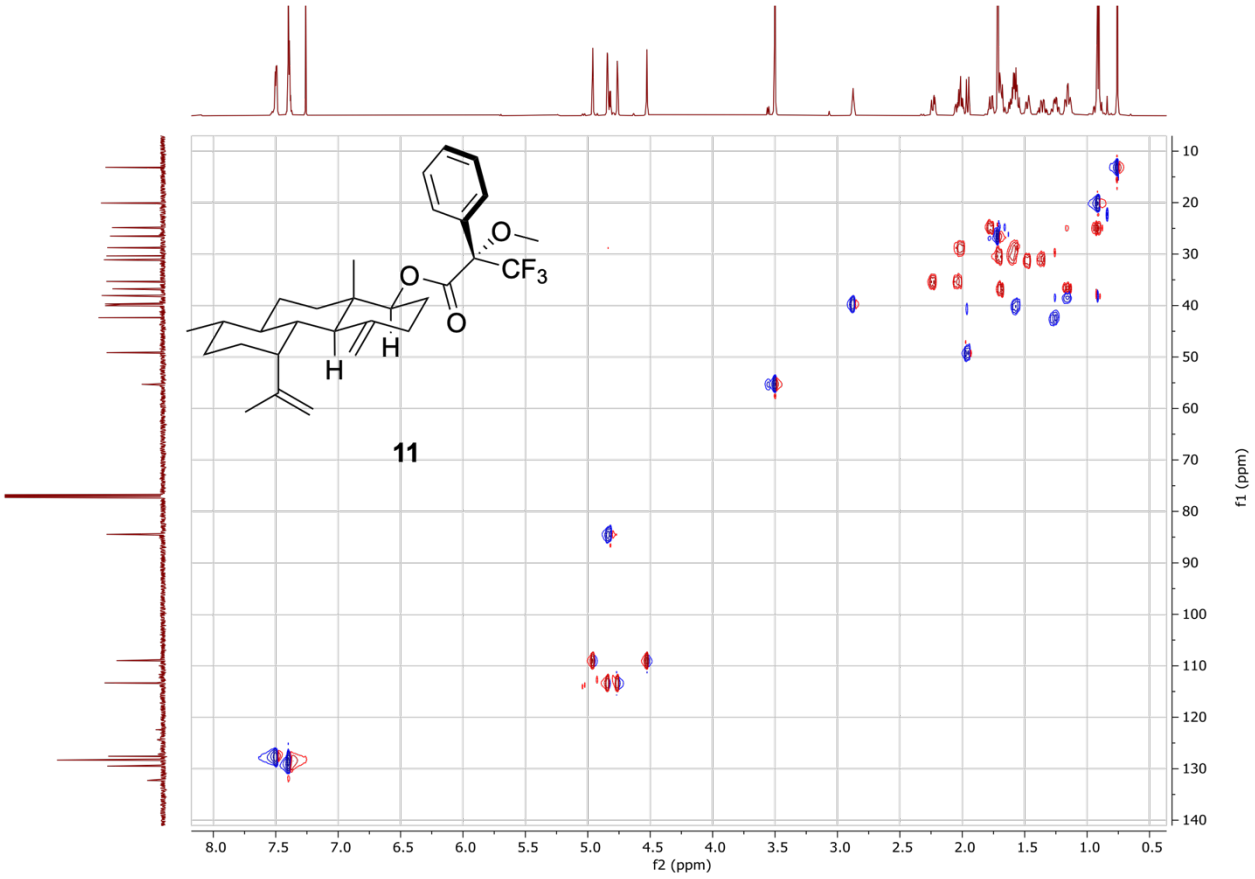

Figure S54. HMBC spectrum of the (*S*)-MTPA ester of **10** (**11**) in chloroform-*d* (600 MHz).

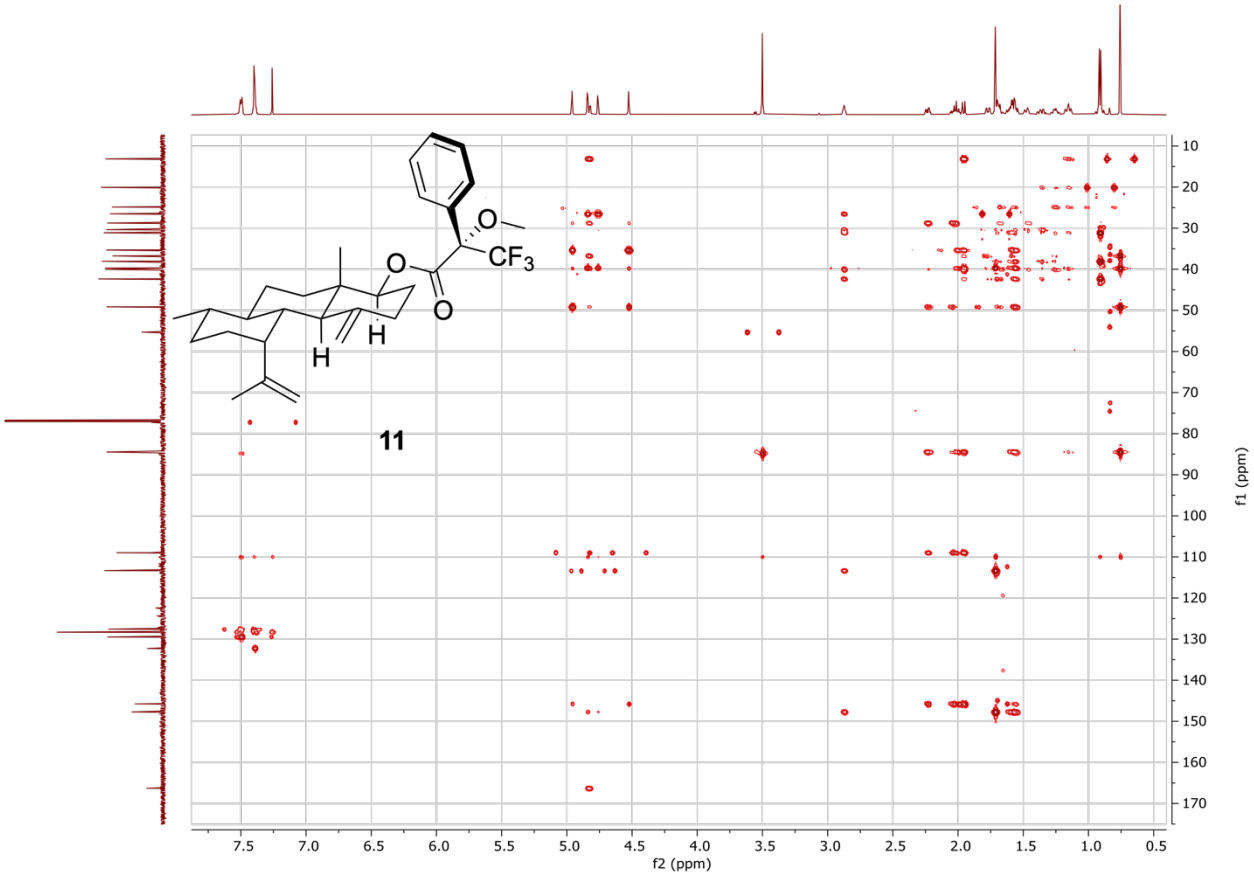

Figure S55. COSY spectrum of the (*S*)-MTPA ester of **10** (**11**) in chloroform-*d* (600 MHz).

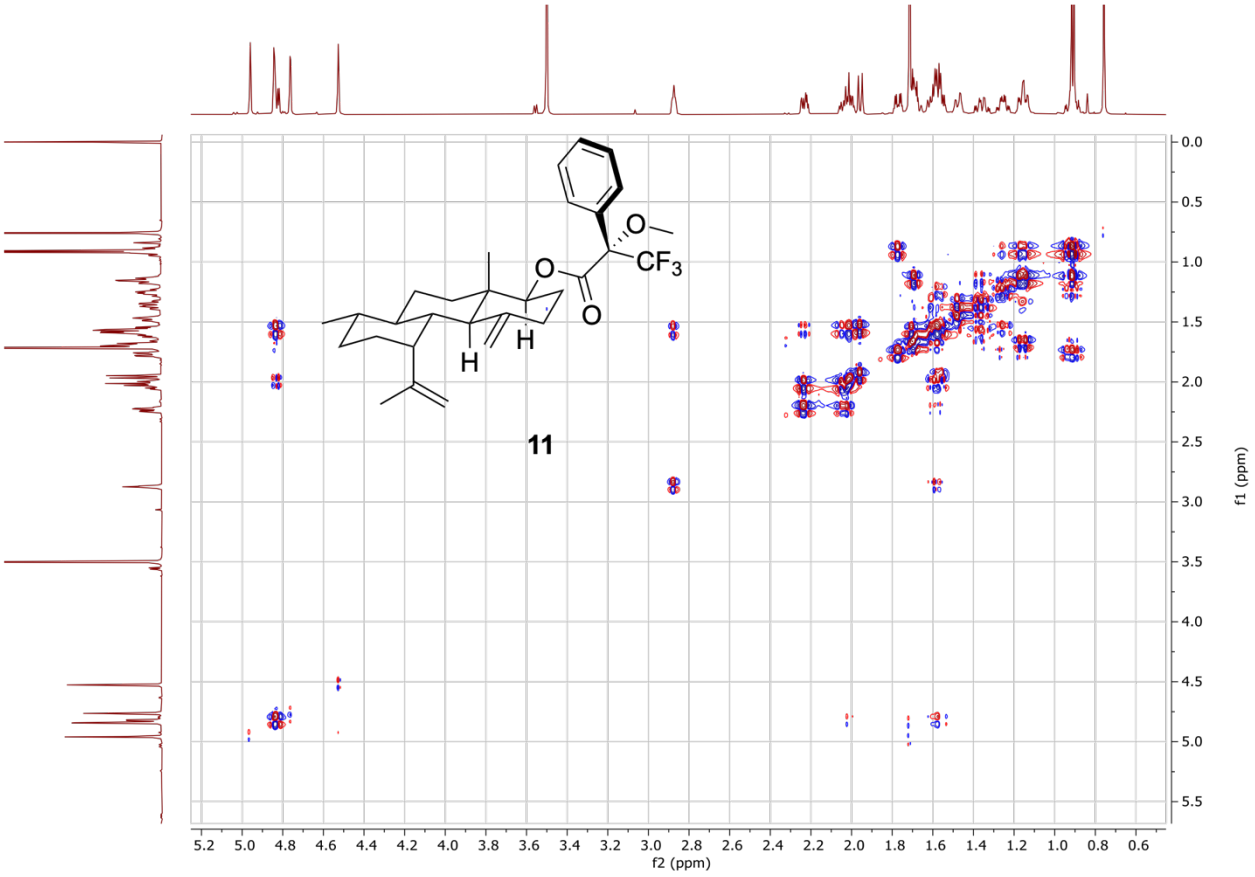

Figure S56. ^{1}H NMR spectrum of the (*R*)-MTPA ester of **10** (**12**) in chloroform-*d* (600 MHz).

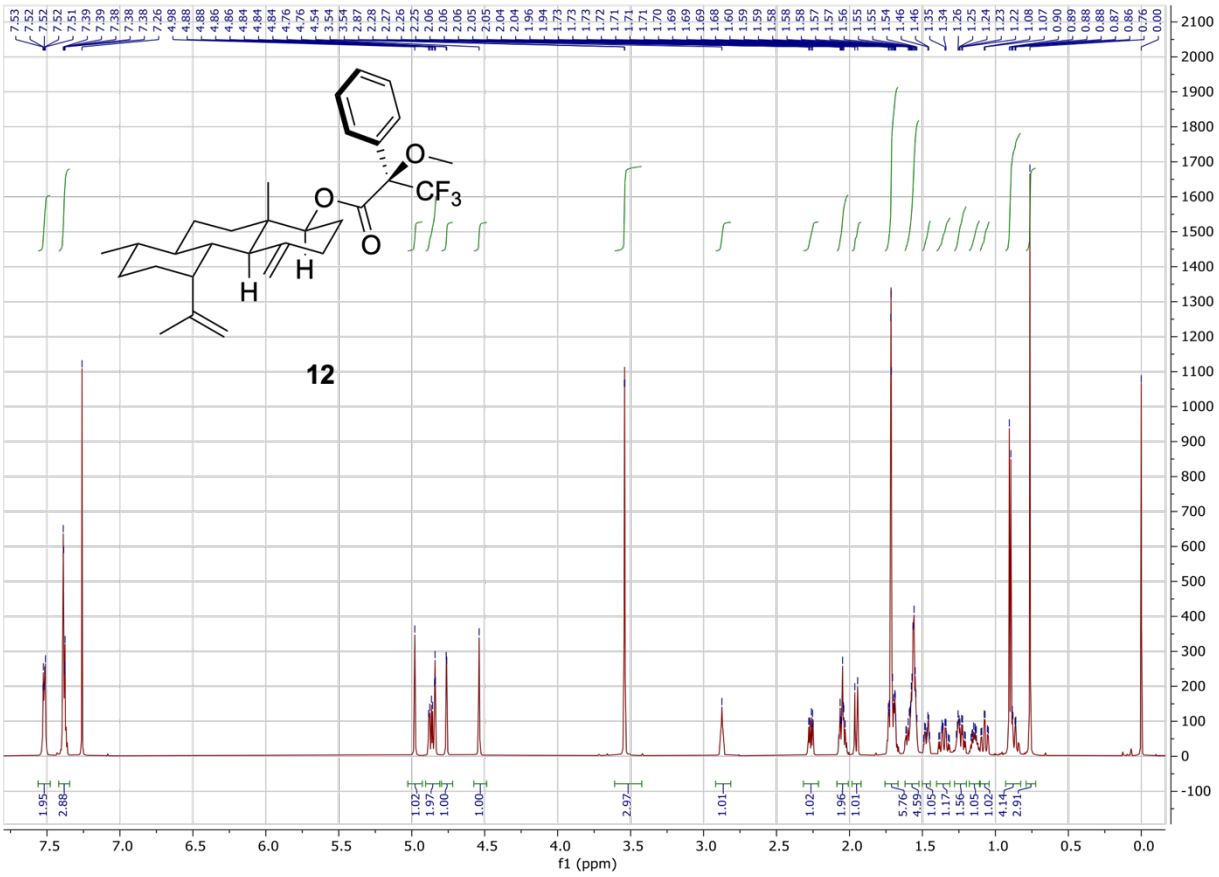

Figure S57. ^{13}C NMR spectrum of the (*R*)-MTPA ester of **10** (**12**) in chloroform-*d* (151 MHz).

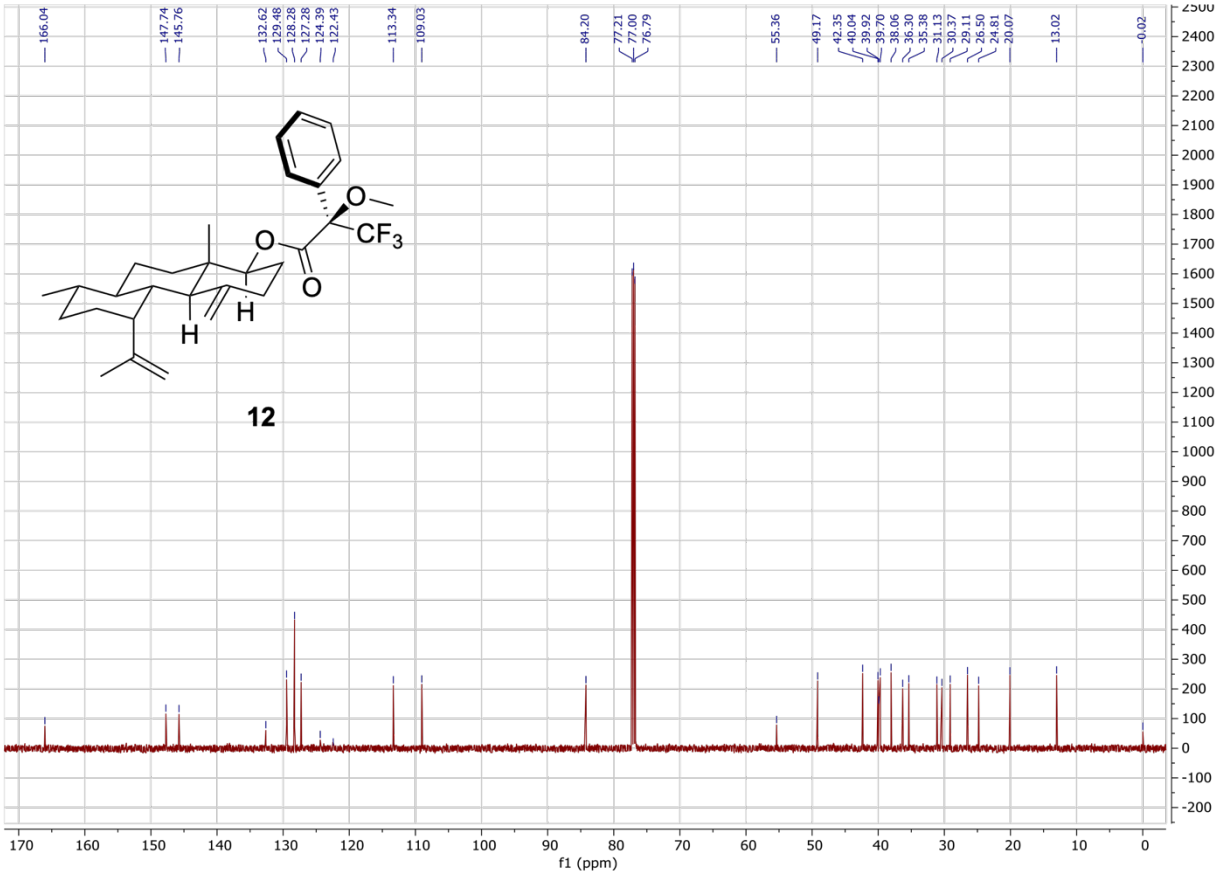

Figure S58. HSQC spectrum of the (*R*)-MTPA ester of **10** (**12**) in chloroform-*d*. Blue cross peaks represent –CH or –CH_3; orange represent –CH_2.

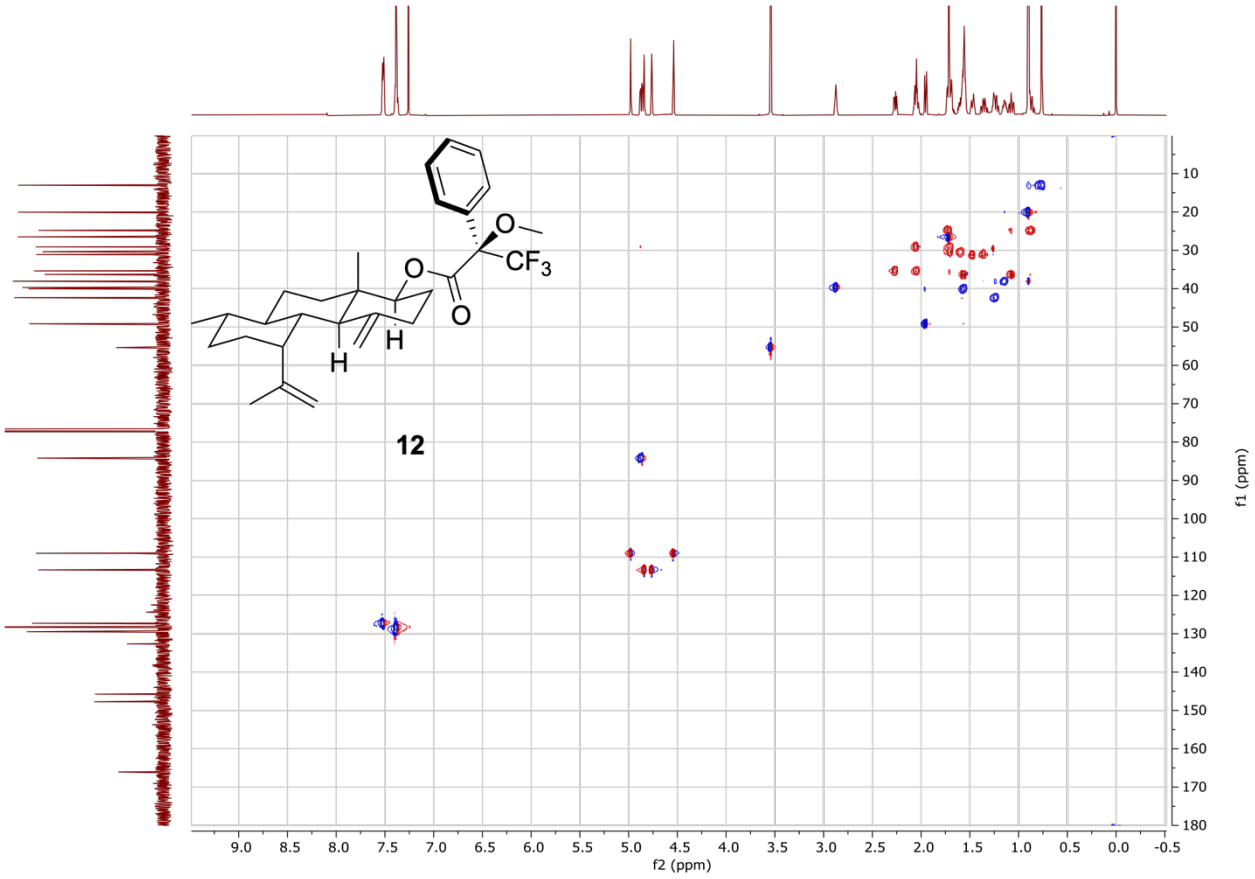

Figure S59. HMBC spectrum of the (*R*)-MTPA ester of **10** (**12**) in chloroform-*d* (600 MHz).

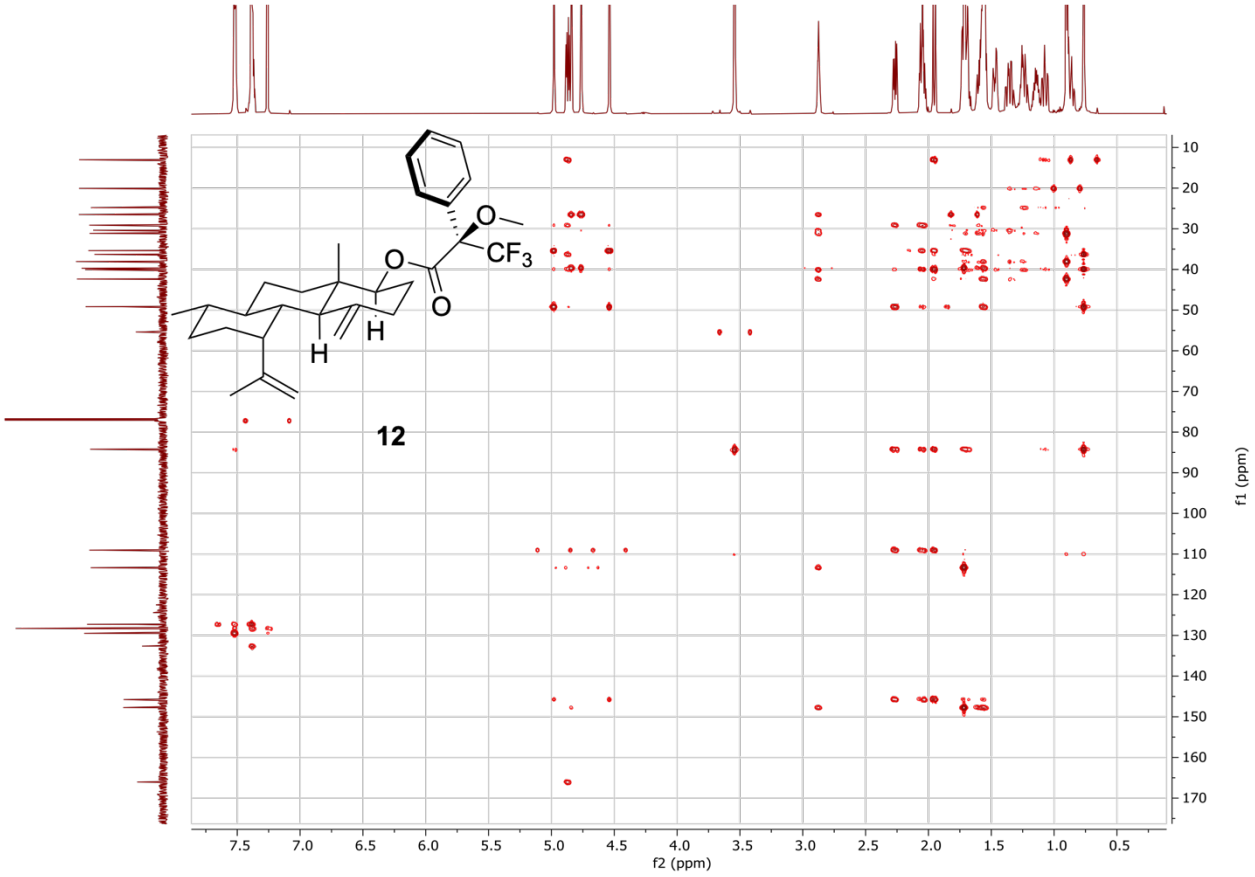

Figure S60. COSY spectrum of the (*R*)-MTPA ester of **10** (**12**) in chloroform-*d* (600 MHz).

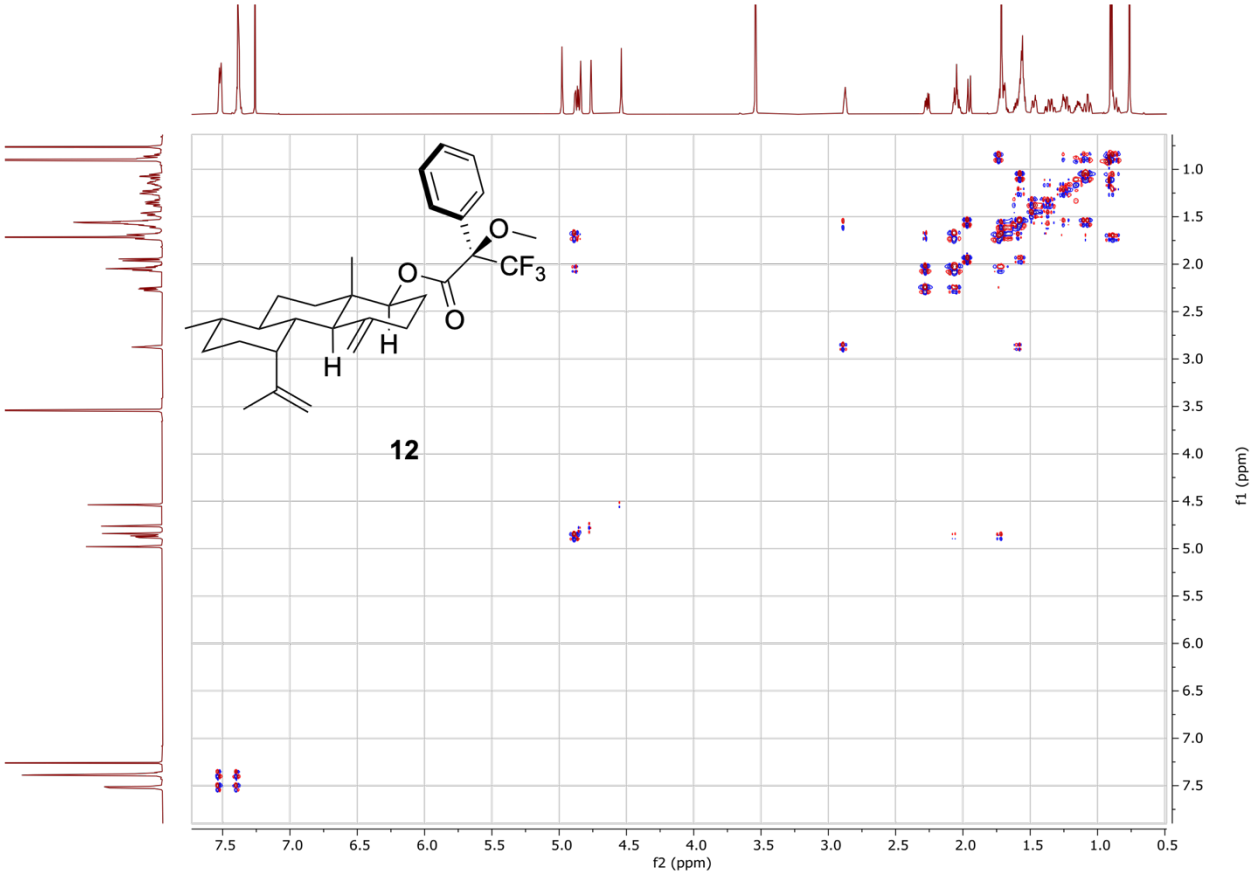

Figure S61. HPLC-UV analysis of the AlbS mutant reactions with GGPP. Absorbance was detected at 210 nm. Related to Fig. 3.

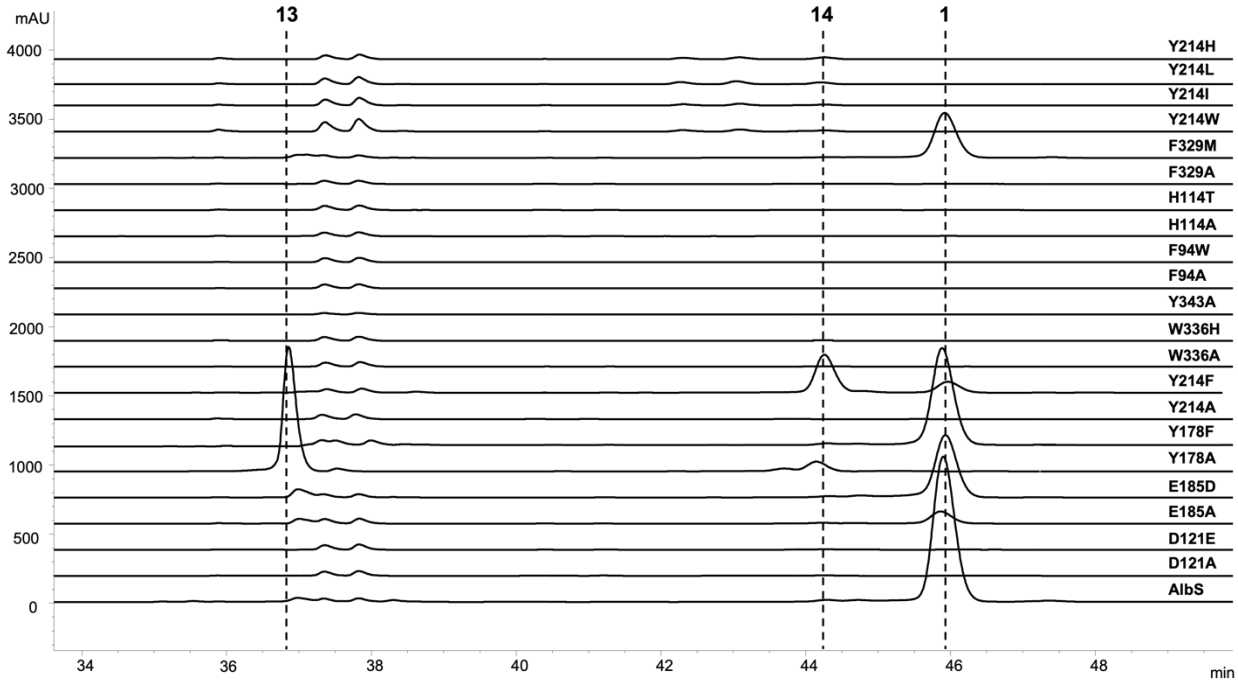

Figure S62. ^{1}H NMR spectrum of prenylgermacrene A (**14**) in benzene-d_6 (600 MHz).

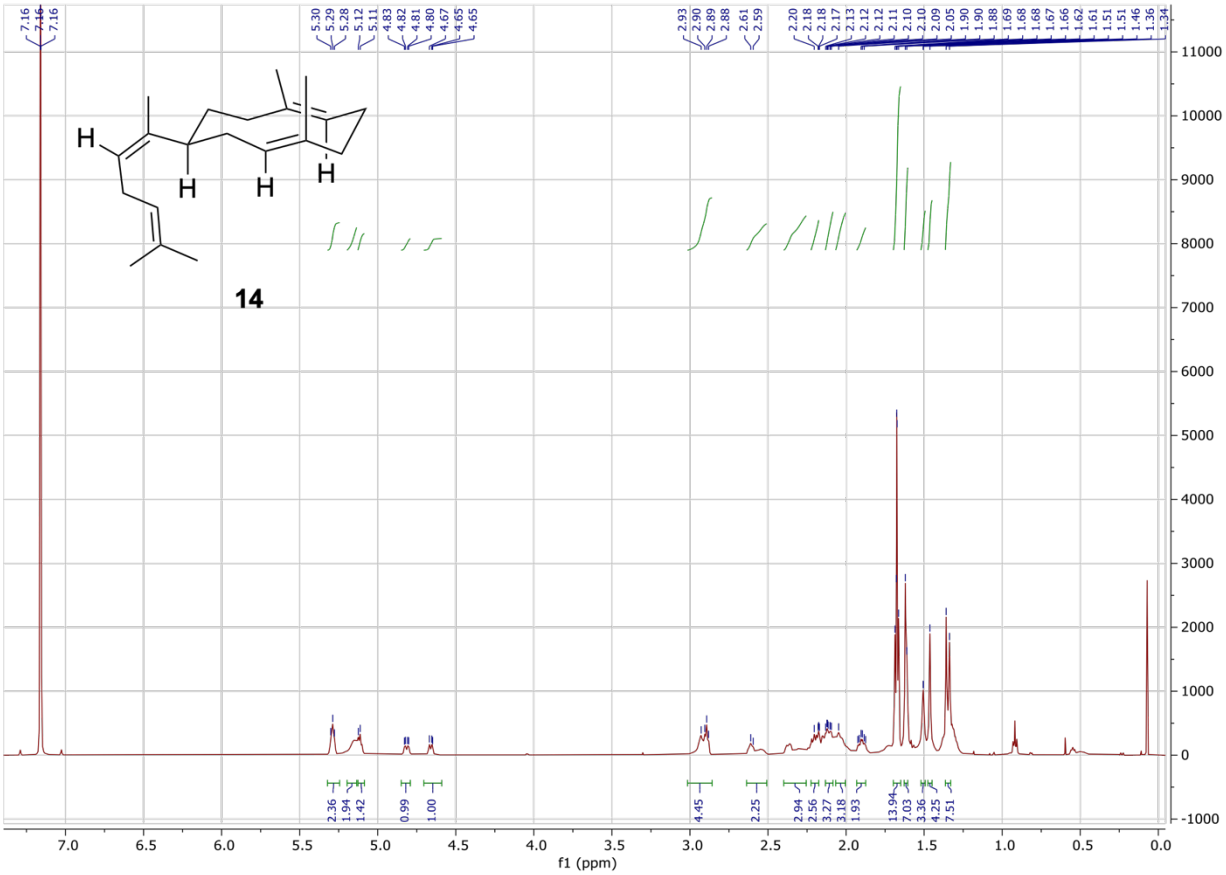

Figure S63 ^{13}C NMR spectrum of prenylgermacrene A (**14**) in benzene-d_6 (151 MHz).

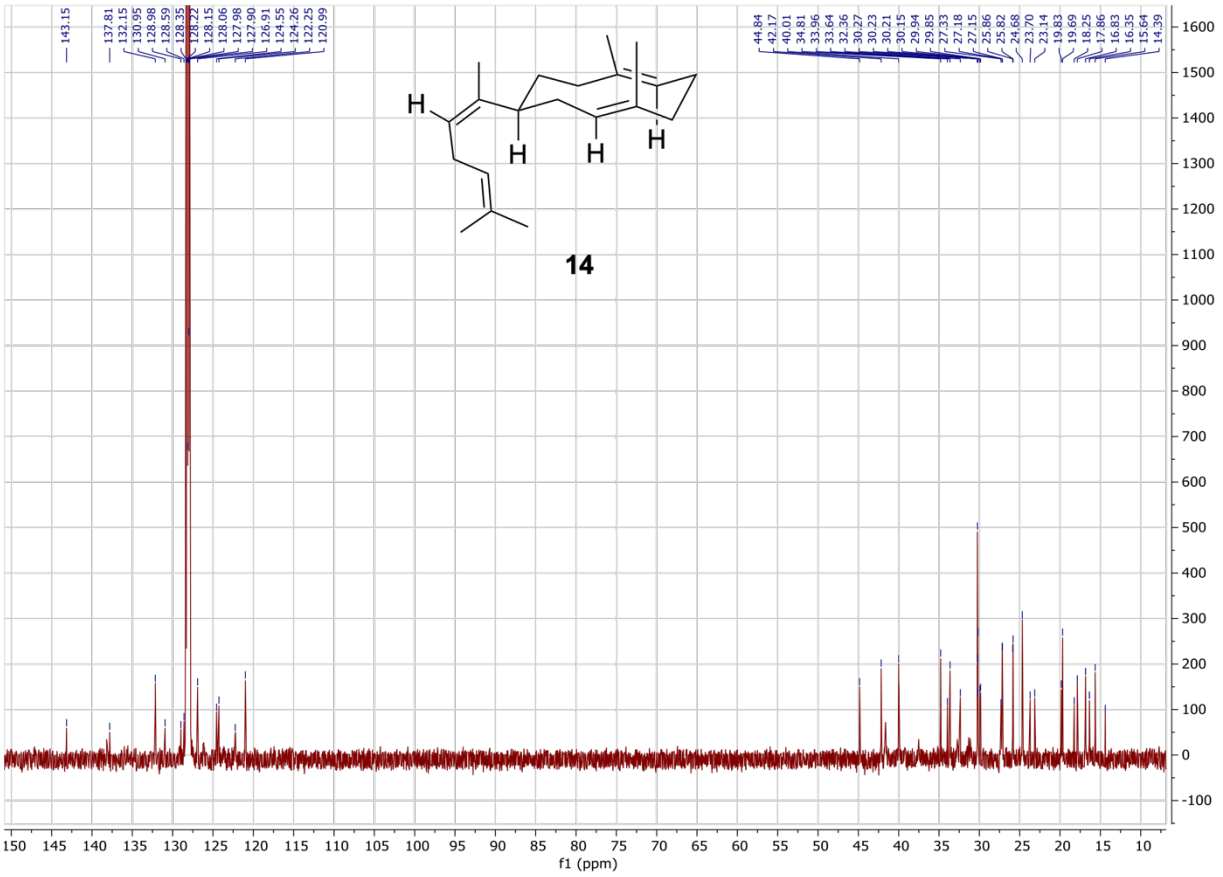

Figure S64. HSQC spectrum of prenylgermacrene A (**14**) in benzene-d_6. Blue cross peaks represent –CH or –CH_3; orange represent –CH_2.

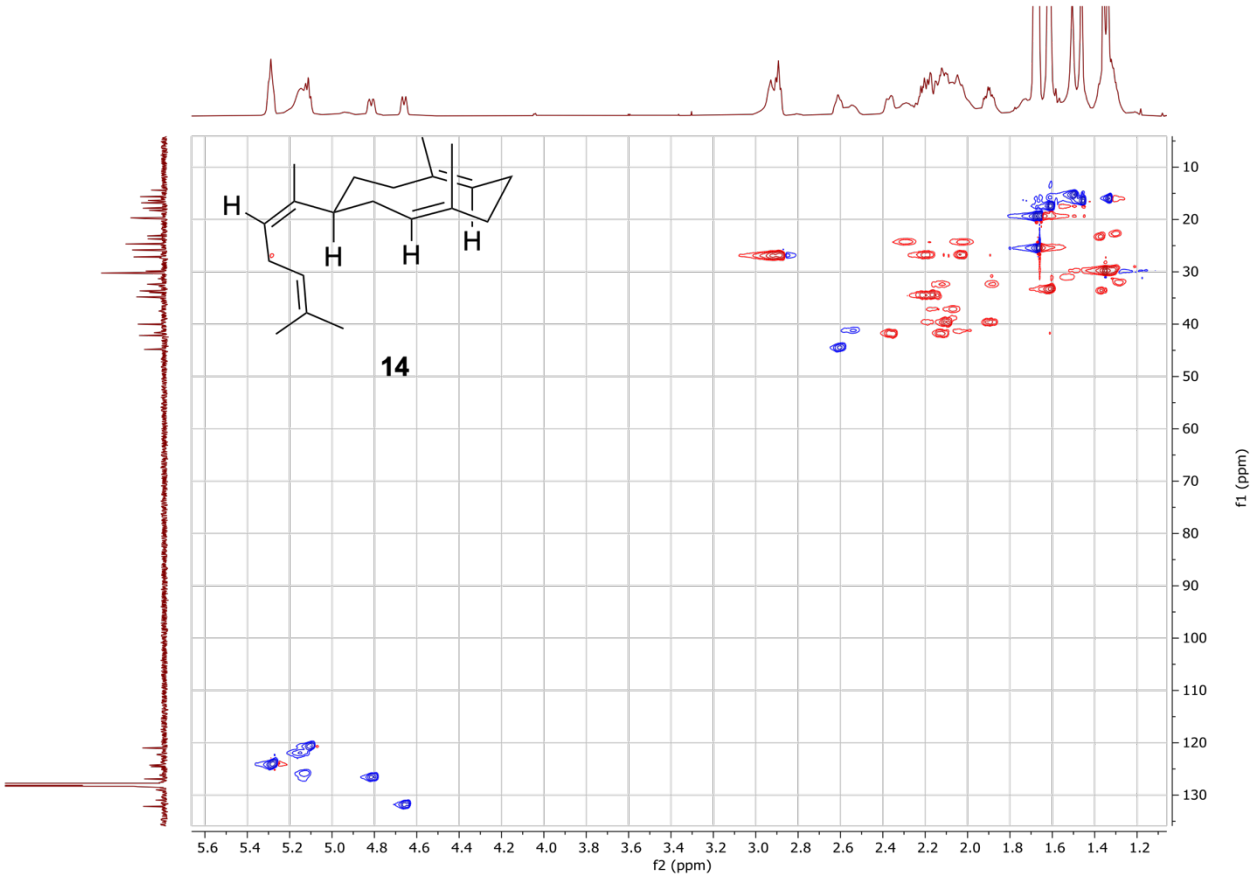

Figure S65. HMBC spectrum of prenylgermacrene A (**14**) in benzene-d_6 (600 MHz).

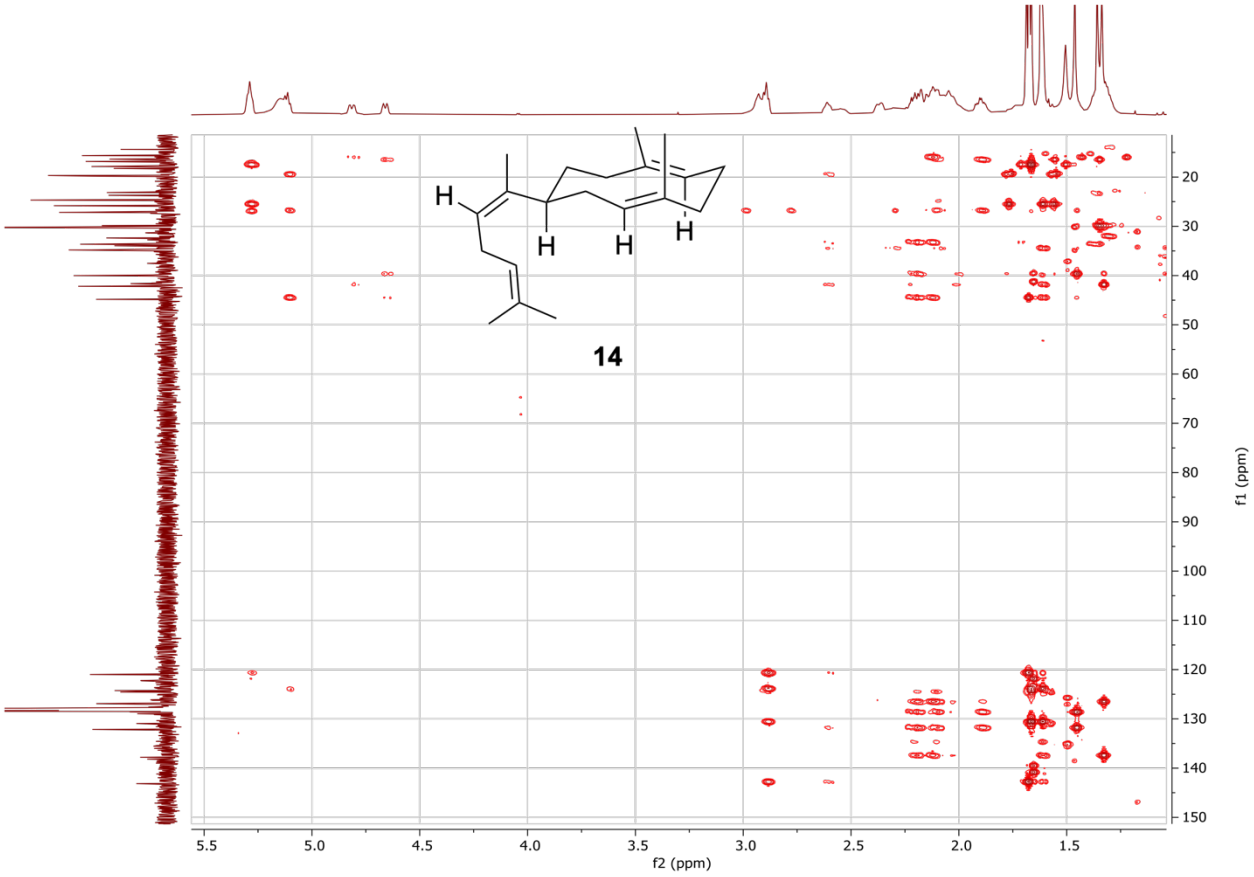

Figure S66. COSY spectrum of prenylgermacrene A (**14**) in benzene-d_6 (600 MHz).

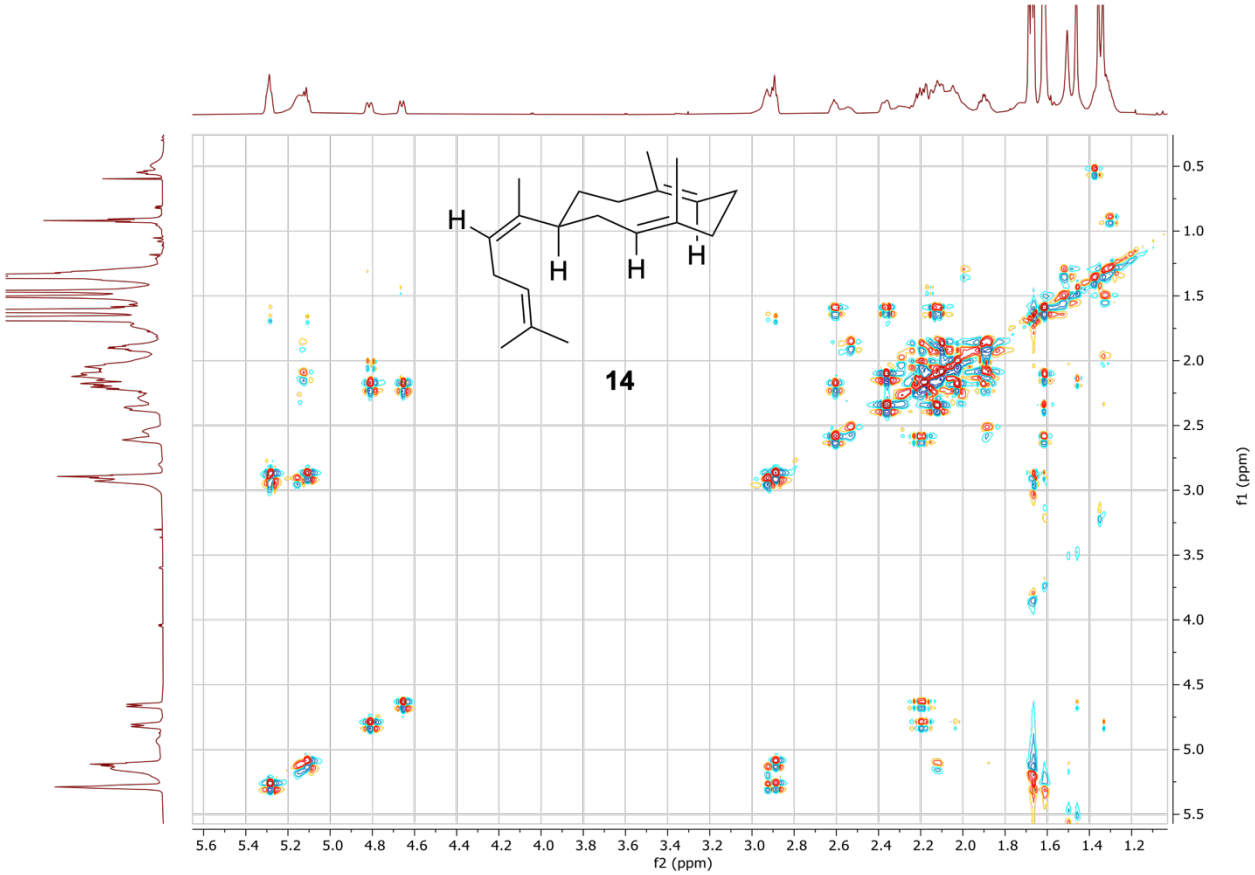

Figure S67. 1D NOESY spectrum of prenylgermacrene A (**14**) in benzene-d_6 with selective excitation of H-12; mixing time = 300 ms.

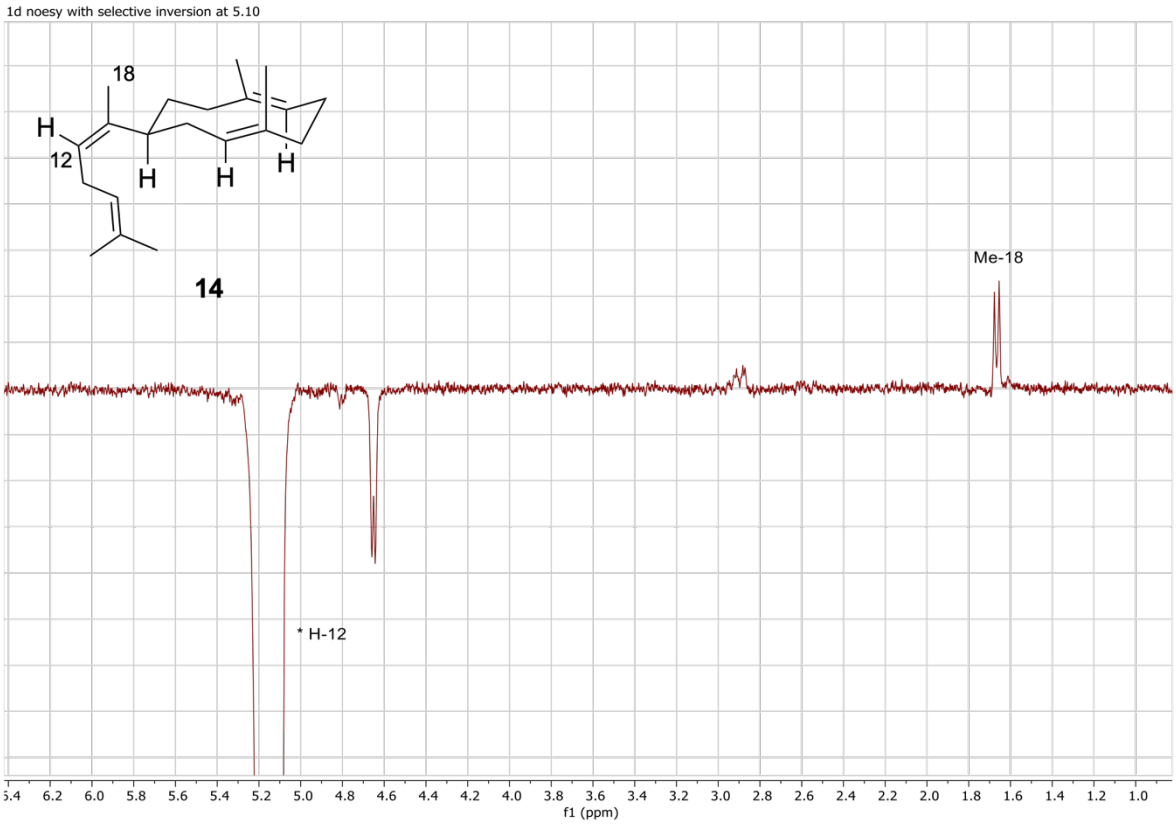

Figure S68. EIMS of prenylgermacrene A (**14**).

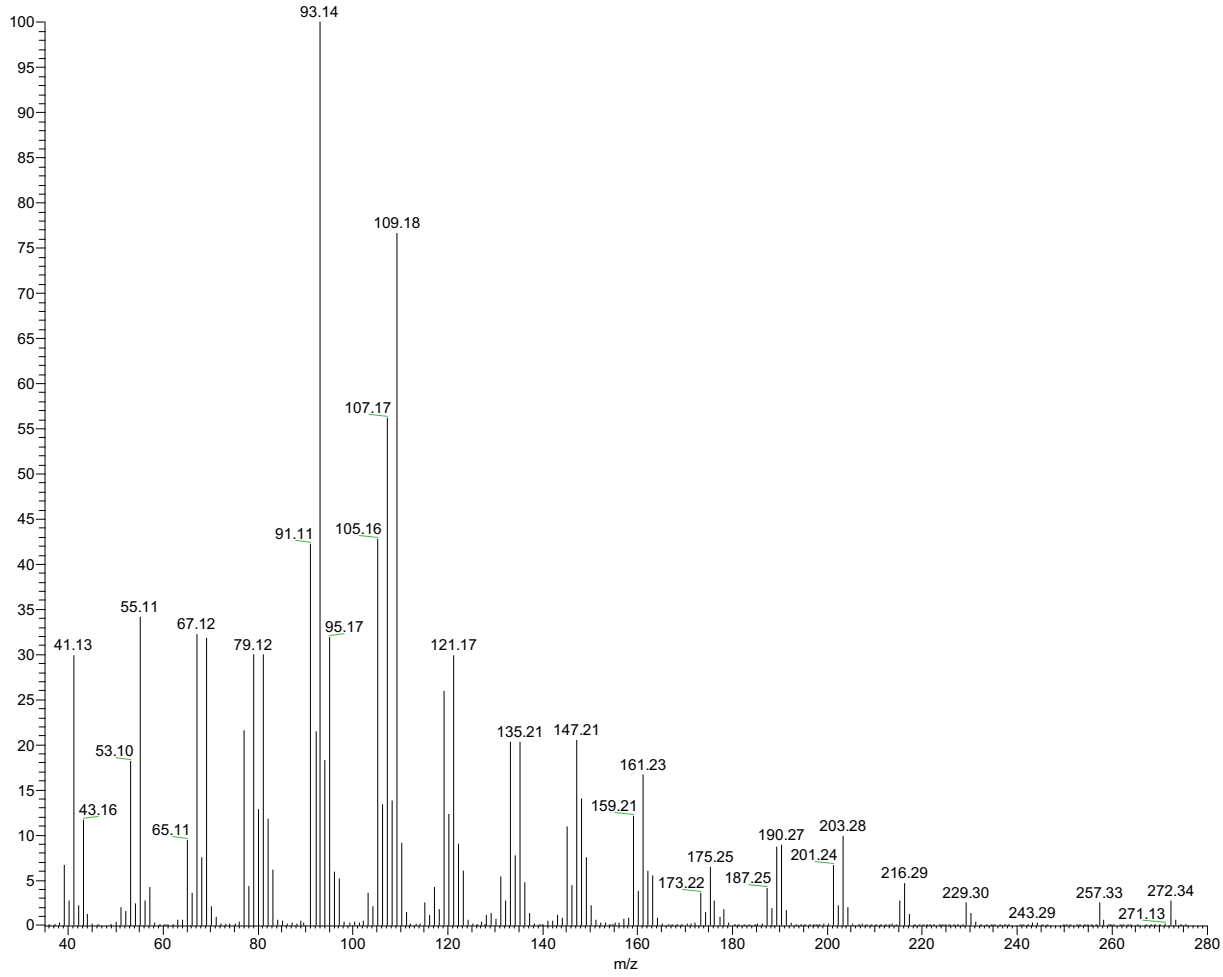

Figure S69. Possible conformations of prenylgermacrene A (**14**). The conformers are denoted as UU, UD, DU, and DD in reference to the U (up) and D (down) orientations of the C-19 and C-20 methyl groups on the 10-membered ring. Based on the olefinic signals of H-2 and H-6 (Figs. S62, 64, and 65, Table S9) and previous calculations for 10-membered sesquiterpenes,[6–9] we predict that **14** is present in its UU (major) and UD (minor) conformers.

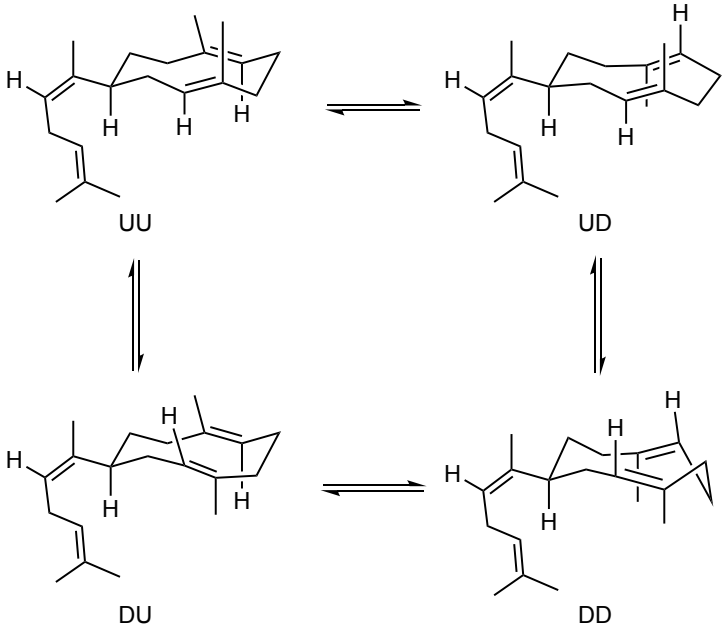

Figure S70. Known diterpenes related to prenylgermacrene A (**14**).

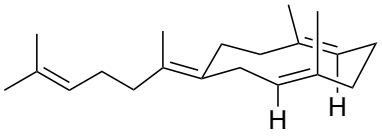

prenylgermacrene B

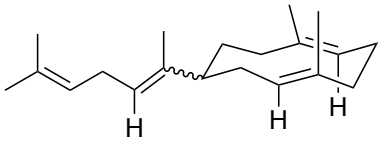

eunicene A

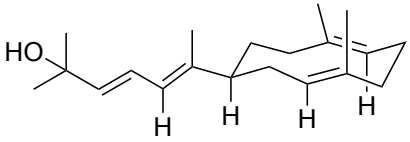

eunicol

Figure S71. ^{1}H NMR spectra 1,1-$^{2}H_2$-IPP and 1*R*-^{2}H-GGPP in D_2O (600 MHz) to assess purity.

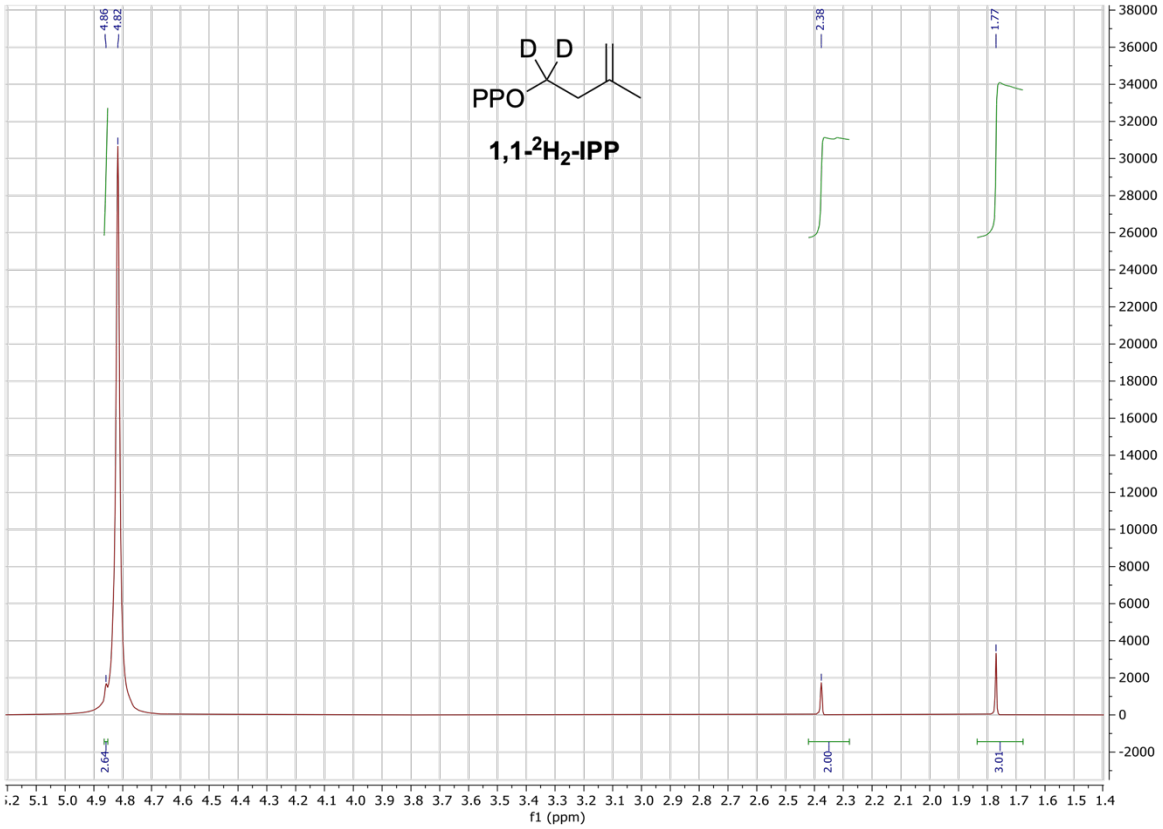

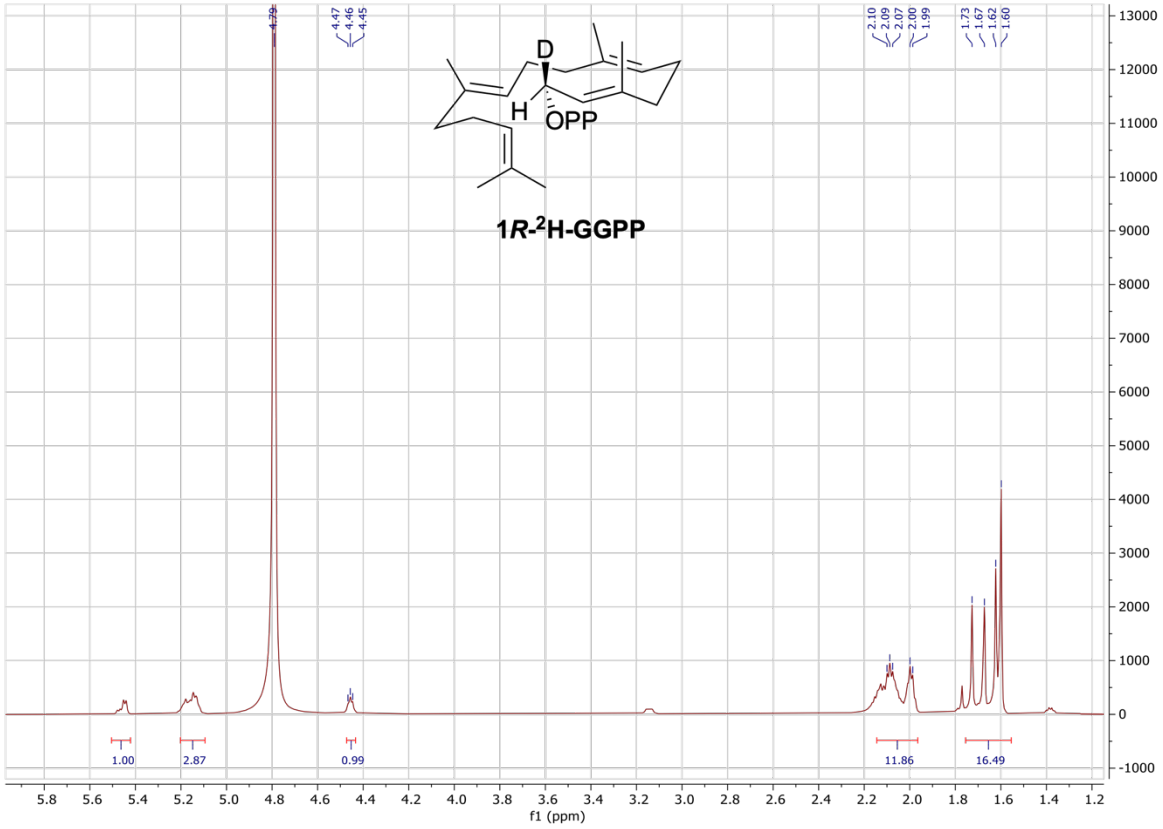

Figure S72. Comparison of the ^{1}H NMR spectra of **1** (bottom), 11-^{2}H-**1** (middle), and 1,11-$^{2}H_2$-**1** (top) in benzene-d_6 (600 MHz). Incubation of AlbS with unlabeled GGPP, 1*R*-^{2}H-GGPP, and 1,1-$^{2}H_2$-GGPP gave **1**, 11-^{2}H-**1**, and 1,11-$^{2}H_2$-**1**, respectively. *Related* to Fig. 5A.

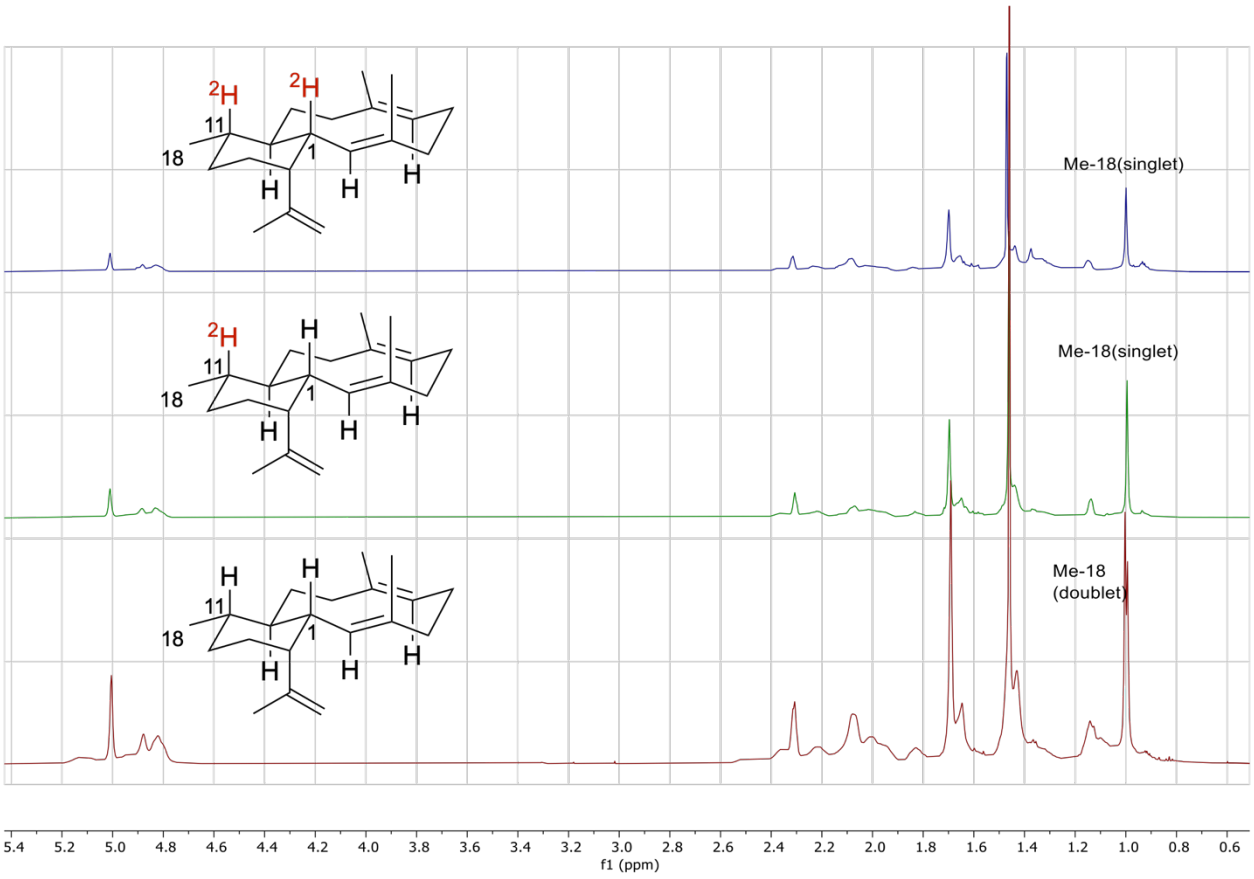

Figure S73. Proposed mechanisms forming **3**–**7** from incubation of AlbS with FPP. The 10-membered monocyclic products undergo thermal Cope rearrangement during GC-MS analysis.

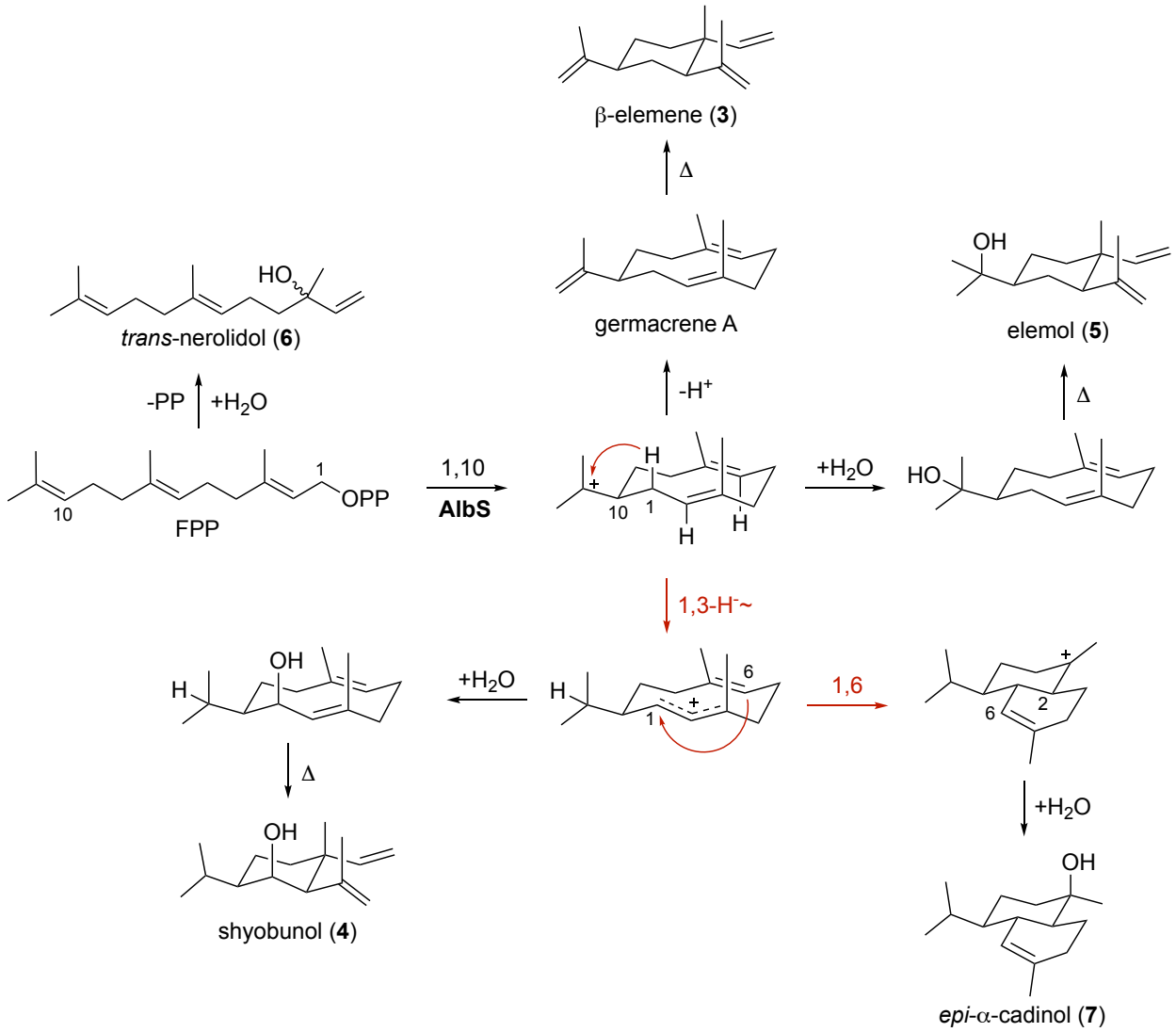

Figure S74. EIMS of benditerpetriene (**2**). (top) **2**; (middle) 1-^{2}H-**2**; (bottom) 1,11-^{2}H$_{2}$-**2**.

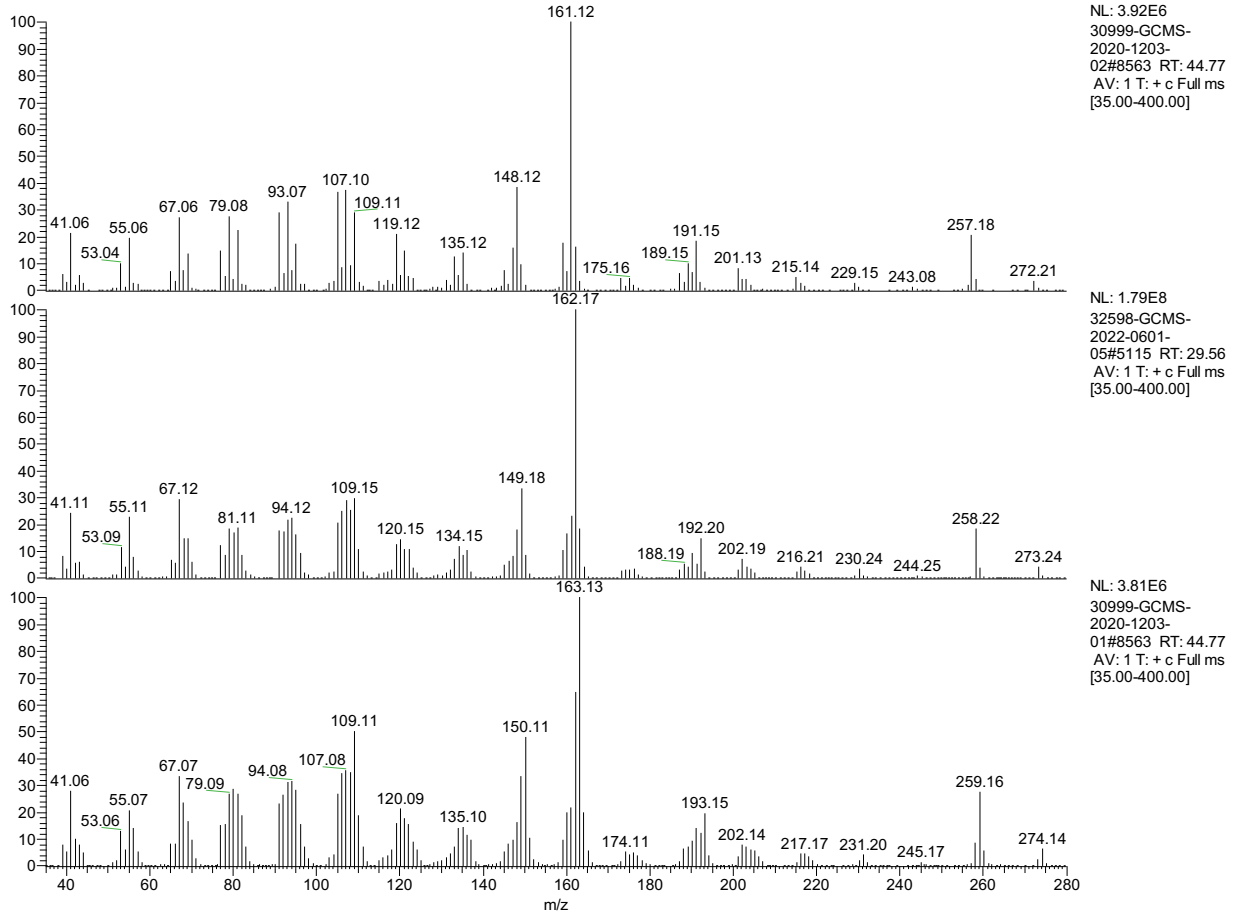

Figure S75. Comparison of the ^{1}H NMR spectra of **2** (bottom), 1-^{2}H-**2** (middle), and 1,11-$^{2}H_2$-**2** (top) in benzene-d_6 (600 MHz). The spectra of **2** and 1,11-$^{2}H_2$-**2** were previously reported.[10] Related to Fig. 5A.

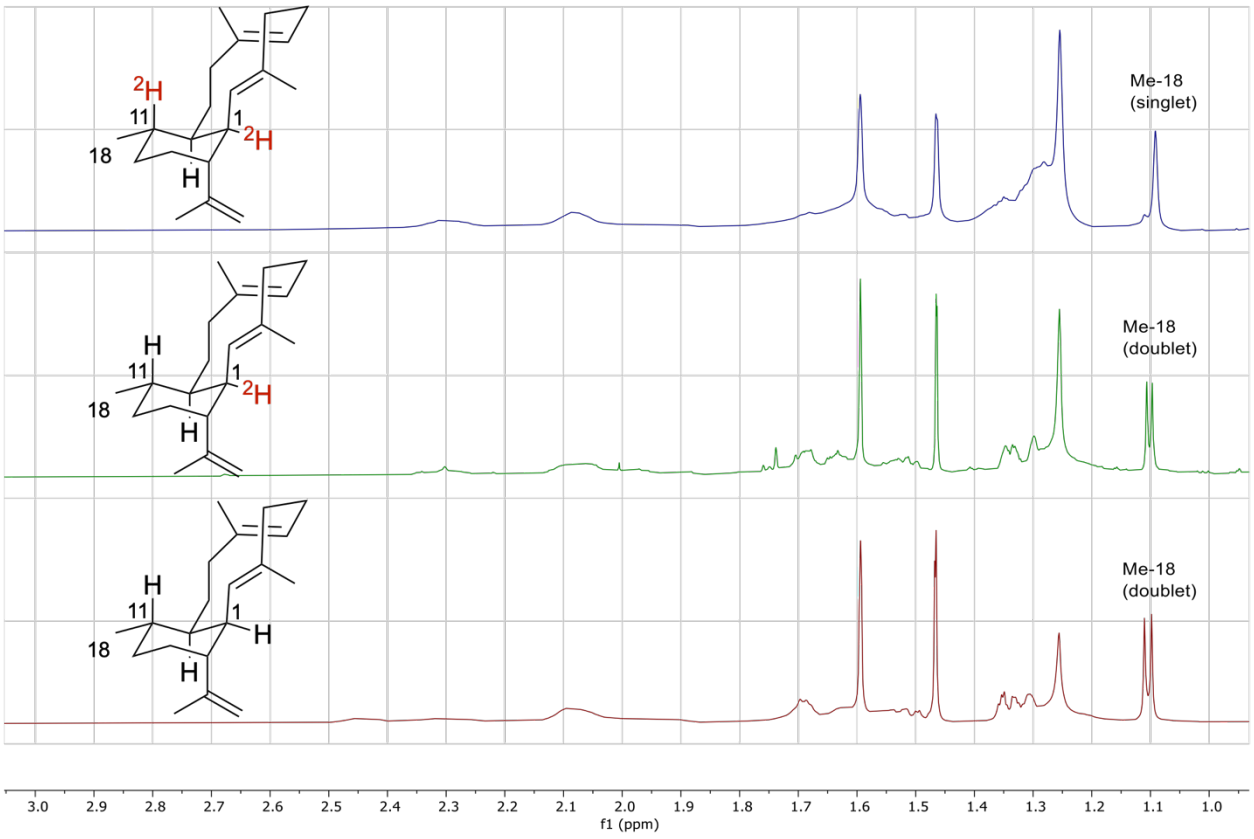

Figure S76. Comparison of the ^{1}H-^{13}C HSQC spectra of **2** (bottom), 1-^{2}H-**2** (middle), and 1,11-$^{2}H_2$-**2** (top) in benzene-d_6 (600 MHz). The spectra of **2** and 1,11$^{2}H_2$-**2** were previously reported.[4] Related to Fig. 5A.

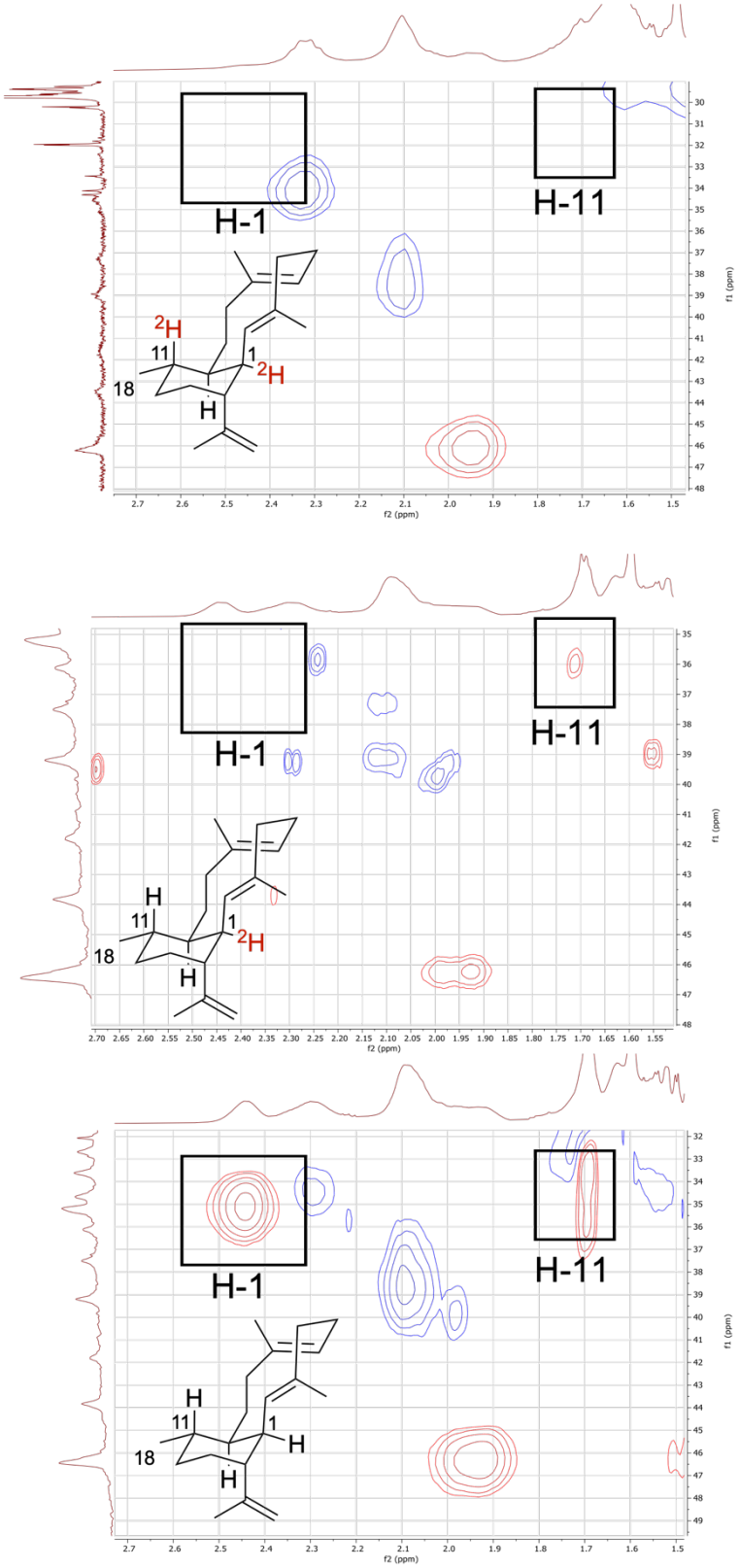

Table S1. Strains used in this study

Strain	Description	Source (Reference)
E. coli NEB Turbo	Host for general cloning	New England Biolabs
E. coli BL21 Star (DE3)	Host for high-level protein production	Invitrogen
Streptomyces albireticuli NRRL B-1670	Used for isolation of genomic DNA for *albS* amplification	NRRL

Table S2. Plasmids used in this study

Plasmid	Description	Source (Reference)
pET28a	Plasmid for heterologous expression in E. coli	Novagen
pCDF-Duet	General plasmid for cloning	Novagen
pJR1064	pET28a-MKI4: pET28a harboring kinases *Ec-Th*iM and *At-IPK*, *Ec-idi*, and GGPP synthase (*bnd3*). Ribosome binding sites were inserted before each gene.	(11)
pJR1064b	pCDF-MKI4: pCDF-Duet harboring the pJR1064 genes	This study
pJR1002	pET28a harboring *albS*	(12)
pJR1071	pET28a harboring *albS* (D121A)	This study
pJR1072	pET28a harboring *albS* (D121E)	This study
pJR1073	pET28a harboring *albS* (E185A)	This study
pJR1074	pET28a harboring *albS* (E185D)	This study
pJR1075	pET28a harboring *albS* (Y178A)	This study
pJR1076	pET28a harboring *albS* (Y214A)	This study
pJR1077	pET28a harboring *albS* (W336A)	This study
pJR1078	pET28a harboring *albS* (W336H)	This study
pJR1079	pET28a harboring *albS* (Y343A)	This study
pJR1080	pET28a harboring *albS* (F94A)	This study
pJR1081	pET28a harboring *albS* (F94W)	This study
pJR1082	pET28a harboring *albS* (H114A)	This study
pJR1083	pET28a harboring *albS* (H114T)	This study
pJR1084	pET28a harboring *albS* (F329A)	This study
pJR1085	pET28a harboring *albS* (F329M)	This study
pJR1086	pET28a harboring *albS* (Y214W)	This study
pJR1087	pET28a harboring *albS* (Y214I)	This study
pJR1088	pET28a harboring *albS* (Y214L)	This study
pJR1089	pET28a harboring *albS* (Y214H)	This study

Table S3. Primers used in this study

Name	Sequence (5′–3′)	Purpose
118_F	CAGCAAATGGGTCGCGGATCCATGAAG GGGATTCCGATGGG	*albS* or mutant amplification for protein expression in *E. coli*
119_R	CTCGAGTGCGGCCGCAAGCTTTCAAGC GGCGGGTTCCCGGA	
D121A_F	GGTCTGGATGGCCGATCGAATGGACCG TAAAGCTGCCATC	AlbS mutagenesis for D121A
D121A_R	TTACGGTCCATTCGATCGGCCATCCAGA CCGACCAGTGGT	
D121E_F	GGTCTGGATGGAAGATCGAATGGACCG TAAAGCTGCCATC	AlbS mutagenesis for D121E
D121E_R	TTACGGTCCATTCGATCTTCCATCCAGA CCGACCAGTGGT	
E185A_F	TCATCTCGCAAGGCGGTCAAAGCCCGG GACGGTATGGATC	AlbS mutagenesis for E185A
E185A_R	GTCCCGGGCTTTGACCGCCTTGCGAGA TGATGCCCCGTAC	
E185D_F	TCATCTCGCAAGGACGTCAAAGCCCGG GACGGTATGGATC	AlbS mutagenesis for E185D
E185D_R	GTCCCGGGCTTTGACGTCCTTGCGAGA TGATGCCCCGTAC	
Y178A_F	CCATGCGAATGGCCGGGGCATCATCTC GCAAGGAGGTCAAAGCCC	AlbS mutagenesis for Y178A
Y178A_R	TGCGAGATGATGCCCCGGCCATTCGCA TGGTCTGAACGAA	
Y178F_F	CCATGCGAATGTTCGGGGCATCATCTCG CAAGGAGGTCAAAGCCC	AlbS mutagenesis for Y178F
Y178F_R	TGCGAGATGATGCCCCGAACATTCGCAT GGTCTGAACGAA	
Y214A_F	ATGCCCGTGGCCCACACGGTGGCCGAC TGGGTCTCGCGCG	AlbS mutagenesis for Y214A
Y214A_R	CCAGTCGGCCACCGTGTGGGCCACGGG CATCGCCGCGGAC	
Y214F_F	ATGCCCGTGTTCCACACGGTGGCCGAC TGGGTCTCGCGCG	AlbS mutagenesis for Y214F
Y214F_R	ATGCCCGTGTTCCACACGGTGGCCGAC TGGGTCTCGCGCG	
W336A_F	GGCGGGGTCAACCACGCGAGCAATCAC ACCTGCCGGTACC	AlbS mutagenesis for W336A
W336A_R	GGTGTGATTGCTCGCGTGGTTGACCCC GCCGGCGAACTGG	
W336H_F	GGCGGGGTCAACCACCACAGCAATCAC ACCTGCCGGTACC	AlbS mutagenesis for W336H
W336H_R	GGTGTGATTGCTGTGTGGTTGACCCCG CCGGCGAACTGG	

Y343A_F	CAATCACACCTGCCGGGCCCTCGTCGG ACAATCCCTGGTG	AlbS mutagenesis for Y343A
Y343A_R	TGTCCGACGAGGGCCCGGCAGGTGTGA TTGCTCCAGTGGT	
Y94A_F	GTGGGAGGCGCCGTTTCCTGGGTCTAT CCCGACGCCACCG	AlbS mutagenesis for Y94A
Y94A_R	GGGATAGACCCAGGAAACGGCGCCTCC CACGTCCTCGCGC	
Y94W_F	GTGGGAGGCTGGGTTTCCTGGGTCTAT CCCGACGCCACCG	AlbS mutagenesis for Y94W
Y94W_R	GGGATAGACCCAGGAAACCCAGCCTCC CACGTCCTCGCGC	
H114A_F	ACCGACTGGGCCCACTGGTCGGTCTGG ATGGACGATCGAA	AlbS mutagenesis for H114A
H114A_R	CATCCAGACCGACCAGTGGGCCAGTC GGTCAGGGCCCTG	
H114T_F	ACCGACTGGACCCACTGGTCGGTCTGG ATGGACGATCGAA	AlbS mutagenesis for H114T
H114T_R	CATCCAGACCGACCAGTGGGTCCAGTC GGTCAGGGCCCTG	
F329A_F	GGGCCCTGCGCCAGGCCGCCGGCGGG GTCAACCACTGGAG	AlbS mutagenesis for F329A
F329A_R	TGACCCCGCCGGCGGCCTGGCGCAGG GCCCCGGCGTAGCG	
F329M_F	GGGCCCTGCGCCAGATGGCCGGCGGG GTCAACCACTGGAG	AlbS mutagenesis for F329M
F329M_R	TGACCCCGCCGGCCATCTGGCGCAGGG CCCCGGCGTAGCG	
Y214W_F	ATGCCCGTGTGGCACACGGTGGCCGAC TGGGTCTCGCGCG	AlbS mutagenesis for Y214W
Y214W_R	CCAGTCGGCCACCGTGTGCCACACGGG CATCGCCGCGGAC	
Y214I_F	ATGCCCGTGATACACACGGTGGCCGAC TGGGTCTCGCGCG	AlbS mutagenesis for Y214I
Y214I_R	CCAGTCGGCCACCGTGTGTATCACGGG CATCGCCGCGGAC	
Y214L_F	ATGCCCGTGCTACACACGGTGGCCGAC TGGGTCTCGCGCG	AlbS mutagenesis for Y214L
Y214L_R	CCAGTCGGCCACCGTGTGGATCACGGG CATCGCCGCGGAC	
Y214H_F	ATGCCCGTGCACCACACGGTGGCCGAC TGGGTCTCGCGCG	AlbS mutagenesis for Y214H
Y214H_R	CCAGTCGGCCACCGTGTGGTGCACGGG CATCGCCGCGGAC	

Table S4. ^{1}H NMR (600 MHz) and ^{13}C NMR (151 MHz) spectroscopic data and key 2D NMR correlations for albireticulene (**1**).[a]

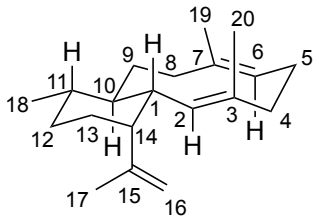

1

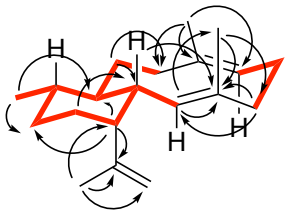

COSY
HMBC

No.	**1**[b]			**1**[c]	
	δ_C	δ_H		δ_C	δ_H
1, CH	45.7	1.98 (br, 1H)		47.1	2.07 (br, 1H)
2, CH	135.7	4.79 (br, 1H)		136.3	4.81 (br, 1H)
3, qC	127	–		133.0	–
4, CH_2	39.6	2.04 (br, 1H), 1.88 (br, 1H)		40.6	2.05 (br, 1H), 1.93 (br, 1H)
5, CH_2	26.2	2.17 (br, 1H), 2.00 (br, 1H)		26.8	2.20 (br, 1H), 2.00 (br, 1H)
6, CH	126.4	4.74 (br, 1H)		127.4	4.79 (br, 1H)
7, qC	137.7	–		138.3	–
8, CH_2	41.3	2.36 (br, 1H), 1.98 (br, 1H)		42.3	2.35 (br, 1H), 1.97 (br, 1H)
9, CH_2	34.6	1.80 (br, 1H), 0.94 (br, 1H)		35.6	1.80 (br, 1H), 1.01 (br, 1H)
10, CH	49.1	1.11 (br, 1H)		50.4	1.11 (br, 1H)
11, CH	36.8	1.04 (br, 1H)		37.5	1.09 (br, 1H)
12, CH_2	29.5	1.46 (br, 2H)		30.7	1.44 (br, 1H), 1.08 (br, 1H)
13, CH_2	38.1	2.03 (br, 1H), 1.59 (br, 1H)		28.5	1.63 (br, 1H), 1.45 (br, 1H)
14, CH	45.7	2.25 (br, 1H)		46.4	2.29 (br, 1H)
15, qC	146.5	–		147.8	–
16, CH_2	112.5	5.04 (br, 1H), 4.88 (br, 1H)		113.1	4.98 (br, 1H), 4.86 (br, 1H)
17, CH_3	25.9	1.66 (s, 3H)		26.3	1.68 (s, 3H)
18, CH_3	21.9	1.04 (br, 3H)		22.4	0.98 (d, J = 5.9, 3H)
19, CH_3	16.8	1.39 (s, 3H)		17.3	1.444 (s, 3H)
20, CH_3	16.3	1.42 (s, 3H)		17.0	1.446 (s, 3H)

[a] d in ppm, J in Hz

[b] NMR taken in toluene-d_8

[c] NMR taken in benzene-d_6

Table S5. Computational NMR chemical shifts of **1** compared to the experimentally obtained values [SMD(Benzene)-mPW1PW91/6-311+G(2d,p)//B3LYP/6-31+G(d,p)]. The mean absolute deviations (MADs) from the experimentally obtained ^{13}C and 1H chemical shifts are 1.3 and 0.1 ppm, respectively.

No.	Absolute Deviation (ppm)	
	δ_C	δ_H
1, CH	0.1	0.0 (br, 1H)
2, CH	0.4	0.1 (br, 1H)
3, qC	2.1	-
4, CH_2	0.5	0.1 (br, 1H) 0.1 (br, 1H)
5, CH_2	0.4	0.0 (br, 1H) 0.1 (br, 1H)
6, CH	0.6	0.0 (br, 1H)
7, qC	3.0	-
8, CH_2	0.1	0.0 (br, 1H) 0.0 (br, 1H)
9, CH_2	0.1	0.1 (br, 1H) 0.0 (br, 1H)
10, CH	1.4	0.0 (br, 1H)
11, CH	1.7	0.1 (br, 1H)
12, CH_2	2.4	0.0 (br, 1H) 0.2 (br, 1H)
13, CH_2	0.5	0.0 (br, 1H) 0.1 (br, 1H)
14, CH	1.7	0.2 (br, 1H)
15, qC	3.0	-
16, CH_2	2.1	0.3 (br, 1H) 0.1 (br, 1H)
17, CH_3	0.2	0.1 (s, 3H)
18, CH_3	2.3	0.0 (d, 3H)
19, CH_3	1.2	0.0 (s, 3H)
20, CH_3	1.5	0.0 (s, 3H)
MAD	1.3	0.1

Table S6. ^{1}H NMR (600 MHz) and ^{13}C NMR (151 MHz) spectroscopic data and key 2D NMR correlations for **8** and **9**.[a]

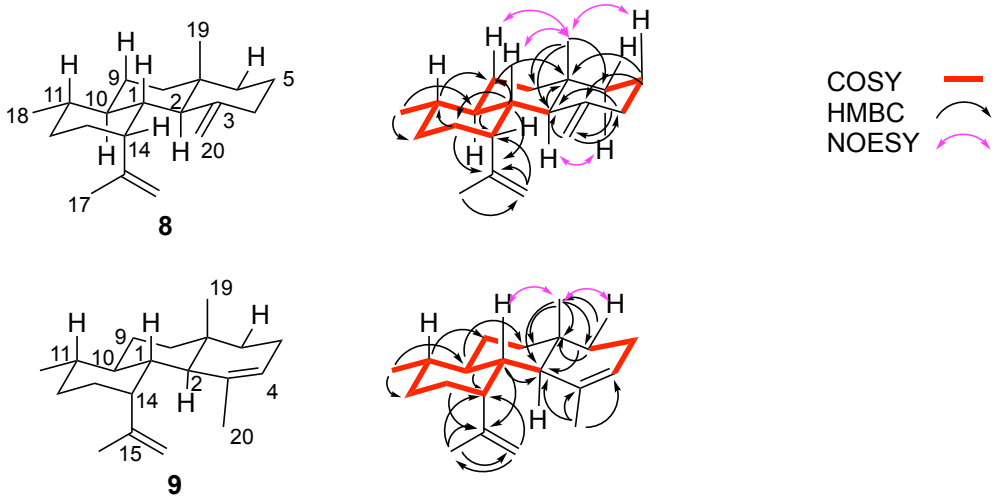

8

9

No.	**8**[b]		No.	**9**[b]	
	δ_C	δ_H		δ_C	δ_H
1, CH	40.7	1.52 (m, 1H)	1, CH	42.6	1.57 (m, 1H)
2, CH	52.2	1.88 (d, *J* = 11.6, 1H)	2, CH	46.3	2.12 (d, *J* = 11.6, 1H)
3, qC	149.2	–	3, qC	138.1	–
4, CH_2	39.1	2.22 (eq, d, *J* = 12.0 1H), 1.87 (ax, m, 1H)	4, CH	124.9	5.44 (m, 1H)
5, CH_2	25.1	1.63 (m, 2H)	5, CH_2	22.7	2.00 (m, 2H)
6, CH_2	42.6	1.35 (eq, m, 1H), 1.23 (ax, m, 1H)	6, CH_2	39.1	1.37 (ax, m, 1H), 1.22 (eq, m, 1H)
7, qC	36.8	–	7, qC	35.3	–
8, CH_2	41.2	1.45 (eq, m, 1H), 1.17 (ax, m, 1H)	8, CH_2	41.1	1.50 (eq, m, 1H), 1.197 (ax, m, 1H)
9, CH_2	25.5	1.74 (eq, m, 1H), 1.03 (ax, m, 1H)	9, CH_2	25.5	1.75 (eq, m, 1H), 1.05 (ax, m, 1H)
10, CH	42.8	1.28 (m, 1H)	10, CH	43.2	1.37 (m, 1H)
11, CH	38.3	1.18 (m, 1H)	11, CH	38.8	1.19 (m, 1H)
12, CH_2	31.4	1.47 (eq, m, 1H), 1.38 (ax, m, 1H)	12, CH_2	31.2	1.47 (eq, m, 1H), 1.33 (ax, m, 1H)
13, CH_2	30.6	1.70 (eq, m, 1H), 1.60 (ax, m, 1H)	13, CH_2	30.8	1.80 (eq, m, 1H), 1.60 (ax, m, 1H)
14, CH	39.5	2.92 (s, 1H)	14, CH	42.5	2.82 (m, 1H)
15, qC	148.3	–	15, qC	147.4	–
16, CH_2	112.9	4.83 (s, 1H), 4.80 (s, 1H)	16, CH_2	113.6	4.93 (m, 1H), 4.90 (m, 1H)
17, CH_3	26.7	1.74 (s, 3H)	17, CH_3	26.6	1.76 (s, 3H)
18, CH_3	20.2	0.92 (dd, *J* = 6.4, 3H)	18, CH_3	20.5	0.91 (dd, *J* = 6.4, 3H)
19, CH_3	17.8	0.74 (s, 3H)	19, CH_3	19.4	0.74 (s, 3H)
20, CH_2	106.6	4.88 (s, 1H), 4.42 (s, 1H)	20, CH_3	23.4	1.85 (s, 3H)

[a] d in ppm, *J* in Hz

[b] NMR taken in $CDCl_3$

Table S7. ^{1}H NMR (600 MHz) and ^{13}C NMR (151 MHz) spectroscopic data and key 2D NMR correlations for **10**.[a]

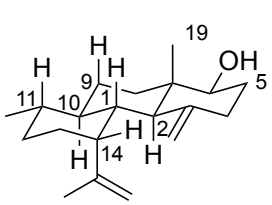

10

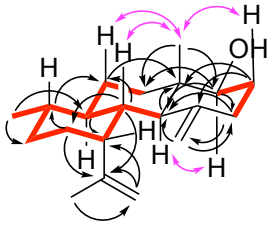

No.	**10**[b]	
	δ_C	δ_H
1, CH	40.2	1.57 (m, 1H)
2, CH	49.1	1.81 (d, *J* = 11.6, 1H)
3, qC	146.9	–
4, CH_2	35.9	2.20 (eq, m, 1H), 1.95 (ax, m, 1H)
5, CH_2	32.9	1.87 (ax, m, 1H), 1.52 (eq, m, 1H)
6, CH	79.7	3.36 (dd, *J* = 11.5, 4.9, 1H)
7, qC	40.7	–
8, CH_2	36.9	1.91 (eq, m, 1H), 1.07 (ax, m, 1H)
9, CH_2	25.1	1.81 (eq, m, 1H), 0.97 (ax, m, 1H)
10, CH	42.4	1.25 (m, 1H)
11, CH	38.2	1.17 (m, 1H)
12, CH_2	31.2	1.47 (eq, m, 1H), 1.36 (ax, m, 1H)
13, CH_2	30.5	1.68 (eq, m, 1H), 1.60 (ax, m, 1H)
14, CH	39.6	2.90 (s, 1H)
15, qC	148	–
16, CH_2	113.1	4.82 (s, 1H), 4.77 (s, 1H)
17, CH_3	12.1	1.7 (s, 3H)
18, CH_3	20.2	0.92 (d, *J* = 6.4, 3H)
19, CH_3	26.6	0.71 (s, 3H)
20, CH_2	108.1	4.93 (s, 1H), 4.49 (s, 1H)

[a] d in ppm, *J* in Hz

[b] NMR taken in $CDCl_3$

Table S8. ^{1}H NMR (600 MHz) spectroscopic data for **11** and **12**.[a]

No.	**11**[b]	**12**[b]	$\Delta\delta^{SR}$	
	δ_H	δ_H	ppm	Hz
1	1.572	1.563	+0.009	+5.4
2	1.956	1.953	+0.002	+1.2
17	0.76	0.76	0	0
8	1.696	1.566	+0.13	+78
	1.153	1.073	+0.08	+48
9	1.772	1.731	+0.041	+24.6
	0.917	0.882	+0.035	+21
10	1.253	1.241	+0.012	+7.2
11	1.156	1.146	+0.01	+6
12	1.477	1.473	+0.004	+2.4
	1.358	1.355	+0.003	+1.8
13	1.710	1.706	+0.004	+2.4
	1.596	1.595	+0.001	+0.6
14	2.875	2.874	+0.001	+0.6
18	0.911	0.898	+0.013	+7.8
19	1.715	1.715	0	0
20	4.840	4.840	0	0
	4.763	4.762	+0.001	+0.6
6	4.83	4.871	-0.041	-24.6
4	2.233	2.268	-0.035	-21
	2.030	2.054	-0.024	-14.4
5	2.012	2.055	-0.043	-25.8
	1.576	1.708	-0.132	-79.2
16	4.960	4.980	-0.02	-12
	4.526	4.538	-0.012	-7.2

[a] d in ppm, *J* in Hz

[b] NMR taken in $CDCl_3$

Table S9. ^{1}H NMR (600 MHz) and ^{13}C NMR (151 MHz) spectroscopic data and key 2D NMR correlations for **14**.[a]

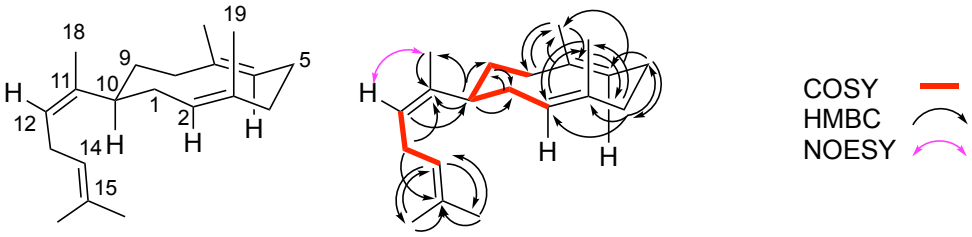

14

No.	**14** (conformer a)[b]		No.	**14** (conformer b)[b]	
	δ_C	δ_H		δ_C	δ_H
1, CH_2	34.9	2.21 (br, 1H), 2.16 (br, 1H)	1, CH_2	34.9	2.17 (br, 1H), 2.03 (br 1H)
2, CH	132.2	4.66 (m, 1H)	2, CH	126.1	5.13 (m, 1H)
3, qC	129.0	–	3, qC	129.0	–
4, CH_2	40.0	2.10 (br, 1H), 1.90 (br, 1H)	4, CH_2	37.6	2.10 (br, 1H), 2.07 (br, 1H)
5, CH_2	27.1	2.20 (br, 1H), 2.03 (br, 1H)	5, CH_2	24.7	2.29 (br, 1H), 2.02 (br, 1H)
6, CH	126.9	4.80 (m, 1H)	6, CH	122.3	5.15 (br, 1H)
7, qC	137.8	–	7, qC	138.1	–
8, CH_2	42.3	2.36 (br, 1H), 2.12 (br, 1H)	8, CH_2	42.3	2.36 (br, 1H), 2.12 (br, 1H)
9, CH_2	33.7	1.61 (br, 2H)	9, CH_2	34.0	1.38 (br, 2H)
10, CH	44.9	2.60 (br, 1H)	10, CH	41.6	2.53 (br, 1H)
11, qC	143.2	–	11, qC	141.1	–
12, CH	121.0	5.10 (br, 1H)	12, CH	121.0	5.10 (br, 1H)
13, CH_2	27.2	2.90 (m, 2H)	13, CH_2	27.3	2.83 (t, J = 7.3, 1H)
14, CH	124.6	5.29 (br, 1H)	14, CH	124.3	5.29 (br, 1H)
15, qC	131.0	–	15, qC	131.0	–
16, CH_3	25.9	1.66 (s, 3H)	16, CH_3	25.8	1.66 (s, 3H)
17, CH_3	17.9	1.62 (s, 3H)	17, CH_3	17.8	1.61 (s, 3H)
18, CH_3	19.8	1.664 (s, 3H)	18, CH_3	19.7	1.686 (s, 3H)
19, CH_3	16.4	1.36 (s, 3H)	19, CH_3	16.4	1.34 (s, 3H)
20, CH_3	16.8	1.46 (s, 3H)	20, CH_3	15.6	1.50 (s, 3H)

[a] d in ppm, J in Hz

[b] NMR taken in benzene-d_6

Supplemental Experimental Procedures

General materials and methods

All ^{1}H, ^{13}C, 1D selective TOCSY, and 2D NMR (^{1}H-^{13}C HSQC, ^{1}H-^{1}H COSY, ^{1}H-^{13}C HMBC) experiments were run on a Bruker AVANCE III Ultrashield 600. ^{1}H NMR and ^{13}C NMR spectra were recorded on a Bruker AVANCE AV400 (400 MHz and 101 MHz) or Bruker AVANCE AV600 (600 MHz and 151MHz). All NMR chemical shifts were referenced to residual solvent peaks or to $Si(CH_3)_4$ as an internal standard. Spectra recorded in D_2O were referenced to residual H_2O at 4.79 ppm for ^{1}H, spectra recorded in $CDCl_3$ were referenced to residual $CHCl_3$ at 7.26 ppm for ^{1}H or 77.00 ppm for ^{13}C, spectra recorded in C_6D_6 were referenced to residual C_6D_5H at 7.16 ppm for ^{1}H or 128.06 ppm for ^{13}C, and spectra recorded in $C_6D_5CD_3$ were referenced at 7.0 ppm for ^{1}H or 137.4 ppm for ^{13}C. All chemicals and reagents for reactions were purchased at the highest commercial quality and used directly. Chemical reactions were monitored by thin layer chromatography (TLC) and high-performance liquid chromatography (HPLC). TLC was performed with 0.25 mm silica gel plates (60 F_{254}) using short-wave UV light to visualize, and I_2 or $KMnO_4$ and heat as developing agents. HPLC was performed on an Agilent 1260 Infinity LC equipped with an Agilent Zorbax SB-C18 column (150 mm × 4.6 mm, 5 µm). Preparative HPLC was carried out on an Agilent 1260 Infinity LC equipped with an Agilent Eclipse XDB-C18 column (250 mm × 21.2 mm, 7 µm). GC-MS analysis was carried out using Thermo Scientific Trace GC ultra-ISQ spectrometer with a DB-5MS glass capillary column (Agilent Technologies, 15 m × 0.25 mm i.d. and 1 µm film). Optical rotations were measured using a JASCO P-2000 polarimeter.

Bacterial strains, plasmids, and chemicals

Strains, plasmids, and PCR primers used in this study are listed in Tables S1–S3. PCR primers were obtained from Sigma-Aldrich. Q5 high-fidelity DNA polymerase and restriction endonucleases were purchased from NEB and used by following the protocols provided by the manufacturers. DNA gel extraction and plasmid preparation kits were purchased from Omega Bio-Tek. DNA sequencing was conducted by Genewiz in standard commercial sources. All strains, plasmids, and PCR primers generated in this study are stored as stocks at –80 ºC or –20 ºC.

Gene cloning

Primers were designed for T5 exonuclease-dependent assembly (TEDA).[13] For site-directed mutagenesis of *albS*, overlap PCR was used with the genome of *Streptomyces albireticuli* sp. NRRL-B-5493 as a template with Q5 DNA polymerase. The PCR products were purified by gel extraction and cloned into the pET28a(+) vector, which was linearized with *Bam*HI and *Hind*III, and transformed into *E. coli* BL21 Star competent cells using TEDA to produce plasmid pJR1002.[12] The plasmid was confirmed by DNA sequencing.

For site-directed mutagenesis, PCR was used to introduce mutations into AlbS. In short, Q5 DNA polymerase was added to a solution of 10 mM Tris-HCl, pH 8.3, containing 7 mM $MgCl_2$, 0.5 mM $MnCl_2$, 50 mM KCl, 0.2 mM dATP, 0.2 mM dGTP, 0.2 mM dCTP, 1 mM dTTP, 10 ng pJR1071, and 0.4 µM primers (Table S3) for amplification of *albS*. Five to 40 cycles of PCR were performed individually with an annealing temperature at 65 °C. The PCR products were cloned into pET28a(+) and confirmed as described above yielding pJR1071–pJR1089.

Using pJR1064, a pET28a-based GGPP production plasmid, we subcloned the genetic fragment containing *thiM*, *ipk*, *idi*, and *bnd3* into pCDF-Duet to yield pJR1064b.

Protein production and purification

Plasmids harboring each gene were transformed into *E. coli* BL21 Star. *E. coli* strains harboring plasmids were grown in lysogeny broth (LB) containing 50 mg mL^{-1} kanamycin for antibiotic selection. Each strain was grown in 4 × 1 L of lysogeny broth (LB) at 37 °C with shaking at 200 rpm until an optical density at 600

nm (OD600) of 0.6 was reached. After addition of 0.3 mM (final concentration) isopropyl β-D-1-thiogalactopyranoside (IPTG) for gene expression, the cells were incubated at 16 °C with shaking for approximately 18 h. Cells were harvested by centrifugation at 4000 *g* for 15 min at 4 °C and the pellet was resuspended in cold lysis buffer (50 mM Tris-HCl, pH 8.0, containing 150 mM NaCl). Cells were lysed with an M-110L Microfluidizer Processor (Quadro Engineering Corp) and the lysates were centrifuged at 40,000 *g* for 30 min at 4 °C. Target proteins from the supernatant were loaded onto a nickel-affinity chromatography column packed with HisPur™ Ni-NTA Resin (Thermo Scientific). The resin was successively washed with lysis buffer containing 20 mM imidazole and eluted with elution buffer (lysis buffer containing 500 mM imidazole). The target protein was immediately desalted using a PD-10 column (GE Healthcare Biosciences) and concentrated using an Amicon Ultra-15 concentrator (Millipore) in 50 mM Tris-HCl, pH 8.0, containing 150 mM NaCl. Protein purities were detected by SDS-PAGE analysis, and concentration was determined by the Bradford assay.[14] Individual aliquots of each protein were flash-frozen in liquid nitrogen and stored at –80 °C for use.

Enzyme activity assay

For each in vitro enzyme reaction, 40 μM AlbS or AlbS mutants were incubated at 37 °C in the presence of 10 mM GGPP, and 10 mM $MgCl_2$ in 50 mM Tris-HCl, pH 8.0, at a total volume of 100 μL. The reactions were incubated for 1 h at 37 °C, quenched with equal volume of acetonitrile, and saturated with NaCl solid. Separation of the two phases by vortexing, the organic phase was analyzed by HPLC and/or GC-MS. For HPLC analysis, enzyme products were monitored at 210 nm with a linear gradient as follows: 5% acetonitrile/water (0–5 min); 5% to 95% acetonitrile/water (5–35 min @ 5% min^{-1}); 95% acetonitrile/water (hold 25 min) at 35 °C with flow rate of 1 mL min^{-1}. For GC-MS analysis, the source, transfer line, and injection port were set to 250, 290, and 250 °C, respectively, and the carrier gas flow rate was set at 1 mL min^{-1}. Products were measured with an electron ionization of 70 eV and mass scan range was from m/z 30–500 @ 1500 u s^{-1} with a temperature gradient as follows: 50°C (0–3 min), ramp to 300 °C @ 4 °C min^{-1} (hold 5 min). Kovats retention index (RI) values were calculated for all products in this study using the GC-MS conditions above in comparison with C8–C30 saturated alkanes (Sigma).

Enzymatic synthesis and purification of terpenes

A preparative enzymatic reaction using AlbS was conducted on a 100 mg GGPP scale. After completion of the reaction, as determined by HPLC analysis, the reaction mixture was extracted three times with equal volumes of hexanes. The combined organic phase was concentrated in vacuo and dissolved in 1.8 mL of acetonitrile. After eliminating insoluble components by centrifugation (16,000 *g*, 10 min), the supernatant was loaded and purified by prep-HPLC using a flow rate of 20 mL min^{-1}. Prep-HPLC was conducted with a linear gradient as follows: 0–5 min, 5% acetonitrile/water; 5% to 95% acetonitrile/water (5–15 min @ 9% min^{-1}); 95% acetonitrile/water (hold 45 min). The products were manually collected by monitoring at 210 nm through comparison with retention time in analytical HPLC. A total of 8.9 mg of **1** were obtained at a yield of 16.7%. For **14**, the same procedure was used to obtain 2.4 mg from a 35 mg GGPP reaction at a yield of 12.5%.

Albireticulene (**1**): colorless oil, R_f = 0.78 (hexanes); *RI* = 1804; $[\alpha]_D^{21}$ = -51.72 (c 1.0, CH_2Cl_2); ^1H and ^{13}C NMR data, see Table S5 and Figs. S10–S22; UV/Vis (acetonitrile:water = 9:1): λ_{max} = 210 nm; IR (cm^{-1}): 2919, 2854, 1444, 1376, 1266, 1247, 883, 851.

Benditerpetriene (**2**): *RI* = 1822. Other spectroscopic data was previously reported.[15]

Gersemiene A (**8**): colorless oil, R_f = 0.8 (hexanes); *RI* = 1939; $[\alpha]_D^{21}$ = -11.85 (c = 0.3, $CHCl_3$); ^1H and ^{13}C NMR data, see Table S6 and Figs. S24–S33; UV/Vis (acetonitrile:water = 9:1): λ_{max} = 210 nm; IR (cm^{-1}): 2917, 2850, 1450, 1375, 1263, 1204, 888, 839.

Gersemiene B (**9**): colorless oil, R_f = 0.82 (hexanes); *RI* = 1932; $[\alpha]_D^{21}$ = -52.72 (c = 1.0, $CHCl_3$); ^1H and ^{13}C NMR data, see Table S6 and Figs. S34–S40; UV/Vis (acetonitrile:water = 9:1): λ_{max} = 210 nm; IR (cm^{-1}): 2921, 2844, 1440, 1375, 1192, 888, 867.

Prenylgermacrene A (**14**): colorless oil, R_f = 0.7 (hexanes); *RI* = 1842; $[\alpha]_D^{21}$ = +0.472 (c = 0.0018, CH_2Cl_2); ^1H and ^{13}C NMR data, see Table S9 and Figs. S62–S67; UV/Vis (acetonitrile:water = 9:1): λ_{max} = 210 nm; IR (cm^{-1}): 2917, 2849, 1448, 1377, 1260, 870, 754.

Enzymatic synthesis of $^2H_2$-1

To a 5 mL reaction mixture of 50 mM Tris-HCl, pH 8.0, containing 20 mM $MgCl_2$, 10 mM 1,1-$^2H_2$-IPP, 10 mM FPP, and 20 μM GGPP synthase (CrtE, for generating GGPP in situ) were added and the reaction was stirred slowly (<100 rpm min^{-1}) at 37 °C for 10 min. AlbS was added to a final concentration of 20 μM and the mixture was stirred for another 2 h. The purification procedure was identical to that described above.

Enzyme activity assays and product purification from *E. coli*

Plasmids pJR1002 and pJR1064b (for producing GGPP from 3-methyl-3-buten-1-ol in cellulo)[4] were transformed into *E. coli* BL21 Star. *E. coli* strains harboring plasmids were grown in lysogeny broth (LB) containing 50 mg mL^{-1} kanamycin and 100 mg mL^{-1} streptomycin for antibiotic selection. Strains were then grown in 12 × 1 L of LB at 37 °C with shaking at 200 rpm until an OD600 of 1.6. IPTG (0.3 mM) and 3-methyl-3-buten-1-ol (4 mM) were then added and the cells were incubated for 24 h at 28 °C. The cells were harvested by centrifugation at 4000 *g* for 15 min at 4 °C and the pellet was dissolved in acetonitrile; NaCl solid was added and the suspension was vortexed to form two phases. The organic phase was analyzed by HPLC and products were purified by prep-HPLC as described above.

Chemical synthesis of IPP, FPP, GGPP, 1,1-$^2H_2$-IPP, and 1*R*-^{2}H-GGPP

The synthesis of prenyl diphosphates was achieved using previously reported methods.[16–23] Products were confirmed by NMR spectroscopy, which matched the literature.

Chemical synthesis of 10

To a solution of **1** (27 mg, 0.10 mmol) and $NaHCO_3$ (30 mg) in CH_2Cl_2 (10 mL), *m*CPBA (75% w/w, 28 mg) was added at -40 °C and the mixture was stirred for 30 min. A saturated Na_2SO_3 aqueous solution was added to quench the reaction after **1** was deterred to be completely consumed by TLC. The reaction mixture was extracted with ethyl acetate and the combined organic extract was concentrated under reduced pressure. The concentrated extract was purified by silica gel chromatography with a gradient elution of hexane/EtOAc (100:0, 95:5, 80:20) to give the major product **10** as a colorless oil (20.6 mg, 72%); R_f = 0.48 (hexanes:ethyl acetate = 4:1); $[\alpha]_D^{21}$ = -32.51 (c = 0.10, $CHCl_3$); ^1H and ^{13}C NMR data, see Table S7; HRESIMS analysis: calc. *m/z* 289.2526 $[M + H]^+$; found *m/z* 289.2523. Mass error: -1.037 ppm.

Modified Mosher ester analysis of 10

Modified Mosher ester analysis[24] was used to identify the stereochemical configuration of the secondary alcohol in **10**. To a solution of **10** (6.0 mg, 0.021 mmol) in dry CH_2Cl_2 (5 mL), anhydrous pyridine (10.0 μL, 0.124 mmol) and (*R*)-(+)-methoxy trifluoromethylphenylacetyl chloride [*R*-(+)-MTPA-Cl] dissolved in dry DCM (1 mL) was successively added. After 24 h, the reaction was quenched with $NaHCO_3$ aqueous solution and then extracted with ethyl acetate. The organic layers were combined, dried over anhydrous Na_2SO_4, and concentrated under reduced pressure to give a crude residue, which was purified by silica gel chromatography with a gradient elution of hexane/EtOAc (100:0, 95:5) to give the desired product, the (*S*)-MTPA ester of **10** (**11**) (8.6 mg, 81%). ^1H and ^{13}C NMR data, see Figs. S51–S55; HRESIMS analysis: calc. *m/z* 527.2744 $[M + H]^+$; found *m/z* 527.2741. Mass error: -0.5690 ppm. The (*R*)-MTPA ester of **10** (**12**) was similarly prepared using (*S*)-(+)-methoxy trifluoromethylphenylacetyl chloride [*S*-(+)-MTPA-Cl].

^{1}H and ^{13}C NMR data, see Figs. S56–S60. HRESIMS analysis: calc. *m/z* 527.2744 $[M + H]^{+}$; found *m/z* 527.2749. Mass error: 0.9483 ppm. The absolute configuration of the secondary alcohol was solved by comparison of ^{1}H NMR chemical shifts (Table S8).[25]

Computational methods

All geometry optimizations were carried out with Gaussian 09 at the mPW1PW91/6-31+G(d,p)//B3LYP/6-31+G(d,p) level of theory.[26–29] NMR calculations[30] were performed with SMD(Benzene)-mPW1PW91/6-311+G(2d,p)//B3LYP/6-31+G(d,p) level using the GIAO method (Table S5).[31–34] The conformational searches were performed with CREST, version 2.11.1 using gfn2//gfnff.[35,36] The optimized structures are available in the ioChem-BD repository.[37] See the following DOI for the coordinates: https://doi.org/10.19061/iochem-bd-6-166.

Accession numbers for proteins

AlbS and its homologues (Fig. S2): AlbS from *Streptomyces albireticuli*, A0A2A2D8W5; *Streptomyces katrae*, A0A0F4JKQ6; *Streptomyces* sp. WAC06614, A0A3R9UKK2; *Streptomyces* sp. WAC07149, A0A3R9VIW7; *Actinomadura rubrisoli*, A0A4V2YVB5; Bnd4 from *Streptomyces* sp. CL12-4, WP_239771469.

Supplemental References

1. Zallot, R., Oberg, N., and Gerlt, J. A. (2019). The EFI web resource for genomic enzymology tools: leveraging protein, genome, and metagenome databases to discover novel enzymes and metabolic pathways. Biochemistry *58*, 4169–4182.

2. Thompson, J. D., Higgins, D. G., and Gibson, T. J. (1994). CLUSTAL W: improving the sensitivity of progressive multiple sequence alignment through sequence weighting, position-specific gap penalties and weight matrix choice. Nucleic Acids Res. *22*, 4673–4680.

3. Robert, X., and Gouet, P. (2014). Deciphering key features in protein structures with the new ENDscript server. Nucleic Acids Res. *42*, W320–W324.

4. Adams, R. P. (2007). Identification of essential oil components by gas chromatography/mass spectrometry (Allured Publishing Corporation).

5. Rabe, P., Schmitz, T., and Dickschat, J. S. (2015). Conformational analysis, thermal rearrangement, and EI-MS fragmentation mechanism of (1(10)*E*,4*E*,6*S*,7*R*)-germacradien-6-ol by ^{13}C-labeling experiments. Angew. Chem. Int. Ed. *54*, 13448–13451.

6. Govindam, S.V.S., Yoshioka, Y., Kanamoto, A., Fujiwara, T., Okamoto, T., and Ojika, M. (2012). Cyclolobatriene, a novel prenylated germacrene diterpene, from the soft coral Lobophytum pauciflorum. Bioorg. Med. Chem. 20, 687–692. 10.1016/j.bmc.2011.12.012.

7. Faraldos, J.A., Wu, S., Chappell, J., and Coates, R.M. (2007). Conformational analysis of (+)-germacrene A by variable-temperature NMR and NOE spectroscopy. Tetrahedron 63, 7733–7742. 10.1016/j.tet.2007.04.037.

8. Terada, Y., and Yamamura, S. (1979). Stereochemical studies on germacrenes: an application of molecular mechanics calculations. Tetrahedron Letters 20, 3303–3306. 10.1016/S0040-4039(01)95391-2.

9. Xu, H., Lackus, N.D., Köllner, T.G., and Dickschat, J.S. (2022). Isotopic labeling experiments solve the hedycaryol problem. Org. Lett. 24, 587–591. 10.1021/acs.orglett.1c04021.

10. Xu, B., Tantillo, D. J., and Rudolf, J. D. (2021). Mechanistic insights into the formation of the 6,10-bicyclic eunicellane skeleton by the bacterial diterpene synthase Bnd4. Angew. Chem. Int. Ed. *60*, 23159–23163.

11. Xu, B., Ning, W., Wei, X., and Rudolf, J. D. (2022). Mutation of the eunicellane synthase Bnd4 alters its product profile and expands its prenylation ability. Preprint at ChemRxiv, 10.26434/chemrxiv-2022-3vsmz.

12. Xu, B., Li, Z., Alsup, T. A., Ehrenberger, M. A., and Rudolf, J. D. (2021). Bacterial diterpene synthases prenylate small molecules. ACS Catal. *11*, 5906–5915.

13. Xia, Y., Li, K., Li, J., Wang, T., Gu, L., and Xun, L. (2019). T5 exonuclease-dependent assembly offers a low-cost method for efficient cloning and site-directed mutagenesis. Nucleic Acids Res. *47*, e15.

14. Kruger, N. J. (2009). The Bradford method for protein quantitation. In The Protein Protocols Handbook, J. M. Walker, ed. (Springer), pp. 17–24.

15. Zhu, C., Xu, B., Adpressa, D.A., Rudolf, J.D., and Loesgen, S. (2021). Discovery and biosynthesis of a structurally dynamic antibacterial diterpenoid. Angew. Chem., Int. Ed. *60*, 14163–14170. 10.1002/anie.202102453.

16. Davisson, V. J., Woodside, A. B., and Poulter, C. D. (1985). Synthesis of allylic and homoallylic isoprenoid pyrophosphates. Meth. Enzymol. *110*, 130–144.

17. Zhao, M., Li, J., Song, Z., Desmond, R., Tschaen, D. M., Grabowski, E. J. J., and Reider, P. J. (1998). A novel chromium trioxide catalyzed oxidation of primary alcohols to the carboxylic acids.

Tet. Lett. *39*, 5323–5326.

18. Davisson, V. J., Woodside, A. B., Neal, T. R., Stremler, K. E., Muehlbacher, M., and Poulter, C. D. (1986). Phosphorylation of isoprenoid alcohols. J. Org. Chem. *51*, 4768–4779.

19. Rudolf, J. D., Dong, L.-B., Cao, H., Hatzos-Skintges, C., Osipiuk, J., Endres, M., Chang, C.-Y., Ma, M., Babnigg, G., Joachimiak, A., et al. (2016). Structure of the *ent*-copalyl diphosphate synthase PtmT2 from *Streptomyces platensis* CB00739, a bacterial type II diterpene synthase. J. Am. Chem. Soc. *138*, 10905–10915.

20. Roe, S. J., Oldfield, M. F., Geach, N., and Baxter, A. (2013). A convergent stereocontrolled synthesis of [3-(14)C]solanesol. J. Labelled Comp. Radiopharm. *56*, 485–491.

21. Dixit, V. M., Laskovics, F. M., Noall, W. I., and Poulter, C. D. (1981). Tris(tetra-n-butylammonium) hydrogen pyrophosphate. A new reagent for the preparation of allylic pyrophosphate esters. J. Org. Chem. *46*, 1967–1969.

22. Scholte, A. A., and Vederas, J. C. (2006). Incorporation of deuterium-labelled analogs of isopentenyl diphosphate for the elucidation of the stereochemistry of rubber biosynthesis. Org. Biomol. Chem. *4*, 730–742.

23. Rinkel, J., Rabe, P. Chen, X., Köllner, T. G., Chen, F., and Dickschat, J. S. (2017). Mechanisms of the Diterpene Cyclases β-Pinacene Synthase from *Dictyostelium discoideum* and Hydropyrene Synthase from *Streptomyces clavuligerus*. Chem. Eur. J. *23*, 10501–10505.

24. Hoye, T. R., Jeffrey, C. S., and Shao, F. (2007). Mosher ester analysis for the determination of absolute configuration of stereogenic (chiral) carbinol carbons. Nat. Protocol. *2*, 2451–2458.

25. Seco, J. M., Quiñoá, E., and Riguera, R. (2004). The assignment of absolute configuration by NMR. Chem. Rev. *104*, 17–118.

26. Gaussian 09, Revision D.01, Frisch, M. J., Trucks, G. W., Schlegel, H. B., Scuseria, G. E., Robb, M. A., Cheeseman, J. R., Scalmani, G., Barone, V., Mennucci, B., Petersson, G. A., et al. (2013). Gaussian, Inc., Wallingford CT.

27. Lee, C., Yang, W., and Parr, R.G. (1988). Development of the Colle-Salvetti correlation-energy formula into a functional of the electron density. Phys. Rev. B *37*, 785–789.

28. Adamo, C., and Barone, V. (1998). Exchange functionals with improved long-range behavior and adiabatic connection methods without adjustable parameters: The mPW and mPW1PW models. J. Chem. Phys. *108*, 664–675.

29. Tantillo, D. J. (2011). Biosynthesis via carbocations: theoretical studies on terpene formation. Nat. Prod. Rep. *28*, 1035 – 1053.

30. Lodewyk, M. W., Siebert, M. R., and Tantillo, D. J. (2012). Computational prediction of ^{1}H and ^{13}C chemical shifts: a useful tool for natural product, mechanistic, and synthetic organic chemistry. Chem.Rev. *112*, 1839–1862.

31. Cheeseman, J.R., Trucks, G. W., Keith, T. A., and Frisch, M. J. (1996). A comparison of models for calculating nuclear magnetic resonance shielding tensors. J. Chem. Phys., *104*, 5497–5509.

32. Wolinski, K., Hinton, J. F., and Pulay, P. (1990). Efficient implementation of the gauge-independent atomic orbital method for NMR chemical shift calculations. J. Am. Chem. Soc.,*112*, 8251–8260.

33. Bagno, A. and Saielli, G. (2015). Addressing the stereochemistry of complex organic molecules by density functional theory-NMR. Wiley Interdiscip. Rev. Comput. Mol. Sci., *5*, 228–240.

34. de Albuquerque, A. C. F., Ribeiro, D. J., and de Amorim, M. B. (2016). Structural determination of complex natural products by quantum mechanical calculations of ^{13}C NMR chemical shifts:

development of a parameterized protocol for terpenes. J. Mol. Model. *22*, 183.

35. Grimme, S. (2019). Exploration of chemical compound, conformer, and reaction space with meta-dynamics simulations based on tight-binding quantum chemical calculations. J. Chem. Theory Comput. *15*, 2847–2862.

36. Pracht, P., Bohle, F., and Grimme, S. (2020). Automated exploration of the low-energy chemical space with fast quantum chemical methods. Phys. Chem. Chem. Phys. *22*, 7169–7192.

37. Álvarez-Moreno, M., De Graaf, C., López, N., Maseras, F., Poblet, J. M., and Bo, C. (2015). Managing the computational chemistry big data problem: the ioChem-BD platform. J. Chem. Inf. Model. *55*, 95–103.